



UNIVERSIDADE ESTADUAL DE CAMPINAS
Faculdade de Engenharia Elétrica e de Computação

Vanessa Mendes Rennó

Advanced Analysis and Simulation of Generalized Wireless Channels

*Análise e Simulação Avançada de
Canais sem Fio Generalizados*

Campinas

2023



UNIVERSIDADE ESTADUAL DE CAMPINAS
Faculdade de Engenharia Elétrica e de Computação

Vanessa Mendes Rennó

Advanced Analysis and Simulation of Generalized Wireless Channels

Análise e Simulação Avançada de Canais sem Fio Generalizados

Thesis presented to the School of Electrical and Computer Engineering of the University of Campinas in partial fulfillment of the requirements for the degree of Doctor in Electrical Engineering, in the area of Telecommunications and Telematics.

Tese apresentada à Faculdade de Engenharia Elétrica e de Computação da Universidade Estadual de Campinas como parte dos requisitos exigidos para a obtenção do título de Doutora em Engenharia Elétrica, na Área de concentração: Telecomunicações e Telemática.

Orientador: Prof. Dr. José Cândido Silveira Santos Filho

Este exemplar corresponde à versão final da tese defendida pela aluna Vanessa Mendes Rennó, e orientada pelo Prof. Dr. José Cândido Silveira Santos Filho.

Campinas

2023

Ficha catalográfica
Universidade Estadual de Campinas
Biblioteca da Área de Engenharia e Arquitetura
Rose Meire da Silva - CRB 8/5974

R295a Rennó, Vanessa Mendes, 1993-
Advanced analysis and simulation of generalized wireless channels /
Vanessa Mendes Rennó. – Campinas, SP : [s.n.], 2023.

Orientador: José Cândido Silveira Santos Filho.
Tese (doutorado) – Universidade Estadual de Campinas, Faculdade de
Engenharia Elétrica e de Computação.

1. Simulação. 2. Canais de desvanecimento. 3. Sistemas de comunicação
sem fio. 4. Modelos estatísticos. 5. Expansões assintóticas. I. Santos Filho,
José Cândido Silveira, 1979-. II. Universidade Estadual de Campinas.
Faculdade de Engenharia Elétrica e de Computação. III. Título.

Informações Complementares

Título em outro idioma: Análise e simulação avançada de canais sem fio generalizados

Palavras-chave em inglês:

Simulation

Fading channels

Wireless communication systems

Statistical models

Asymptotic expansions

Área de concentração: Telecomunicações e Telemática

Titulação: Doutora em Engenharia Elétrica

Banca examinadora:

José Cândido Silveira Santos Filho [Orientador]

Victoria Dala Pegorara Souto

Waslon Terlizzie Araújo Lopes

Michel Daoud Yacoub

Paulo Cardieri

Data de defesa: 18-05-2023

Programa de Pós-Graduação: Engenharia Elétrica

Identificação e informações acadêmicas do(a) aluno(a)

- ORCID do autor: <https://orcid.org/0000-0001-8498-5270>

- Currículo Lattes do autor: <http://lattes.cnpq.br/9121098337331787>

COMISSÃO JULGADORA - TESE DE DOUTORADO

Candidata: Vanessa Mendes Rennó, RA: 229995

Data da Defesa: 18 de Maio de 2023

Título da Tese: “Advanced Analysis and Simulation of Generalized Wireless Channels (Análise e Simulação Avançada de Canais sem Fio Generalizados)”.

Prof. Dr. José Cândido Silveira Santos Filho (FEEC/UNICAMP) (Presidente)

Prof^a. Dr^a. Victoria Dala Pegorara Souto (Inatel)

Prof. Dr. Waslon Terllizzie Araújo Lopes (UFPB)

Prof. Dr. Michel Daoud Yacoub (FEEC/UNICAMP)

Prof. Dr. Paulo Cardieri (FEEC/UNICAMP)

A ata de defesa, com as respectivas assinaturas dos membros da Comissão Julgadora, encontra-se no SIGA (Sistema de Fluxo de Dissertação/Tese) e na Secretaria de Pós-Graduação da Faculdade de Engenharia Elétrica e de Computação.

To my parents, Roberto and Regina.

Acknowledgements

I thank God for the gift of life, giving me health, ability, intelligence, and perseverance to follow my journey.

To my parents, Roberto and Regina, for their unconditional love, encouragement, and support in all my dreams.

To Vinícius, my fiancé, with whom I share all my fears and secrets. Thank you for always encouraging me to complete this work. Having you in my life made this journey lighter.

To my brother, Alexandre, for his companionship, friendship, and many pieces of advice.

I deeply thank my beloved family for being my inspiration and always showing me the right way. I love them so much.

I would like to thank my advisor, Prof. Dr. José Cândido, for the moments of kind dedication, excellent advice, patience and guidance throughout the development of this work. Thank you for so many lessons shared and belief in my work.

To Unicamp, through the professors and employees, for the excellence in teaching.

To all my friends, for their loyalty, friendship, affection, and moments of relaxation.

This work was supported by the São Paulo Research Foundation (FAPESP) under Grant no. 2018/20179-9. I thank FAPESP for the financial support.

I will be forever grateful to everyone who accompanied me on this journey. I conclude the realization of this dream with the certainty that I wouldn't get this far alone.

*“Maybe I couldn’t do the best, but I fought for
the best to be done. I’m not what I should be,
but thank God, I’m not what I used to be.”
(Martin Luther King)*

Resumo

Esta tese visa avançar no campo da comunicação por canais sem fio abordando dois tópicos-chaves: (i) a simulação de processos de desvanecimento de canais sem fio generalizados e (ii) a análise assintótica de modelos de desvanecimento da classe gaussiana.

Apesar da flexibilidade matemática e ótimo ajuste aos dados empíricos, as distribuições de desvanecimento α - μ , η - μ , κ - μ e α - η - κ - μ não têm, até o momento, uma estrutura de simulação tão geral quanto os próprios modelos. De fato, a estrutura de simulação disponível é bastante limitada, aplicável apenas a valores inteiros e meio-inteiros do parâmetro real μ . Essa é uma restrição pouco realista. Na primeira parte deste trabalho, propõe-se um método de simulação unificado para os processos de desvanecimento α - μ , η - μ , κ - μ e α - η - κ - μ , que acomoda valores arbitrários de todos os parâmetros de desvanecimento. Não menos importante, o método é simples, corresponde exatamente às estatísticas de primeira ordem dos modelos de desvanecimento e se aproxima bem às estatísticas de segunda ordem. Este último requisito é especialmente complicado e, de fato, um problema antigo na simulação de desvanecimento. São deduzidas expressões analíticas para as estatísticas relevantes do método proposto. Além disso, um parâmetro de simulação crucial é otimizado para melhorar o ajuste das estatísticas de segunda ordem. Como consequência, são obtidas representações em série e expressões assintóticas úteis para estatísticas essenciais de primeira e segunda ordens dos modelos de desvanecimento investigados. Os resultados são validados por simulação de Monte Carlo.

Modelos de desvanecimento de base gaussiana consideram diferentes aspectos de propagação do canal sem fio, como correlação, não-linearidade, *clustering*, ondas espalhadas e componentes dominantes. A fim de caracterizar a natureza dinâmica dos processos aleatórios que modelam tais canais, estatísticas de segunda ordem e métricas correspondentes são frequentemente empregadas. Infelizmente, a análise exata dessas estatísticas para condições de desvanecimento generalizadas resulta em expressões intrincadas. Para contornar essa desvantagem, na segunda parte deste trabalho, é fornecida uma análise assintótica geral para estatísticas de segunda ordem em regime de alta relação sinal-ruído para uma ampla gama de canais com desvanecimento de classe gaussiana. A estrutura proposta produz expressões simples e em forma fechada, que caracterizam o impacto de cada aspecto físico do desvanecimento no canal, fornecendo assim uma descrição completa, prática e intuitiva do comportamento dinâmico do sistema. As expressões assintóticas obtidas são exaustivamente validadas, tanto reduzindo-as a casos particulares conhecidos como via simulações de Monte Carlo.

Palavras-chaves: Simulação, canais de desvanecimento, estatísticas de segunda ordem, análise assintótica.

Abstract

This thesis aims to advance the field of wireless communications by addressing two key topics: (i) simulation of generalized wireless fading channels and (ii) asymptotic analysis for a broad Gaussian class of fading models.

Despite their mathematical flexibility, great fit to empirical data, and increasing popularity, the α - μ , η - μ , κ - μ , and α - η - κ - μ fading models have to date no simulation framework as general as the models themselves. Indeed, the available simulation framework is quite limited, only applicable to integer and half-integer values of the (real-valued) μ -parameter. This is an impractical constraint. In the first part of this work, we overcome this drawback by proposing a unified simulation method for α - μ , η - μ , κ - μ , and α - η - κ - μ fading processes that accommodates full-range values of all fading parameters. Not less important, the proposed method is simple, exactly matches the fading models' first-order statistics, and well approximates their second-order statistics. This last requirement is especially tricky, by far the most challenging, and, indeed, a long-standing problem in fading simulation. We derive analytical expressions for the proposed method's relevant statistics. Also, we optimize a crucial simulation parameter to improve the match for the second-order statistics. In passing, we obtain useful series representations and asymptotic expressions for essential first- and second-order statistics for the fading models investigated. The results are fully validated via Monte Carlo simulation.

Gaussian-based fading models incorporate different propagation aspects of the wireless channel, such as correlation, non-linearity, clustering, scattered waves, and dominant components. In order to characterize the dynamic nature of random processes that model such fading channels, second-order statistics and corresponding metrics are often employed. Unfortunately, the exact analysis of these statistics for generalized fading conditions leads to intricate expressions. To overcome this drawback, in the second part of this work, we provide a general asymptotic analysis for second-order statistics at high signal-to-noise ratio regime for a broad Gaussian class of fading channels. The proposed structure leads to simple, unified, and closed-form expressions that characterize the impact of each physical aspect of fading in the channel, thus providing a complete, practical, and intuitive description of the dynamic behavior of the system. The asymptotic expressions obtained are thoroughly validated, both by reducing them to known particular cases and via Monte Carlo simulations.

Keywords: Simulation, fading channels, second-order statistics, asymptotic analysis.

List of Figures

Figure 1.1 – Illustration of LCR and AFD metrics for an arbitrary random fading signal.	26
Figure 2.1 – The classic simulation framework for α - μ , η - μ , κ - μ , and α - η - κ - μ fading.	39
Figure 2.2 – The proposed simulation framework for α - μ , η - μ , and κ - μ fading.	40
Figure 2.3 – The proposed simulation framework for α - η - κ - μ fading.	40
Figure 4.1 – LCR and AFD of the proposed α - μ , η - μ , and κ - μ simulator versus theoretical fading model's statistics in a worse-than-Rayleigh condition.	69
Figure 4.2 – LCR and AFD of the proposed α - μ , η - μ , and κ - μ simulator versus theoretical fading model's statistics in a better-than-Rayleigh condition.	70
Figure 4.3 – LCR and AFD of the proposed α - η - κ - μ simulator versus theoretical fading model's statistics.	71
Figure 4.4 – Analytical-asymptotic, simulated, and theoretical LCR and AFD for known particular cases of the Gaussian-class fading model.	73
Figure 4.5 – Analytical-asymptotic, simulated, and theoretical LCR and AFD for the commutative scenario of the Gaussian-class fading model.	74
Figure 4.6 – Analytical-asymptotic, simulated, and theoretical LCR and AFD for various in-phase-quadrature scenarios of the Gaussian-class fading model.	75
Figure A.1 – Illustrative example of the proposed simulation framework for α - μ , η - μ , and κ - μ fading.	89
Figure A.2 – Illustrative example of the proposed simulation framework for α - η - κ - μ fading.	90

List of Tables

Table 2.1 – Parameterization of fading models for the classic simulator.	39
Table 3.1 – Asymptotic LCR and AFD for particular fading models.	64

List of Acronyms

3G	Third-generation
3GPP	Third Generation Partnership Project
4G	Fourth-Generation
5G	Fifth-Generation
6G	Sixth-Generation
ACC	Autocorrelation Coefficient
ACF	Autocorrelation Function
AFD	Average Fade Duration
CDF	Cumulative Distribution Function
D2D	Device-to-Device
i.i.d.	Independent and Identically Distributed
LCR	Level Crossing Rate
LOS	Line-of-Sight
MIMO	Multiple-Input Multiple-Output
mmWave	Millimeter Wave
NB	Narrowband
PDF	Probability Density Function
RIS	Reconfigurable Intelligent Surfaces
RV	Random Variable
SNR	Signal-to-Noise Ratio
UWB	Ultra-Wideband
V2V	Vehicle-to-Vehicle

List of Symbols

\sim	asymptotically equal to around zero
$\lfloor \cdot \rfloor$	floor operation
$\lceil \cdot \rceil$	ceil operation
$\mathbf{1}$	unitary matrix
$\mathbf{0}$	null matrix
α	nonlinearity of the transmission medium factor
$a_{i,0}$	asymptotic \check{X}_i^2 coefficient
$a_{B,0}$	asymptotic B coefficient
a_n	cumulative distribution function's coefficient of the Maclaurin series
a_0	first coefficient term of the cumulative distribution function's Maclaurin series/asymptotic cumulative distribution function coefficient
B	sample of fading signal power
β	signal power in fading
$b_{i,0}$	asymptotic \check{X}_i^2 exponential
$b_{B,0}$	asymptotic B exponential
b_n	cumulative distribution function's exponential of the Maclaurin series
b_0	first exponential term of the cumulative distribution function's Maclaurin series/asymptotic cumulative distribution function exponential
\mathbf{C}	Cholesky decomposition of the covariance matrix
c_n	level crossing rate's coefficient of the Maclaurin series
c_0	first coefficient term of the level crossing rate's Maclaurin series/ asymptotic level crossing rate coefficient
\mathbf{D}	diagonal matrix
d	in-phase–quadrature imbalance of the referred derivative
$\det(\cdot)$	determinant operation
δ	placeholder parameter for α , η and κ
d_n	level crossing rate's exponential of the Maclaurin series
d_0	first exponential term of the level crossing rate's Maclaurin series/ asymptotic level crossing rate exponential
$\mathbb{E}(\cdot)$	expectation
e_0	asymptotic $h_{R_{\text{ref}}}(\cdot)$ coefficient
$\exp(\cdot)$	exponential function
${}_0\tilde{F}_1(; a; z)$	regularized hypergeometric function
${}_2\tilde{F}_1(a; b; c; x)$	regularized form of Gauss hypergeometric function
${}_2F_1(\cdot)$	hypergeometric function
${}_3F_2(\cdot)$	regularized generalized PQ hypergeometric function
f_D	maximum Doppler shift in Hz
f_0	asymptotic $h_{R_{\text{ref}}}(\cdot)$ exponential
$f_Z(\cdot)$	probability density function of a generic random variable Z
$F_Z(\cdot)$	cumulative distribution function of a generic random variable Z
$f_{Z_1, Z_2}(\cdot)$	joint probability density function of the generic random variables Z_1 and Z_2
$f_{Z_1 Z_2}(\cdot)$	conditional probability density function of the generic random variables Z_1 and Z_2

$\Gamma(\cdot)$	Gamma function
$\Gamma(\cdot, \cdot)$	upper incomplete Gamma function
$h_{R_{\text{ref}}}(\cdot)$	support function that writes R_{ref} in terms of \check{R}
$\ddot{\Psi}(\cdot)$	second time derivative of the autocorrelation function at 0
$\xi_{i,j}$	i -th line and j -th column of the inverse matrix \mathbf{R}^{-1}
\mathbf{I}	identity matrix
\mathbf{I}^c	identity complementary matrix
$I_v(\cdot)$	modified Bessel function of the first kind and arbitrary order v
κ	ratio of the total power of the dominant components to the total power of the scattered waves
\mathbf{K}	$\mathbf{D}^{-1}\mathbf{m}$ matrix
k	ratio between the dominant power and the average scattered power in the commutative scenario
k_i	ratio between the dominant power and the average scattered power of the i -th cluster
κ_x	ratio between the total power of the dominant in-phase components and the power of the in-phase scattered waves
κ_y	ratio between the total power of the quadrature dominant components and the power of the quadrature scattered waves
k_x	ratio between the dominant power and the scattered average power of the in-phase components of the in-phase and quadrature commutative scenario
k_y	ratio between the dominant power and the scattered average power of the quadrature components of the in-phase and quadrature commutative scenario
$L_n^\lambda(x)$	generalized Laguerre Polynomial
λ_x	total average value of the in-phase component
λ_{x_i}	average values of the in-phase components
λ_y	total average value of the quadrature component
λ_{y_i}	average values of the quadrature components
m	Nakagami fading parameter/inverse of normalized power variance/ mean value in the commutative scenario
\mathbf{m}	mean vector of the multivariate Gaussian
M	total integer-number of multipath clusters
m_i	mean value of the X_i component
M_x	integer number of in-phase Gaussian components
M_y	integer number of quadrature Gaussian components
m_x	in-phase mean value in the in-phase and quadrature commutative scenario
m_y	quadrature mean value in the in-phase and quadrature commutative scenario
μ	total real-number of multipath clusters
μ_L	the desired μ -parameter rounding down to the nearest integer or half-integer value
μ_U	the desired μ -parameter rounding up to the nearest integer or half-integer value
μ_x	total real-number of in-phase multipath clusters
μ_y	total real-number of quadrature multipath clusters
μ_{xL}	the desired μ_x -parameter rounding down to the nearest integer value
μ_{yL}	the desired μ_y -parameter rounding down to the nearest integer value
μ_{xU}	the desired μ_x -parameter rounding up to the nearest integer value
μ_{yU}	the desired μ_y -parameter rounding up to the nearest integer value
η	ratio of the total power of the in-phase scattered waves to the total power of the quadrature scattered waves

N	number of samples in R_{ref} -sequence
N_L	number of samples in R_L -sequence
N_U	number of samples in R_U -sequence
$N_Z(\cdot)$	level crossing rate of a generic random variable Z
p	ratio between the number of multipath clusters of the in-phase and quadrature signals
p_L	the desired p -parameter rounding down
p_{mix}	mixture probability
p_U	the desired p -parameter rounding up
q	ratio between two ratios: the first is the ratio of the powers of the dominant in-phase and quadrature components, and the second is the ratio of the scattered wave powers of the in-phase and quadrature components
$Q_v(\cdot, \cdot)$	generalized Marcum- Q function
r	signal envelope in fading
R	sample of fading signal envelope
R_I	samples drawn independently according to the desired fading parameters
ref	supporting subscript for L or U
\mathbf{R}	normalized covariance matrix
\mathbf{R}^{-1}	inverse normalized covariance matrix
R_L	reference sequence with lower parameters
R_{ref}	the output sequence of the random-mixture stage
r_{th}	any given target envelope level
R_U	reference sequence with upper parameters
\dot{R}	time derivative of R
\tilde{R}	global output sequence of the proposed simulator
\hat{r}	effective value of R
\hat{r}^α	expected value $\mathbb{E}(R^\alpha)$
\hat{r}_x^2	expected value $\mathbb{E}(X)$ /sum of the power of the in-phase multipath clusters and the power of the in-phase dominant components
\hat{r}_y^2	expected value $\mathbb{E}(Y)$ /sum of the power of the quadrature multipath clusters and the power of the quadrature dominant components
ρ	correlation coefficient in the commutative scenario / non-zero commutative cross-correlation between the in-phase and quadrature components
$\rho_{i,j}$	correlation coefficient between coefficients X_i and X_j
ρ_x	in-phase correlation coefficient in the in-phase and quadrature commutative scenario
ρ_y	quadrature correlation coefficient in the in-phase and quadrature commutative scenario
Σ	covariance matrix of the multivariate Gaussian
σ	root of the power of the scattered components in the commutative scenario
σ^2	scattered wave powers of multipath clusters
σ_i^2	X_i component variance
$\dot{\sigma}_i^2$	\dot{X}_i component variance
σ_x	root of the power of the scattered in-phase components in the in-phase and quadrature commutative scenario
σ_x^2	scattered wave powers of in-phase multipath clusters

σ_y	root of the power of the scattered quadrature components in the in-phase and quadrature commutative scenario
σ_y^2	scattered wave powers of quadrature multipath clusters
$(\cdot)^T$	transpose operation
$T_Z(\cdot)$	average fade duration of a generic random variable Z
$U(\cdot)$	confluent hypergeometric function
$\mathbb{V}(\cdot)$	variance
\mathbf{X}	multivariate Gaussian vector
\mathbf{X}_I	matrix of $M \times N$ autocorrelated X_i components
X_i	mutually independent in-phase Gaussian processes / i -th vector component of a multivariate Gaussian
\check{X}_i^2	independent random variable asymptotically equivalent to X_i^2
\dot{X}_i	time derivative of X_i
Y_i	mutually independent quadrature Gaussian processes
z	subscript that can represent the in-phase or quadrature component
Z	in-phase or quadrature component

List of Publications

Journal Papers

- V. M. Rennó, F. R. A. Parente, and J. C. S. Santos Filho, “Asymptotic Analysis of Second Order Statistics for Gaussian Class Fading Channels,” *IEEE Trans. Wireless Commun.*, 2023, submitted.
- V. M. Rennó and J. C. S. Santos Filho, “On the Generation of Autocorrelated α - μ , η - μ , and κ - μ Fading Sequences,” *IEEE Trans. Antennas Propag.*, 2022.
DOI: 10.1109/TAP.2022.3209206.

Conference Articles

- V. M. Rennó, F. R. A. Parente, and J. C. S. Santos Filho, “Análise Assintótica Unificada de Estatísticas de Segunda Ordem para Canais de Classe Gaussiana,” in *XL Simpósio Brasileiro de Telecomunicações e Processamento de Sinais (SBrT2022)*, Santa Rita do Sapucaí, Brasil, Sep. 2022.
DOI: 10.14209/sbrt.2022.1570812932.
- V. M. Rennó, and J. C. S. Santos Filho, “Um Simulador Aprimorado para Processos α - η - κ - μ ,” in *XXXIX Simpósio Brasileiro de Telecomunicações e Processamento de Sinais (SBrT2021)*, Fortaleza, Brasil, Sep. 2021. Best Paper Award.
DOI: 10.14209/sbrt.2021.1570723489.
- V. M. Rennó and J. C. S. Santos Filho, “On The Generation of Autocorrelated α - η - κ - μ Fading Sequences,” in *IEEE Statistical Signal Processing Workshop (SSP)*, Rio de Janeiro, Brasil, Jul. 2021.
DOI: 10.1109/SSP49050.2021.9513839
- V. M. Rennó and J. C. S. Santos Filho, “Um Simulador Fase-Envoltória para o Processo α - μ ,” in *XXXVIII Simpósio Brasileiro de Telecomunicações e Processamento de Sinais (SBrT2020)*, Florianópolis, Brasil, Nov. 2020.
DOI: 10.14209/SBRT.2020.1570648767.

Contents

1	Introduction	21
1.1	Statistical Fading Models	22
1.2	Fading Channel Statistics	25
1.3	Fading Channel Simulation	26
1.4	Fading Channel Analysis at High Signal-to-Noise Ratio	28
1.5	Summary of Contributions and Dissertation Outline	30
2	Advanced Simulation of Generalized Wireless Channels	32
2.1	Target Statistics	33
2.1.1	The α - μ Fading Model	33
2.1.2	The η - μ Fading Model	34
2.1.3	The κ - μ Fading Model	35
2.1.4	The α - η - κ - μ Fading Model	36
2.2	Classic Simulation Framework	38
2.3	Proposed Simulation Framework	39
2.3.1	The Random-Mixture Stage	40
2.3.2	The Rank-Matching Stage	43
2.3.3	The Output Statistics	44
2.4	Leveraging the Mixture Probabilities	45
2.4.1	Design Principle for Mixture Probabilities	45
2.4.2	Maclaurin Series for Target Statistics	46
2.4.3	Asymptotic Expressions for $h_{R_{\text{ref}}}(\cdot)$	50
2.4.4	Asymptotic Design of Mixture Probabilities	50
2.5	Conclusions	51
3	Unified Asymptotic Analysis of Generalized Wireless Channels	53
3.1	Preliminaries	54
3.1.1	Physical Model	54
3.1.2	First-Order Statistics	55
3.2	Asymptotic Second-Order Statistics	57
3.2.1	LCR and AFD at High SNR	57
3.2.2	Particular Scenarios	59
3.2.2.1	Correlated In-Phase–Quadrature Components	60
3.2.2.2	Uncorrelated In-Phase–Quadrature Components	61
3.2.2.3	Commutative Scenario	62
3.2.3	Particular Fading Models	63

3.3	Conclusions	65
4	Numerical and Simulation Results	67
4.1	Simulation Results for the Proposed Simulation Framework	67
4.2	Numerical Results for the Proposed Asymptotic Analysis	72
4.3	Conclusions	76
5	Final Words	77
5.1	Concluding Remarks	77
5.2	Future Research Directions	78
	Bibliography	80
	Appendices	88
A	Supporting Material for Chapter 2	89
A.1	Illustrative Example for the Proposed Simulator	89
B	Supporting Material for Chapter 3	91
B.1	The Determinant of R for Correlated In-Phase–Quadrature Components .	91
B.2	The Inverse of R for Correlated In-Phase–Quadrature Components	92
B.3	The Determinant of R for Uncorrelated In-Phase–Quadrature Components	93
B.4	The Inverse of R for Uncorrelated In-Phase–Quadrature Components . . .	94
C	Permission to Reproduce Copyrighted Material	95

1 Introduction

Over the years, the advance of wireless communication systems has been one of the most crucial factors in the growing revolution that has been taking place in the telecommunications world scenario. Increasingly sophisticated technologies and services have become more accessible due to lower manufacturing costs and large-scale commercialization. This improvement is mainly due to a key feature of wireless communications: mobility.

As expected by Edholm's law [1], wireless data rates have doubled every eighteen months for the last three decades. The direct consequence predicts that a link speed in the order of Terabits per second (Tbps) must be reached before 2030 [2]. Furthermore, studies indicate that billions of devices will be connected to the network [3, 4]. With this progressive demand, current wireless communication generations, as third-generation (3G), fourth-generation (4G), and even fifth-generation (5G), will not be able to support such traffic requirements. As a consequence, there are many challenges to be overcome by the next generation of wireless networks, such as the restrictions imposed by the transmission medium, the support of a massive growth in the number of connected devices, as well as a vast and diversified set of services and applications, the demand for ubiquitous and reliable coverage, capable of providing access anywhere and at anytime, and a more efficient energy consumption [5–7].

To cover the goal of high data transmission rates, standards organizations such as the Third Generation Partnership Project (3GPP) have already reported that frequency bands above 6 GHz, the so-called millimeter wave (mmWave) bands, should be used to meet these high-rate demands [8, 9]. Furthermore, enabling technologies such as non-orthogonal multiple access [10, 11], massive multiple-input multiple-output systems [12, 13], as well as futuristic technologies such as reconfigurable intelligent surfaces (RIS) [14, 15] should be considered. Therefore, aiming to meet all the requirements imposed by the new generations of wireless communication systems, academic and industrial researchers have focused their efforts on the design and development of 5G and sixth-generation (6G) wireless networks.

The communication channel is one of the components in a wireless transmission system that naturally affects the performance and requirements imposed by the future generations of wireless communication [16]. The channel is the propagation medium itself, which allows the connection between transmitter and receiver. In wireless systems, the channel is the air interface, where information travels through electromagnetic radi-

ation [17]. Along the channel, the signal can suffer considerable losses. In wireless environments, the signal is subject to reflection, diffraction, scattering, and path loss. Due to these physical phenomena, the signal reaches the mobile receiver as a large number of waves with random amplitudes and phases, coming from different paths, which is called multipath propagation [16–18].

As a result of path loss and multipath propagation, the amplitude and phase of the received signal randomly fluctuate over time. This fluctuation is known as fading. Due to the multitude of factors involved, almost always unpredictable, the modeling of the communication channel is treated in a probabilistic way. In other words, statistical models are used to describe the random fluctuations of the channel under the fading effect. Therefore, the characterization of the wireless propagation environment is done through probabilistic models, and the study of the communication channel proves essential in the creation and improvement of current and new technologies [19–22]. Moreover, despite the high spectral availability that the mmWave band offers to enable the emerging high transmission rates, the associated technical challenges are great, such as the propagation phenomena being perceived more strongly compared to lower frequency bands [23]. Overcoming these challenges requires an in-depth characterization of the communication channel.

The remainder of this chapter is structured as follows. Section 1.1 revisits many established statistical fading models and corresponding application scenarios. Section 1.2 introduces the fading channel’s most important first- and second-order statistics. Section 1.3 addresses the need for simulating fading channels in communication systems design. Section 1.4 presents the asymptotic analysis of fading channels at high signal-to-noise ratio (SNR). Finally, Section 1.5 exposes the objectives, contributions, and structure of this dissertation.

1.1 Statistical Fading Models

In a wireless communication environment, the received signal is the sum of wave components scattered by random obstructions. This interference between versions of the same transmitted signal arriving at the receiver at different times is known as short-term fading, or also as multipath fading. As a consequence, the multipath waves arrive at the receiving antenna in a combined way, forming a signal that can vary greatly in both amplitude and phase within a short period of time or distance [16]. Furthermore, the relative motion of the transmitter and the receiver, along with the motion of objects between them, results in random frequency modulation of the signal due to different Doppler shifts in each of the multipath components [17]. Thus, the fading channel has a

time-varying impulsive response.

Given the stochastic nature of the multipath fading phenomenon, probabilistic models have been proposed to describe the behavior of the wireless channel, each of which exploits certain physical aspects of the electromagnetic propagation [19–22, 24]. The accurate description of channel statistics is essential to correctly characterize the system that it interacts with.

A simple and popular statistical model for short-term fading is the Rayleigh distribution [20]. The model is described by the sum of two Gaussian random variable (RV), one in phase and another in quadrature, with zero mean and identical variances. Later, fading models such as Hoyt [25] and Rice [24] were proposed to contemplate the physical effects of unequally distributed Gaussian components. In the Hoyt distribution, the variances of the in-phase and quadrature components may have dissimilar values, and in the Rice distribution, these components may have non-zero means.

The Weibull [26] and Nakagami [27] fading models were also developed from the Rayleigh distribution. Such models consider Gaussian components with identical characteristics. In the Weibull distribution, the non-linearity of the transmission medium is considered. In the Nakagami distribution, through the m -parameter, the clustering of multipath wave signals is addressed.

Each aforementioned statistical distribution represents the isolated effect of a single physical aspect of fading, except for Rayleigh, which is a distribution with no shape parameters. Thus, to better characterize the communication channel, more flexible statistical models that combine more than one physical aspect of the propagation medium were proposed later on.

The α - μ [21], η - μ , and κ - μ [22] distributions have gained attention due to their great flexibility and are widely used to characterize the fading phenomenon. Each distribution represents the combined effect of two key aspects of short-term fading in wireless channels. Specifically, the distribution parameters account for the non-linearity of the transmission medium (α), power imbalance between the in-phase and quadrature components (η), existence of a dominant wave component (κ), and multipath wave clusterization (μ). Despite being relatively recent fading models, their usefulness has been largely proven in practice. Next we quote a few examples. In [28], Chong *et al.* showed that the α - μ distribution best fits fading measurements at 400 MHz when wireless devices are located just 1.5 cm above the surface, under the effect of wind-blown foliage or human movement. In [29], Rodrigo-Penarrocha *et al.* used the α - μ distribution in a measurement campaign for a vehicle-to-vehicle (V2V) scenario. The authors tested several fading models and concluded that the α - μ distribution provided an excellent fit to the experimental data while

being mathematically very simple to model the composite short- and long-term fading in the urban area of Valencia, Spain. In [30], Yoo *et al.* validated the use of the η - μ distribution through an indoor environment and real-time measurements, for body-centered communication channels. In [31], Bhargav *et al.* modeled the impact of background noise and co-channel interference in a body area network operating at 2.48 GHz successfully by using the κ - μ fading model. An extended version of the κ - μ fading model, namely the κ - μ shadowed model [32], was also used by Canete *et al.* in [33] to model measurements in ultrasonic underwater acoustic channels as well as body-centric and device-to-device (D2D) communications. A great number of other measurement campaigns involving the referred distributions can be found in the literature [34, 35].

Given the development of more sophisticated communication systems, even more general envelope-based fading models, namely α - η - μ and α - κ - μ [36], were created. The former combines the α - μ and η - μ distributions, and the latter, the α - μ and κ - μ distributions.

The α - η - κ - μ complex fading distribution arises from a physically-based model that encompasses the most relevant fading aspects found in the context of wireless communications [19]. It accounts for key features of short-term propagation phenomena, such as non-linearity of the medium, power of the scattered waves, power of the dominant components, and the number of multipath clusters. Due to its flexibility and, most importantly, generality, the α - η - κ - μ model is suitable to most diverse propagation conditions and comprises several short-term fading scenarios found in the literature [20–22, 24–27, 36].

As α - η - κ - μ distribution is a new and wide-ranging model, several issues still need to be explored and investigated, attracting the attention of the scientific community. For example, in [37], the authors investigated how the α - η - κ - μ fading model affects the channel capacity under different adaptive transmission policies. The authors of [38] showed that the statistics of the α - η - κ - μ distribution provide the best fit for the envelope of a signal propagating in mmWave scenarios, that is, it provides a better modeling for 5G applications. In addition, they derived second-order analytical statistics for the α - η - κ - μ fading model. The authors of [39] studied the performance of Wyner’s classic listening model, where the main channels and interceptors are modeled by the α - η - κ - μ distribution. The authors of [40] investigated the performance analysis of multi-hop wireless communication systems through the α - η - κ - μ channel. The authors of [41] developed a simulator of independent α - η - κ - μ envelope samples and analyzed the performance of the algorithm in spectral sensing application.

More recently, Parente *et al.* [42] explored a general Gaussian-class model that contemplates several other models as particular cases, from Rayleigh to α - η - κ - μ [19]. This new model makes the analysis more flexible by allowing multipath clusters to be

arbitrarily correlated. This is a realistic scenario for emerging communication systems. For example, narrowband (NB) RIS and mmWave channels have a good agreement when modeled by the well-known Rayleigh and Rice distributions [8, 13–15, 43]. However, recent experimental studies have shown that mmWave systems operating over ultra-wideband (UWB) channels can suffer a high correlation between the multipath clusters, a scenario where the assumption of independent multipath clusters is no longer realistic [8, 44].

Here we gathered some examples of fading models commonly addressed in the literature, along with related applications and research studies. Next we introduce key statistics for fading channels.

1.2 Fading Channel Statistics

Fading models are probabilistic representations that characterize the random nature of the communication channel. These distributions are represented through fading parameters that portray the physical characteristics of the propagation medium. The corresponding random variables are described by statistical functions related to the physical parameters of the model. The main functions are the probability density function (PDF) and the cumulative distribution function (CDF) [45]. These are the so-called first-order statistics, which contemplate the static behavior of the channel for any fixed instant of time. Such statistics can be used to assess system performance in terms of outage probability or bit error rate [45]. However, these metrics do not provide information about the dynamic behavior of the channel over time, mainly caused by the relative movement between transmitter and receiver, or by obstructions between them. Channel variations over time produce a random frequency modulation of the signal due to different Doppler shifts in each multipath component [17].

The dynamic, time-varying nature of a fading channel is characterized by its second- and higher-order statistics. The main second-order statistics are the level crossing rate (LCR) and the average fade duration (AFD) [46]. The LCR measures the average number of ascending (or descending) crosses per second for a given envelope level. In turn, the AFD is the average time the fading signal spends below a certain threshold level. Fig. 1.1 exemplifies these phenomena. These statistics are essential for appropriately designing key transmission parameters such as power and bandwidth allocation, symbol rate and block length selection, maximum latency requirements, and interleaving depth of error-correction codes. For addressing these issues, more than metrics that solely consider the static channel behavior, such as outage probability and bit error rate, are required.

The fading channel analysis using first- and second-order statistics is crucial to obtaining a complete evaluation of the static and dynamic effects of fading on the perfor-

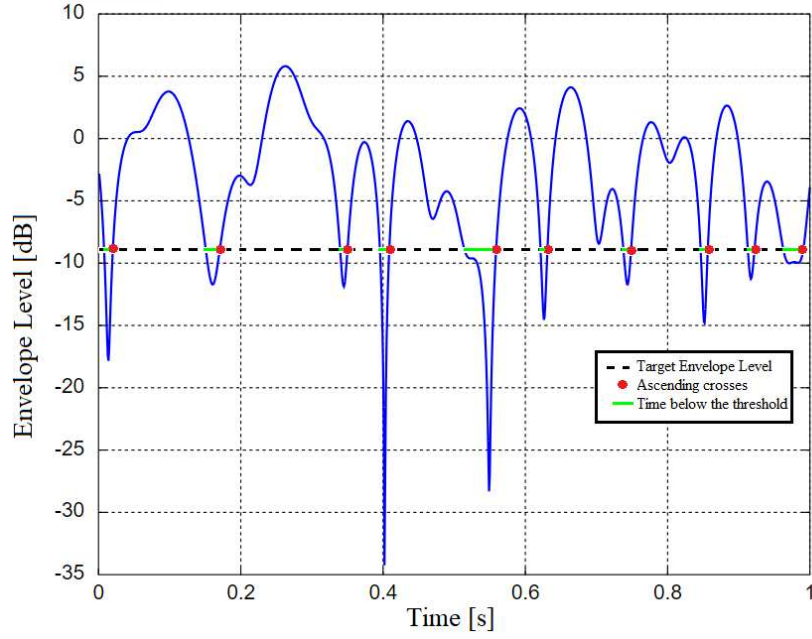


Figure 1.1 – Illustration of LCR and AFD metrics for an arbitrary random fading signal.

mance of wireless communication systems. These statistics for fading models commonly found in the literature have been extensively studied [21, 23, 35, 38, 47–50].

1.3 Fading Channel Simulation

Every modern communication system has been designed with the aid of extensive computer-based simulations. They are used to test, revise, improve, and finely tune equipment, algorithms, and techniques while helping to avoid, minimize, or complement field trials, usually much expensive and time-consuming. Analytical tools are certainly preferable, but often they either solve the problem in simplistic ways or prove impractical. In such cases, the simulation may be the only appropriate solution. A simulator allows for replicating real characteristics of an environment, usually through software. In the context described here, the simulation is used to emulate a fading environment, containing many of the propagation phenomena.

As the systems become increasingly complex with each new generation of network standards and protocols, an efficient and realistic simulation framework proves critical [51, 52]. Yet many challenges remain unchanged in wireless communications, such as the severe restrictions imposed by the transmission medium. In particular, a realistic fading simulator is needed to emulate the random, time-varying nature of the mobile radio channel. The simulator should obviously mimic the channel odds at any fixed instant of time, i.e., the channel's first-order statistics [41]. Moreover, and much more challenging, a fading simulator should also mimic how the channel variations unfold over time, i.e., the

channel's higher-order statistics [53]. These statistics affect dynamic metrics such as the average outage rate and duration.

As the statistical distributions used to describe the behavior of the wireless channel are associated with physical models (in fact, they derive from them), it is possible, in principle, to implement a simulator with direct use of these fading models. Such simulators are commonly called classic and carry the motivation of having been inspired by the physical models of each fading environment. However, sometimes the structure of classic simulators is not flexible enough to accommodate the range of parameters observed in real systems. In the α - μ , η - μ , κ - μ , α - η - μ , α - κ - μ e α - η - κ - μ fading distributions, the μ -parameter, which accounts for the number of multipath clusters, was originally proposed to be real-valued [19,21,22,36]. This relaxation of the μ -parameter proves indeed realistic, being chiefly motivated by the dramatic improvement in the models' flexibility and, above all, in their fit to empirical fading data [29,30,33,34,38]. In short, the classic simulators is limited to integer and half-integer values of the μ -parameter, too strong a constraint in practice.

In such cases, using alternative simulation schemes becomes the only solution. In [41,54–57], efficient simulators were proposed for various fading models that generate independent channel samples. Such generators are useful to meet the random process first-order requirements. However, to generate autocorrelated sequences (second-order statistics), the simulation becomes more intricate. That occurs because, except for the ultra-particular case where the fading model is Gaussian, linear filtering changes the first-order statistics of the input samples. For example, by linearly filtering a white Gamma sequence, the colored output sequence is no longer Gamma [58]. Therefore, other techniques are needed in the general non-Gaussian case.

The common method for generating an autocorrelated non-Gaussian sequence is to modify an autocorrelated Gaussian sequence by a memoryless non-linear transformation [59]. The transformation is chosen so that the target PDF is achieved and the Gaussian auto-correlation coefficient (ACC) is chosen so that the target ACC is achieved. In this method, the knowledge of the inverse function of the target CDF is essential. The inverse is needed to establish the proper non-linear transformation. However, many statistical distributions do not have their inverses CDFs in closed form. An alternative to producing an autocorrelated sequence would be to generate a set of N independent samples, via any existing methods [41,54–57], and appropriately order the samples to meet the autocorrelation function (ACF) of the desired fading model. However, there are $N!$ possible arrangements of N samples to be tested. In principle, an extensive comparison across all arrays could be used to find the ACF that best fits, but for practical applications (large N), this brute-force approach becomes computationally infeasible.

Therefore, as far as we know, there is no comprehensive simulation method for the α - μ , η - μ , κ - μ , and, more generally, α - η - κ - μ fading models that accounts for the channel's static and dynamic behaviors combined while allowing for full-range values of the fading parameters. The available schemes are quite limited [19, 21, 22]. They arise from the physical models that originated the fading statistics, written as sums of Gaussian components. There is a severe drawback, though. Of course, in the referred simulation scheme, the number of Gaussian components must be integer-valued.

It is worth noting that the problem addressed here — generating autocorrelated sequences of the fading models random processes, thereby covering the static and dynamic properties of the channels — is far more complex than the somewhat related problem of generating independent samples of the fading models random variables. The latter can be solved via traditional techniques, such as the inversion and rejection methods, including the dedicated solution provided in [41]. In these solutions, no constraints are imposed on the values of the μ -parameter. Here, we face a much deeper challenge: maintaining the no-constraints requirement for the μ -parameter value while generating a random sequence that meets the higher-order statistics of the α - μ , η - μ , κ - μ , and α - η - κ - μ fading models. In fact, this has been a long-standing open issue in Gaussian-class fading simulation.

1.4 Fading Channel Analysis at High Signal-to-Noise Ratio

New propagation scenarios are emerging with the unprecedented requirements in data rate for the next generation of wireless communications and its enabling technologies, such as massive multiple-input multiple-output (MIMO) systems [12, 13], non-orthogonal multiple access [10, 43], and RIS [14, 15]. To meet the growing demand for high data rates, these new communication scenarios can exploit the so-called mmWave bands [13]. On the one hand, there is high spectral availability for mmWave communications. On the other, there are many technical challenges associated with propagation phenomena. Therefore, to take advantage of the new resources offered by mmWave bands, it is necessary to carry out an in-depth characterization of the wireless channel [38].

While traveling from source to destination, the transmitted signal is subject to wave clustering, medium non-linearity, correlation between components, scattering, and power dominance [16]. Given the stochastic nature of the phenomenon, several probabilistic models have been proposed to describe the behavior of the wireless channel, each of which exploiting certain physical aspects of the electromagnetic propagation [19, 21, 22]. Many of the widely used models were obtained based on the assumption that the multiple wave clusters are Gaussian processes. Accordingly, they are called Gaussian-class fading models [45, 60]. Also, many fading models assume that there is independence between the

multipath clusters or between their in-phase and quadrature components [19, 21, 22].

However, recent experimental studies have shown that mmWave systems operating over UWB channels can suffer a high correlation between the multipath clusters [8, 14, 15, 44]. Even more, receiver imperfections and correlated Gaussian noise can produce non-identical Gaussian components [31, 61]. For these new propagation scenarios, the assumption of independence between different wave clusters may not be valid anymore. However, it turns out that the more fading parameters are considered in a model, the more complex becomes the performance metrics analysis, which generally does not result in closed-form expressions [19]. Furthermore, it is often hard to obtain practical intuition about how each fading parameter interferes with the analyzed metrics.

In order to consider the new challenges of emerging propagation scenarios, Parente *et al.* [42] explored a general Gaussian-class fading model that contemplates several other models as particular cases, from the simplistic Rayleigh to the multiparameter α - η - κ - μ distribution [19]. This new model makes the analysis more flexible by allowing multipath clusters to be arbitrarily correlated, a more realistic scenario for current and next generations of communication systems. Also, the framework introduced in [42] was conceived in an asymptotic fashion, circumventing the complexity of the exact approach. The analysis builds on a crucial point discussed in [62], which demonstrated that the asymptotic PDF — at the origin — of the channel determines the system performance in the regime of high SNR. More importantly, this tail regime is of most practical interest for many wireless applications, such as in (i) optical-wireless communications, where systems commonly operate at very high SNR, e.g., in the order of 70 dB [63, 64], and in (ii) radiofrequency systems, in which severe fading conditions require a high SNR value to achieve the target level of symbol error and outage probability [62].

Motivated by this, several works have studied asymptotic channel statistics in the high SNR regime. However, the analyses are restricted to specific fading scenarios (e.g., see [65–68] and references therein). Unfortunately, these efforts do not directly render comprehensive insights into how each physical aspect of fading impacts the system performance in emerging wireless channels, such as in intricate 5G and 6G networks, where machines, things, and humans mutually communicate.

In [42], in order to avoid the intricacy of the exact approach and provide comprehensive insights into the system performance, the authors went further into the high SNR regime and introduced an unified asymptotic characterization based on the referred Gaussian-class general fading model, which considers an arbitrary correlation between the multipath components. All in all, the main motivation behind that work was to provide an unified asymptotic analysis with exact closed-form solutions for the diversity and coding gains of wireless channels subject to all known physical aspects of fading,

including multipath correlation. But [42] addressed first-order statistics only. No higher-order statistics were considered. We help fill that gap in this thesis, by asymptotically analyzing the corresponding second-order statistics.

1.5 Summary of Contributions and Dissertation Outline

This dissertation comprises three main contributions:

1. Design a fading simulator for autocorrelated α - μ , η - μ , κ - μ , and α - η - κ - μ fading processes with arbitrary real values of all fading parameters;
2. Conduct an asymptotic analysis at high SNR for the second-order statistics of the general Gaussian-class fading model introduced in [42]; and
3. Validate these contributions by extensive Monte Carlo simulations for new and known wireless propagation scenarios.

To achieve these goals, in Chapter 2 we design and analyze a general and unified simulation method for α - μ , η - μ , κ - μ , and α - η - κ - μ fading channels that embraces arbitrary real values of the μ -parameter. Not less important, the proposed method matches the exact first-order statistics of the fading models and closely approaches their second-order statistics. Our method relies on a cascade of two simulation techniques: random mixture [69] and rank matching [70]. This combination has proven effective for Nakagami- m fading, a very special case of the α - μ , η - μ , κ - μ , and α - η - κ - μ models [53]. Here, we extend and refine the idea far beyond, by showing that and how a cascade of random mixture and rank matching can be adapted to offer an improved, general, and unified simulation framework for the α - μ , η - μ , κ - μ , and α - η - κ - μ fading models. To our knowledge, there is no other simulation method in the literature that meets these requirements for the referred fading models. In addition, we develop a new simple approach for optimizing the random-mixture stage and, as a byproduct, we derive new series representations and asymptotic coefficients for essential first- and second-order statistics of the fading models analyzed here. These representations and coefficients constitute a valuable original contribution of this work, which can be used elsewhere in the analysis and design of communication systems over fading channels.

In Chapter 3, we investigate the time-varying nature of Gaussian random processes and propose an asymptotic analysis for the dynamic metrics of a general class of fading models [42]. More specifically, we provide new, simple, closed-form expressions for fundamental second-order statistics in high SNR regime, namely, LCR and AFD. The framework includes several Gaussian-class fading distributions as particular cases, which

considers the correlation between the multipath components as an additional parameter. Our analytical results are extensively validated, by reducing them to known particular cases, such as fading channels commonly reported in the literature [19], as well as to various correlation scenarios for the in-phase and quadrature components.

In Chapter 4, we provide several numerical and simulation results that illustrate the behavior of the proposed simulator in Chapter 2 and the derived asymptotic analysis for second-order statistics in Chapter 3. Different fading scenarios characterized by wireless fading channel distributions are addressed, such as α - μ , η - μ , κ - μ , α - η - κ - μ , and the general Gaussian class fading model from [42].

Chapter 5 concludes this work with final considerations. Possible future works for the continuity of this research are also presented.

2 Advanced Simulation of Generalized Wireless Channels

The α - μ , η - μ , κ - μ , and α - η - κ - μ fading models have mathematical flexibility, great fit to empirical data, and increasing popularity. However, they have to date no simulation framework as general as the models themselves. Indeed, the available simulation framework is quite limited, only applicable to integer and half-integer values of the real-valued μ -parameter. In this chapter, we overcome this drawback by proposing a unified simulation method for the α - μ , η - μ , and κ - μ fading processes and a general simulation framework for α - η - κ - μ fading model that accommodate full-range values of all fading parameters. Not less important, the proposed methods are simple, exactly match the fading models' first-order statistics, and well approximate their second-order statistics. This latter requirement is especially tricky, by far the most challenging, and, indeed, a long-standing problem in fading simulation. We derive analytical expressions for relevant statistics of the proposed simulation methods. Also, we optimize a crucial simulation parameter to improve the match for the second-order statistics. In passing, we obtain useful series representations and asymptotic expressions for essential first- and second-order statistics of the fading models investigated.

The rest of this chapter is organized as follows. In Section 2.1, the α - μ , η - μ , κ - μ , and α - η - κ - μ fading models are revisited, along with their main statistics. In Section 2.2, the traditional simulation framework for these models, called classic method, is also revisited. The proposed simulation frameworks are detailed and statistically analyzed in Section 2.3. The optimization of a key simulation parameter is done in Section 2.4, as well as the required derivation of asymptotic expressions for the fading models' target statistics. Finally, Section 2.5 presents some conclusions. Numerical results are postponed to Chapter 4.

This chapter contains research findings presented in the following articles:

- V. M. Rennó and J. C. S. Santos Filho, "On the Generation of Autocorrelated α - μ , η - μ , and κ - μ Fading Sequences," *IEEE Trans. Antennas Propag.*, 2022.
DOI: 10.1109/TAP.2022.3209206.
- V. M. Rennó and J. C. S. Santos Filho, "On The Generation of Autocorrelated α - η - κ - μ Fading Sequences," in *IEEE Statistical Signal Processing Workshop (SSP)*, Rio de Janeiro, Brasil, Jul. 2021.
DOI: 10.1109/SSP49050.2021.9513839

- V. M. Rennó and J. C. S. Santos Filho, “Um Simulador Aprimorado para Processos α - η - κ - μ ,” in *XXXIX Simpósio Brasileiro de Telecomunicações e Processamento de Sinais (SBrT2021)*, Fortaleza, Brasil, Sep. 2021. Best Paper Award.

DOI: 10.14209/sbrt.2021.1570723489.

2.1 Target Statistics

In this section, for completeness, we reproduce essential first- and second-order statistics of the α - μ , η - μ , κ - μ , and α - η - κ - μ fading models. Later, we will rely on these statistics to design, analyze, and finely tune our simulation framework.

2.1.1 The α - μ Fading Model

The α - μ distribution is a general model of short-term fading, originally proposed in [21]. Its statistical behavior encompasses the non-linearity of the wireless transmission medium and the clusterization of multipath radio waves. This non-linearity is represented by a power α -parameter, so that the channel envelope arises as the α -th root of the sum of squares of 2μ multipath wave components [21]:

$$R = \sqrt[\alpha]{\sum_{i=1}^{\mu} X_i^2 + \sum_{i=1}^{\mu} Y_i^2}, \quad (2.1)$$

where X_i and Y_i are zero-mean, independent and identically distributed (i.i.d.) Gaussian variates, $\mathbb{E}(X_i^2) = \mathbb{E}(Y_i^2) = \hat{r}^\alpha/2\mu$, and $\mathbb{E}(\cdot)$ denotes expectation.

From (2.1), the PDF of the α - μ envelope is found as [21]

$$f_R(r) = \frac{\alpha\mu^\mu r^{\alpha\mu-1}}{\hat{r}^{\alpha\mu}\Gamma(\mu)} \exp\left(\frac{-\mu r^\alpha}{\hat{r}^\alpha}\right), \quad (2.2)$$

where $r \geq 0$, $\alpha > 0$, $\mu = \mathbb{E}^2(R^\alpha)/\mathbb{V}(R^\alpha) > 0$, $\hat{r} = \sqrt[\alpha]{\mathbb{E}(R^\alpha)}$, $\Gamma(\cdot)$ is the gamma function [71], and $\mathbb{V}(\cdot)$ denotes variance. The corresponding CDF is obtained as [21]

$$F_R(r) = 1 - \frac{\Gamma\left(\mu, \mu \frac{r^\alpha}{\hat{r}^\alpha}\right)}{\Gamma(\mu)}, \quad (2.3)$$

where $\Gamma(\cdot, \cdot)$ is the upper incomplete gamma function [71].

The time-varying dynamics of a fading channel can be characterized by second-order statistics. Here we focus on two of these statistics: LCR and AFD. In particular, and following a standard practice, we consider isotropic scattering and omnidirectional reception, for which the LCR and AFD of the α - μ fading channel are given respectively by [21]

$$N_R(r) = \frac{\sqrt{2\pi} f_D \mu^{(\mu-\frac{1}{2})} r^{\alpha(\mu-\frac{1}{2})}}{\Gamma(\mu) \hat{r}^{\alpha(\mu-\frac{1}{2})} \exp\left(\mu \frac{r^\alpha}{\hat{r}^\alpha}\right)} \quad (2.4)$$

$$T_R(r) = \frac{\Gamma(\mu, \mu \frac{r^\alpha}{\hat{r}^\alpha}) \exp\left(\mu \frac{r^\alpha}{\hat{r}^\alpha}\right) \hat{r}^{\alpha(\mu-\frac{1}{2})}}{\sqrt{2\pi} f_D \mu^{(\mu-\frac{1}{2})} r^{\alpha(\mu-\frac{1}{2})}}, \quad (2.5)$$

where f_D is the maximum Doppler shift in Hz.

2.1.2 The η - μ Fading Model

The η - μ distribution is a general model that represents the short-term variations of the fading signal in a non-line-of-sight (LOS) condition [22]. It is written in terms of two key parameters, namely η and μ , and may appear in two different formats. The μ -parameter is related to the number of multipath wave clusters, whereas the η -parameter is related to the power ratio (Format 1) or correlation (Format 2) between the in-phase and quadrature wave components. The envelope of the η - μ fading signal can be written as [22]

$$R = \sqrt{\sum_{i=1}^{2\mu} X_i^2 + \sum_{i=1}^{2\mu} Y_i^2}, \quad (2.6)$$

where X_i and Y_i are zero-mean Gaussian variates. In Format 1, X_i and Y_i are mutually independent, $\mathbb{E}(X_i^2) = \eta \hat{r} / (\mu(\eta+1))$, and $\mathbb{E}(Y_i^2) = \hat{r} / (\mu(\eta+1))$ [19], the power ratio being $\eta = \mathbb{E}(X_i^2) / \mathbb{E}(Y_i^2) > 0$. In Format 2, X_i and Y_i are mutually correlated and have identical variances, the correlation coefficient being $\eta = \mathbb{E}(X_i Y_i) / \mathbb{E}(X_i^2) = \mathbb{E}(X_i Y_i) / \mathbb{E}(Y_i^2)$, $-1 < \eta < 1$. For convenience, in [22] the η -parameter was used in both formats and, based on it, two auxiliary parameters were defined, namely h and H . In each format, these parameters assume a different meaning and a different range of values. In Format 1, $h = (2 + \eta^{-1} + \eta) / 4$ and $H = (\eta^{-1} - \eta) / 4$; in Format 2, $h = 1 / (1 - \eta^2)$ and $H = \eta / (1 - \eta^2)$. These formats can be obtained from one another via the bilinear transformation $\eta_1 = (1 - \eta_2) / (1 + \eta_2)$, where η_1 denotes the η -parameter in Format 1 and η_2 denotes the η -parameter in Format 2.

From (2.6), the η - μ envelope PDF is given by [22]

$$f_R(r) = \frac{4\sqrt{\pi} \mu^{\mu+\frac{1}{2}} h^\mu}{\Gamma(\mu) H^{\mu-\frac{1}{2}} \hat{r}} \left(\frac{r}{\hat{r}}\right)^{2\mu} \exp\left(-2\mu h \left(\frac{r}{\hat{r}}\right)^2\right) \times I_{\mu-\frac{1}{2}}\left[2\mu H \left(\frac{r}{\hat{r}}\right)^2\right], \quad (2.7)$$

where $r \geq 0$, $\mu = [\mathbb{E}^2(R^2) / (2\mathbb{V}(R^2))] \times [1 + (H/h)^2] > 0$, $\hat{r} = \sqrt{\mathbb{E}(R^2)}$, and $I_v[\cdot]$ is the modified Bessel function of the first kind and order v [71]. The CDF of the η - μ envelope is [22]

$$F_R(r) = 1 - Y_\mu\left[\frac{H}{h}, \sqrt{2\mu h} \frac{r}{\hat{r}}\right], \quad (2.8)$$

where

$$Y_v(\lambda, \beta) \triangleq \frac{2^{-v+\frac{3}{2}} \sqrt{\pi} (1 - \lambda^2)^v}{\Gamma(v) \lambda^{v-\frac{1}{2}}} \int_\beta^\infty x^{2v} \exp(-x^2) I_{v-\frac{1}{2}}[\lambda x^2] dx. \quad (2.9)$$

In [48], the LCR and AFD of the η - μ fading channel were derived for Format 1 only. This is also the format we cover in this work. As already detailed, one format can be

converted into another. For isotropic scattering and omnidirectional reception, the LCR of η - μ fading is obtained as [48]

$$N_R(r) = \frac{f_D \sqrt{\pi} ((1 + \eta)\mu)^{2\mu - \frac{1}{2}}}{2^{2\mu - 2} \eta^\mu \Gamma^2(\mu)} \left(\frac{r}{\hat{r}}\right)^{4\mu - 1} \int_0^{\pi/2} (\sin(2\theta))^{2\mu - 1} \sqrt{1 + \eta - (1 - \eta) \cos(2\theta)} \times \exp\left(\frac{-\mu((1 + \eta)^2 + (1 - \eta)^2 \cos(2\theta))}{2\eta}\right) \left(\frac{r}{\hat{r}}\right)^2 d\theta, \quad (2.10)$$

and the AFD is obtained from its general representation as

$$T_R(r) = \frac{F_R(r)}{N_R(r)}, \quad (2.11)$$

in which $F_R(\cdot)$ is given by (2.8), and $N_R(\cdot)$, by (2.10).

2.1.3 The κ - μ Fading Model

For a LOS condition, the short-term variations of the fading signal can be modeled by the κ - μ distribution [22]. Its statistical behavior is governed by the parameters κ and μ . The former describes the ratio of the total power of the dominant components to the total power of the scattered waves, and the latter is related to the number of multipath clusters. In this fading model, all scattered waves have identical powers, but in each cluster there is an arbitrary dominant component. Accordingly, the κ - μ fading envelope can be described as [22]

$$R = \sqrt{\sum_{i=1}^{\mu} (X_i + \lambda_{x_i})^2 + \sum_{i=1}^{\mu} (Y_i + \lambda_{y_i})^2}, \quad (2.12)$$

where X_i and Y_i are zero-mean i.i.d. Gaussian variates, with $\mathbb{E}(X_i^2) = \mathbb{E}(Y_i^2) = \hat{r}/(2\mu(\kappa + 1))$ [19]. The parameters λ_{x_i} and λ_{y_i} are respectively the mean values of the in-phase and quadrature components of the i -th multipath cluster. By letting $\lambda_x^2 \triangleq \sum_{i=1}^{\mu} \lambda_{x_i}^2$ and $\lambda_y^2 \triangleq \sum_{i=1}^{\mu} \lambda_{y_i}^2$, and by the meaning of the κ -parameter, we have $\lambda_x^2 + \lambda_y^2 = \kappa \hat{r}/(\kappa + 1)$ [19, 22].

From (2.12), the κ - μ envelope PDF is given as [22]

$$f_R(r) = \frac{2\mu(1 + \kappa)^{\frac{\mu+1}{2}}}{\kappa^{\frac{\mu-1}{2}} \exp(\mu\kappa)\hat{r}} \left(\frac{r}{\hat{r}}\right)^{\mu} \exp\left(-\mu(1 + \kappa) \left(\frac{r}{\hat{r}}\right)^2\right) I_{\mu-1} \left[2\mu\sqrt{\kappa(1 + \kappa)} \frac{r}{\hat{r}}\right], \quad (2.13)$$

where $r \geq 0$, $\kappa > 0$, $\mu = [\mathbb{E}^2(R^2)/\mathbb{V}(R^2)] \times [(1 + 2\kappa)/(1 + \kappa)^2] > 0$ and $\hat{r} = \sqrt{\mathbb{E}(R^2)}$. The corresponding CDF is obtained as [22]

$$F_R(r) = 1 - Q_{\mu} \left[\sqrt{2\kappa\mu}, \sqrt{2\mu(1 + \kappa)} \frac{r}{\hat{r}} \right], \quad (2.14)$$

where $Q_v[\cdot, \cdot]$ is the generalized Marcum- Q function [72].

The LCR and AFD of the κ - μ fading channel were derived in [49] for the isotropic scenario, respectively, as

$$N_R(r) = \frac{\sqrt{2\pi\mu}f_D(1+\kappa)^{\frac{\mu}{2}}}{\kappa^{\frac{\mu-1}{2}}\exp(\mu\kappa)\hat{r}} \left(\frac{r}{\hat{r}}\right)^{\mu} \exp\left(-\mu(1+\kappa)\left(\frac{r}{\hat{r}}\right)^2\right) I_{\mu-1}\left[2\mu\sqrt{\kappa(1+\kappa)}\frac{r}{\hat{r}}\right] \quad (2.15)$$

$$T_R(r) = \frac{1 - Q_{\mu}\left[\sqrt{2\kappa\mu}, \sqrt{2\mu(1+\kappa)}\frac{r}{\hat{r}}\right]}{\sqrt{2\pi\mu}f_D(1+\kappa)^{\frac{\mu}{2}} \left(\frac{r}{\hat{r}}\right)^{\mu} \exp\left(-\mu(1+\kappa)\left(\frac{r}{\hat{r}}\right)^2\right) I_{\mu-1}\left[2\mu\sqrt{\kappa(1+\kappa)}\frac{r}{\hat{r}}\right]} \frac{\kappa^{\frac{\mu-1}{2}}\exp(\mu\kappa)}{1}. \quad (2.16)$$

2.1.4 The α - η - κ - μ Fading Model

The α - η - κ - μ envelope R can be written as [19, Eq. (9)]

$$R^{\alpha} = \sum_{i=1}^{\mu_x} (X_i + \lambda_{x_i})^2 + \sum_{i=1}^{\mu_y} (Y_i + \lambda_{y_i})^2, \quad (2.17)$$

where $\alpha > 0$ represents the nonlinearity of the transmission medium; $\{X_i\}_{i=1}^{\mu_x}$ and $\{Y_i\}_{i=1}^{\mu_y}$ are zero-mean, mutually independent Gaussian processes with variances σ_x^2 and σ_y^2 , respectively; λ_{x_i} and λ_{y_i} are respectively the mean values of the in-phase and quadrature components of the i -th multipath cluster; and μ_x and μ_y are respectively the number of multipath clusters for the in-phase and quadrature components. Then, the first- and higher-order statistics of R can be obtained in terms of in-phase parameters (μ_x , σ_x , and λ_x) and quadrature parameters (μ_y , σ_y , and λ_y). This is the so-called *Raw Parameterization* [19].

It is sometimes convenient to write the first- and higher-order statistics of R in terms of physical parameters found elsewhere in the literature. For instance, the following parameters, in which Z denotes either X or Y conveniently described in terms of in-phase and quadrature signals, can be used: $\kappa_z > 0$, defined as the ratio of the total power of the dominant components to the total power of scattered waves, i.e., $\kappa_z = \lambda_z^2/(\mu_z\sigma_z^2)$; and $\hat{r}_z^2 > 0$, defined as the mean value $\mathbb{E}(Z)$, given as a function of the power of the multipath clusters and the power of the dominant components, i.e., $\hat{r}_z^2 = \mu_z\sigma_z^2 + \lambda_z^2$. This is the so-called *Local Parameterization* [19]. Note that the α - η - κ - μ envelope R to the power of α (i.e., R^{α}) can be written as the sum of two κ - μ powers with parameters $(\kappa_x, \mu_x/2, \hat{r}_x)$ and $(\kappa_y, \mu_y/2, \hat{r}_y)$.

Additionally, the first- and higher-order statistics of R can be represented in terms of the so-called *Global Parameterization* [19]. In this case, the following parameters are used: (i) $\alpha > 0$ denotes the nonlinearity of the transmission medium; (ii) $\eta > 0$, defined as the ratio of the total power of the in-phase scattered waves to the total power of the quadrature scattered waves, i.e., $\eta = \mu_x\sigma_x^2/(\mu_y\sigma_y^2)$; (iii) $\kappa > 0$, defined as the ratio

of the total power of the dominant components to the total power of the scattered waves, i.e., $\kappa = (\lambda_x^2 + \lambda_y^2)/(\mu_x\sigma_x^2 + \mu_y\sigma_y^2)$; (iv) $\mu > 0$, defined as the total number of multipath clusters, i.e., $\mu = (\mu_x + \mu_y)/2$; (v) $q > 0$, defined as the ratio of two ratios, namely the ratio of the power of the dominant components to the power of the scattered waves of the in-phase signal and its counterpart for the quadrature signal, i.e., $q = \lambda_x^2\mu_y\sigma_y^2/(\lambda_y^2\mu_x\sigma_x^2)$; (vi) $p > 0$, defined as the ratio between the number of multipath clusters of the in-phase and quadrature signals, i.e., $p = \mu_x/\mu_y$; and (vii) $\hat{r} > 0$, defined as $\sqrt[p]{\mathbb{E}(R^\alpha)}$, i.e., $\hat{r}^\alpha = \mu_x\sigma_x^2 + \lambda_x^2 + \mu_y\sigma_y^2 + \lambda_y^2$.

In [19], the α - η - κ - μ first-order statistics, that is, its PDF and CDF, were introduced. Later on, in [73], new efficient representations were provided for these statistics. In particular, to the analysis that follows, we shall use a series representation of the α - η - κ - μ PDF, obtained as [73]

$$f_R(r) = \frac{\alpha(\xi\mu)^\mu}{\exp\left(\frac{(1+pq)\kappa\mu}{\delta}\right)} \left(\frac{p}{\eta}\right)^{\frac{p\mu}{1+p}} \frac{r^{\alpha\mu-1}}{\hat{r}^{\alpha\mu}} \exp\left(-\frac{r^\alpha p \xi \mu}{\hat{r}^\alpha \eta}\right) \sum_{n=0}^{\infty} \left(\frac{r^\alpha \xi \mu (p-\eta)}{\hat{r}^\alpha \eta}\right)^n \times \quad (2.18)$$

$$L_n^{\frac{\mu}{1+p}-1}\left(\frac{\eta\kappa\mu}{\delta(\eta-p)}\right) {}_0\tilde{F}_1\left(; \mu+n; \frac{p^2 q r^\alpha \kappa \xi \mu^2}{\hat{r}^\alpha \delta \eta}\right),$$

where $r \geq 0$, $\xi = (1+\eta)(1+\kappa)/(1+p)$, $\delta = (1+q\eta)(1+p)/(1+\eta)$, ${}_0\tilde{F}_1(; a; z)$ is the regularized hypergeometric function [71], and $L_n^\lambda(x)$ is the generalized Laguerre Polynomial [71, Eq. (22.3.9)]. Likewise, the α - η - κ - μ CDF is obtained as [73]

$$F_R(r) = \exp\left(-\frac{\kappa\mu}{\delta}\right) \left(\frac{\eta}{p}\right)^{\frac{\mu}{1+p}} \sum_{n=0}^{\infty} \left(1 - \frac{\eta}{p}\right)^n L_n^{\frac{\mu}{1+p}-1}\left(\frac{\eta\kappa\mu}{\delta(\eta-p)}\right) \times \quad (2.19)$$

$$\left(1 - Q_{n+\mu}\left(\sqrt{\frac{2pq\kappa\mu}{\delta}}, \left(\frac{r}{\hat{r}}\right)^{\frac{\alpha}{2}} \sqrt{\frac{2p\xi\mu}{\eta}}\right)\right).$$

In [38], key second-order statistics, including the LCR and AFD, were obtained for α - η - κ - μ fading. Alternative formulas were presented in [50], including a series representation we shall use for the LCR, given as

$$N_R(r) = \frac{2d\sqrt{-\ddot{\Psi}(0)}(\xi\mu)^{\mu-\frac{1}{2}}}{\sqrt{\pi}(1+d)\exp\left(\frac{(1+pq)\kappa\mu}{\delta}\right)} \left(\frac{\eta}{p}\right)^{\frac{1}{2}-\frac{p\mu}{1+p}} \frac{r^{\alpha(\mu-\frac{1}{2})}}{\hat{r}^{\alpha(\mu-\frac{1}{2})}} \exp\left(-\frac{\xi\mu p r^\alpha}{\eta\hat{r}^\alpha}\right) \sum_{n=0}^{\infty} \sum_{j=0}^{\infty} \frac{1}{j!} \left(\frac{p^2 q \kappa \xi \mu^2 r^\alpha}{\eta \delta \hat{r}^\alpha}\right)^j \times$$

$$\left(\frac{(p-\eta)\xi\mu r^\alpha}{\eta\hat{r}^\alpha}\right)^n L_n^{\frac{\mu}{1+p}-1}\left(-\frac{\eta\kappa\mu}{\delta(p-\eta)}\right) {}_2\tilde{F}_1\left(-\frac{1}{2}, n + \frac{\mu}{1+p}; j+n+\mu; 1 - \frac{p}{d^2\eta}\right), \quad (2.20)$$

where ${}_2\tilde{F}_1(a; b; c; x)$ is the regularized form of Gauss's hypergeometric function [71, Eq. (15.1.1)], $\ddot{\Psi}(\cdot)$ is the second time derivative of the autocorrelation function, and d denotes the in-phase-quadrature imbalance of the referred derivative, as detailed in [50]. Consequently, $2(-\ddot{\Psi}(0))^{1/2} = (-\ddot{\Psi}_x(0))^{1/2} + (-\ddot{\Psi}_y(0))^{1/2}$ and $d = (-\ddot{\Psi}_x(0))^{1/2}/(-\ddot{\Psi}_y(0))^{1/2}$.

Here we consider the isotropic scenario, for which $\ddot{\Psi}_Z(0) = -2\pi^2 f_Z^2$, where f_Z is the maximum Doppler shift, and Z can be X or Y for in-phase and quadrature components, respectively. Finally, the α - η - κ - μ AFD is obtained from its general representation as in (2.11), where $F_R(r)$ and $N_R(r)$ are given by (2.19) and (2.20), respectively.

As mentioned, the α - η - κ - μ distribution includes most other fading models as special cases, as detailed in [19, Section VI].

2.2 Classic Simulation Framework

The classic framework for generating random sequences that fulfill the first- and higher-order statistics of the α - μ , η - μ , κ - μ , and α - η - κ - μ fading channels is to mirror their physical models based on Gaussian components, as in (2.1), (2.6), (2.12), and (2.17), respectively [19, 21, 22]. The Gaussian sequences are individually generated using any established technique and are then combined as in the models [74]. This simulation framework is shown in Fig. 2.1, which can be specialized for each of the fading models covered here, as detailed in Table 2.1.

However, since the number of Gaussian input components is obviously discrete, the classic simulation framework only applies to integer and half-integer values of the μ -parameter. This is a severe limitation in practice. The real-valued nature of the μ -parameter is largely responsible for the great flexibility of the α - μ , η - μ , κ - μ , and α - η - κ - μ distributions and for their notable fit to empirical fading data. For example, non-integer values of the μ -parameter are known to occur if there exists (i) a nonzero correlation between the clusters of multipath waves, (ii) a nonzero correlation between the in-phase and quadrature components, or (iii) any degree of non-Gaussianity in these components. Moreover, electromagnetic scattering is known to occur continuously throughout surfaces, and not at discrete points. Indeed, non-integer numbers of multipath clusters have been detected empirically and extensively reported in the literature [28–31, 33–35, 38].

Let us briefly review the big picture. The physical models of α - μ , η - μ , κ - μ , and α - η - κ - μ fading in (2.1), (2.6), (2.12), and (2.17) can be used (as they have been) as a simulation framework, but this approach only holds for integer and half-integer values of the μ -parameter. In contrast, those physical models give rise to first- and second-order statistics, namely (2.2)–(2.5), (2.7)–(2.11), (2.13)–(2.16), and (2.18)–(2.20), that have no constraints to be used (as they have been) for arbitrary real values of the μ -parameter and, most importantly, only if so used they fully shine when applied to practical wireless channels. Next, we provide a simulation framework that addresses this need.

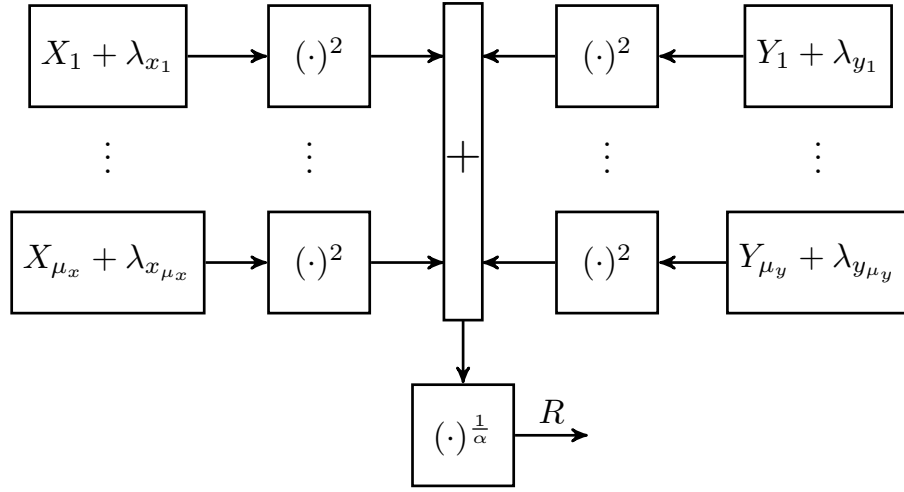
Figure 2.1 – The classic simulation framework for α - μ , η - μ , κ - μ , and α - η - κ - μ fading.

Table 2.1 – Parameterization of fading models for the classic simulator.

Fading Models	α	λ_{x_i}	λ_{y_i}	μ_x	μ_y	$\mathbb{E}(X_i)$	$\mathbb{E}(Y_i)$	$\mathbb{E}(X_i^2)$	$\mathbb{E}(Y_i^2)$
α - μ	α	0	0	μ	μ	0	0	$\frac{\hat{r}^\alpha}{2\mu}$	$\frac{\hat{r}^\alpha}{2\mu}$
η - μ	2	0	0	2μ	2μ	0	0	$\frac{\eta \hat{r}^2}{(\mu(\eta+1))}$	$\frac{\eta \hat{r}^2}{(\mu(\eta+1))}$
κ - μ	2	λ_{x_i}	λ_{y_i}	μ	μ	0	0	$\frac{\hat{r}^2}{(2\mu(\kappa+1))}$	$\frac{\hat{r}^2}{(2\mu(\kappa+1))}$
α - η - κ - μ	α	λ_{x_i}	λ_{y_i}	μ_x	μ_y	0	0	$\frac{\eta(p+1)\hat{r}^\alpha}{(2\mu p(\eta+1)(\kappa+1))}$	$\frac{(p+1)\hat{r}^\alpha}{(2\mu(\eta+1)(\kappa+1))}$

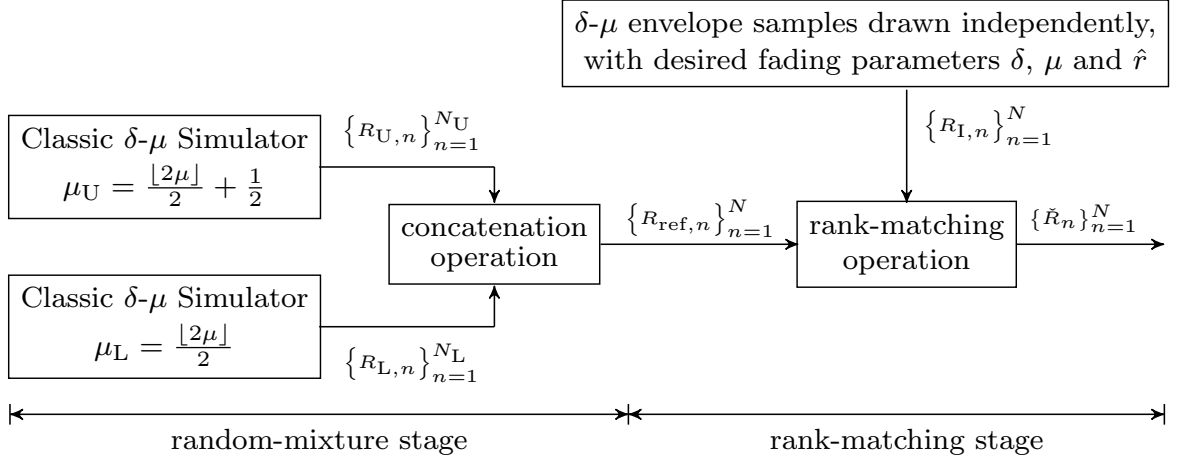
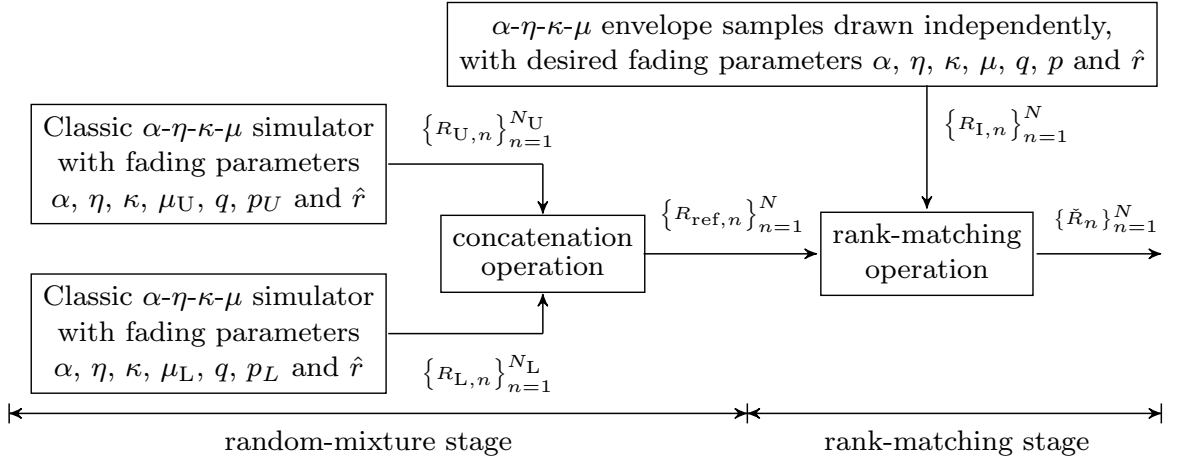
2.3 Proposed Simulation Framework

In this section, we propose a general and unified simulation framework for α - μ , η - μ , and κ - μ fading channels, illustrated in Fig. 2.2. We also propose a more general simulation scheme for the α - η - κ - μ fading model, illustrated in Fig. 2.3.

The proposed simulation methods share the same principle, being a cascade of two simulation techniques: *random mixture* [69] and *rank matching* [70]. This kind of approach was introduced in [53] for the Nakagami- m channel, a particular case of the α - μ , η - μ , κ - μ , and α - η - κ - μ fading scenarios. Our proposal, in both cases, not only adequately reproduces the first- and second-order statistics of these fading processes, but also removes a critical limitation of the classic simulation method by accommodating arbitrary real values of the μ -parameter. As far as we know, there is to date no simulation scheme for the referred fading models with all those features combined.

A block diagram of the proposed simulation framework is depicted in Fig. 2.2, for the α - μ , η - μ , and κ - μ fading channels, and in Fig. 2.3, for the α - η - κ - μ fading channel. These simulation schemes will be described and analyzed in the following sections.

Here, for a unified treatment of the α - μ , η - μ , and κ - μ (Fig. 2.2) scenarios, let δ be a placeholder parameter, with $\delta = \alpha$ for α - μ fading, $\delta = \eta$ for η - μ fading, or

Figure 2.2 – The proposed simulation framework for α - μ , η - μ , and κ - μ fading.Figure 2.3 – The proposed simulation framework for α - η - κ - μ fading.

$\delta = \kappa$ for κ - μ fading. Accordingly, from now on, we will refer to a δ - μ channel, in which δ denotes α , η , or κ , depending on the channel model at hand. Therefore, let δ , μ , and \hat{r} be the desired fading parameters of an N -sample δ - μ sequence to be generated. For the α - η - κ - μ scenario (Fig. 2.3), α , η , κ , μ , q , p , and \hat{r} are the desired fading parameters of the N -sample α - η - κ - μ sequence to be generated.

2.3.1 The Random-Mixture Stage

In this section, the random-mixture stage of the simulation schemes presented in Fig. 2.2 and Fig. 2.3 will be discussed separately. In Sections 2.3.2 and 2.3.3, the rank-matching stage and output statistics will be treated in a unified way. The difference between the simulation schemes in the random-mixture stage (cf. Fig. 2.2 and Fig. 2.3) occurs because the α - η - κ - μ fading model allows for different numbers of multipath clusters for the in-phase and quadrature components, through the parameter p , as explained and analyzed below.

For the case represented in Fig. 2.2, where the goal is to generate an α - μ , η - μ , or κ - μ fading sequence, first, in the random-mixture stage, two δ - μ reference sequences are generated using the classic method described in Section 2.2. As required in that method, these reference sequences are generated by combining (an integer number of) Gaussian components. More precisely, one reference sequence (say, R_L , with “L” standing for “lower”) is specified by rounding the desired μ -parameter down to the nearest integer or half-integer value, i.e.,

$$\mu_L = \frac{\lfloor 2\mu \rfloor}{2}, \quad (2.21)$$

where $\lfloor \cdot \rfloor$ denotes floor. In a similar vein, the other reference sequence (say, R_U , with “U” standing for “upper”) is specified by rounding the μ -parameter up to the nearest integer or half-integer value, i.e.,

$$\mu_U = \frac{\lfloor 2\mu \rfloor}{2} + \frac{1}{2}. \quad (2.22)$$

For example, if the desired fading parameter is $\mu = 1.6$, then $\mu_L = 1.5$ and $\mu_U = 2$, that is, $\mu_L \leq \mu < \mu_U$. In short, one δ - μ reference sequence R_L is generated with fading parameters δ , μ_L , and \hat{r} , and another δ - μ reference sequence R_U is generated with fading parameters δ , μ_U , and \hat{r} . Recall that δ is in fact α , η , or κ , depending on the fading model considered.

For the case represented in Fig. 2.3, in the random-mixture stage, two α - η - κ - μ reference sequences are generated separately through the classic method, also described in Section 2.2. As required by that method, these reference sequences must comprise an integer number of Gaussian components. To this end, from the desired values of μ and p , the corresponding desired values of μ_x and μ_y are calculated using the relationships between the Global and Raw parameterizations. Recall that, in general, μ , p , μ_x , and μ_y are all real-valued. Then, one reference sequence (R_L) is specified by rounding μ_x and μ_y down to the nearest integers, i.e., $\mu_{xL} = \lfloor \mu_x \rfloor$ in-phase components and $\mu_{yL} = \lfloor \mu_y \rfloor$ quadrature components. In a similar way, the other reference sequence (R_U) is specified by rounding μ_x and μ_y up to the nearest integers, i.e., $\mu_{xU} = \lceil \mu_x \rceil$ in-phase components and $\mu_{yU} = \lceil \mu_y \rceil$ quadrature components, where $\lceil \cdot \rceil$ denotes the ceiling operation. For these sequences, the μ and p values must be adapted accordingly, since they are the only global parameters solely given in terms of μ_x and μ_y . So, the R_L -sequence has parameters

$$\mu_L = \frac{\mu_{xL} + \mu_{yL}}{2} \quad (2.23)$$

and

$$p_L = \frac{\mu_{xL}}{\mu_{yL}}, \quad (2.24)$$

and the R_U -sequence has parameters

$$\mu_U = \frac{\mu_{xU} + \mu_{yU}}{2} \quad (2.25)$$

and

$$p_U = \frac{\mu_{xU}}{\mu_{yU}}. \quad (2.26)$$

All in all, one α - η - κ - μ reference sequence R_L is generated with fading parameters α , η , κ , μ_L , q , p_L , and \hat{r} , and another α - η - κ - μ reference sequence R_U is generated with fading parameters α , η , κ , μ_U , q , p_U , and \hat{r} . Note that both sequences bear an integer number of multipath clusters for the in-phase and quadrature components. In particular, when $\mu_{xL} = 0$, R_L specializes to an α - κ - μ sequence with parameters α , κ_y , $\mu_{yL}/2$, and $\hat{r}_y^{2/\alpha}$. Similarly, when $\mu_{yL} = 0$, it specializes to an α - κ - μ sequence with parameters α , κ_x , $\mu_{xL}/2$, and $\hat{r}_x^{2/\alpha}$. The parameters κ_x , κ_y , \hat{r}_x , and \hat{r}_y are those referring to the Local parameterization, described in Section 2.1.4.

The output sequence of the random-mixture stage in both situations described above (say, R_{ref}) can now be formed, by concatenating the reference sequences R_L and R_U , in any order. Of course, for R_{ref} to contain N samples, the lengths of R_L (say, N_L) and R_U (say, N_U) must satisfy $N_L + N_U = N$. Let $N_L = \text{round}(p_{\text{mix}}N)$ and $N_U = N - N_L$, where $0 \leq p_{\text{mix}} \leq 1$. Indeed, p_{mix} and $1 - p_{\text{mix}}$ are key simulation parameters, called mixture probabilities. They govern the relative frequency of samples from R_L and R_U that form R_{ref} . As a result, any statistics of R_{ref} can be written as a weighted sum of the corresponding statistics of R_L and R_U . The weights are given by the respective mixture probabilities, p_{mix} and $1 - p_{\text{mix}}$.

A central task in the random-mixture stage is to design suitable mixture probabilities that render a good approximation to whatever statistics of interest. In [69], for instance, this task was addressed for independent Nakagami- m samples using a moment-based approach, yielding

$$p_{\text{mix}} = \frac{2\mu_L(\mu_U - \mu)}{\mu}. \quad (2.27)$$

The scenario here is quite different, requiring a complete redesign of the mixture probabilities as detailed in Section 2.4.

As desired, the random-mixture stage allows for arbitrary real values of all fading parameters, including the μ -parameter.

A remark is in order. Even though the δ - μ channels are particular cases of the α - η - κ - μ channel, it is more efficient to simulate δ - μ channels using their dedicated scheme in Fig. 2.2 than by specializing the α - η - κ - μ scheme in Fig. 2.3, as follows. Considering a δ - μ fading channel in the scheme shown in Fig. 2.3 and $\mu < 1$, we have $\mu_{xL} = \mu_{yL} = 0$ and $\mu_{xU} = \mu_{yU} = 1$. This results in $\mu_L = 0$ and $\mu_U = 1$, where the output of the random-mixture stage will be the R_U sequence alone, with $\mu_U = 1$. On the other hand, when using the dedicated method given in Fig. 2.2, if $0.5 \leq \mu < 1$, we have $\mu_L = 0.5$ and $\mu_U = 1$, where the output sequence of the random-mixture stage is formed by both R_L and R_U

sequences. Moreover, when $\mu < 0.5$ in Fig. 2.2, we have $\mu_L = 0$ and $\mu_U = 0.5$, so the output of the random-mixture stage will be the R_U sequence alone with $\mu_U = 0.5$. Note that $\mu_U = 0.5$ is closer to the range under consideration for the desired μ -parameter than if we use the scheme in Fig. 2.3, where $\mu_U = 1$ for the same range of μ -values. The point here is that the finer tuning of μ_L and μ_U causes the dedicated method in Fig. 2.2 to better fit the δ - μ second-order statistics than the general method in Fig. 2.3.

2.3.2 The Rank-Matching Stage

The output of the random-mixture stage provides the input to the rank-matching stage [70]. In this second stage, for both simulators described in Fig. 2.2 and Fig. 2.3, a global output δ - μ or α - η - κ - μ sequence (say, \check{R}) is obtained from the reference sequence R_{ref} , coming from the random-mixture stage, and from a set of N δ - μ or α - η - κ - μ samples (say, R_I) drawn independently according to the desired fading parameters δ , μ , and \hat{r} , or α , η , κ , μ , q , p , and \hat{r} (e.g., via the rejection method in [41]). The global output sequence \check{R} is a mere rearrangement of the samples in R_I , in a way that the samples in \check{R} exactly match the ranking of the samples in the reference sequence R_{ref} , that is, their minima occur in the same position, their second minima occur in the same position, and so on. This operation is called rank matching [70]. It can be implemented in Matlab as follows:

$$\begin{aligned} [R_{\text{ref}}, \text{index}] &= \text{sort}(R_{\text{ref}}); \\ R_I &= \text{sort}(R_I); \\ R_I(\text{index}) &= R_I; \\ \check{R} &= R_I. \end{aligned}$$

Notice how the random-mixture and rank-matching stages are interconnected. Due to the random-mixture stage, R_{ref} follows either a α - μ , η - μ , κ - μ or α - η - κ - μ process with fading parameters conditioned to $\text{ref} = L$, with probability p_{mix} , or a α - μ , η - μ , κ - μ or α - η - κ - μ process with fading parameters conditioned to $\text{ref} = U$, with probability $1 - p_{\text{mix}}$. Due to the rank-matching stage, whatever the value of p_{mix} , the global output sequence \check{R} satisfies the exact first-order statistics of the fading models with the desired fading parameters, since \check{R} is just a reordering of the samples in R_I [70]. However, p_{mix} affects \check{R} 's second- and higher-order statistics. Next, we analyze \check{R} 's second-order statistics in a unified way for the α - μ , η - μ , κ - μ , and α - η - κ - μ fading models as a function of p_{mix} . Then, in Section 2.4, we optimize p_{mix} to render \check{R} a good fit to the exact second-order statistics for the fading models discussed here.

As desired, the proposed cascade of random-mixture and rank-matching stages

allows for full-range values of all α - μ , η - μ , κ - μ , and α - η - κ - μ fading parameters. (See Appendix A for an illustrative example of the proposed simulation scheme.)

2.3.3 The Output Statistics

In [58], it was demonstrated that the generation of \check{R} from R_{ref} and R_I via the rank-matching operation is asymptotically equivalent to the generation of \check{R} , from R_{ref} alone, via the traditional inversion method, as the length N goes to infinity. Therefore, considering this asymptotic scenario (in practice, N is desirably very large), the output \check{R} of the proposed simulator can be written in terms of the reference R_{ref} as

$$\check{R} = F_R^{-1} (F_{R_{\text{ref}}} (R_{\text{ref}})), \quad (2.28)$$

where $F_{R_{\text{ref}}}(\cdot)$ is the CDF of the δ - μ envelope, with parameters δ , μ_{ref} and \hat{r} , when the simulator presented in Fig. 2.2 is considered, or the CDF of the α - η - κ - μ envelope with parameters α , η , κ , μ_{ref} , q , p_{ref} , and \hat{r} , when the simulator shown in Fig. 2.3 is considered. Furthermore, $F_R^{-1}(\cdot)$ is the inverse CDF of the fading models with desired parameters, i.e., δ , μ and \hat{r} for the δ - μ envelope, and α , η , κ , μ , q , p , and \hat{r} for the α - η - κ - μ envelope. (Recall that, conditioned on $\text{ref} = \text{L}$ or $\text{ref} = \text{U}$, the reference sequence R_{ref} produced by the random-mixture stage is a δ - μ or α - η - κ - μ process with fading parameters δ , μ_{ref} , and \hat{r} or α , η , κ , μ_{ref} , q , p_{ref} , and \hat{r} , respectively.) The CDF of the α - μ , η - μ , κ - μ , and α - η - κ - μ fading models are given by (2.3), (2.8), (2.14), and (2.19), respectively, and the inverse CDF can be calculated numerically using any standard mathematical software.

In the analysis that follows, instead of (2.28), it is more convenient to use its inverse relationship, in which R_{ref} is written in terms of \check{R} , i.e.,

$$R_{\text{ref}} = F_{R_{\text{ref}}}^{-1} (F_R(\check{R})) \triangleq h_{R_{\text{ref}}}(\check{R}), \quad (2.29)$$

where $F_R(\cdot)$ is the CDF of the δ - μ or α - η - κ - μ envelope with the desired parameters and $F_{R_{\text{ref}}}^{-1}(\cdot)$ is the inverse CDF of the δ - μ or α - η - κ - μ envelope with parameters from the random-mixture stage, conditioned to $\text{ref} = \text{L}$ or $\text{ref} = \text{U}$.

Now, based on (2.29), we are able to derive any statistics of \check{R} in terms of the corresponding statistics of R_{ref} . For example, \check{R} 's LCR and AFD are directly obtained as

$$N_{\check{R}}(r) = N_{R_{\text{ref}}}(h_{R_{\text{ref}}}(r)) \quad (2.30)$$

$$T_{\check{R}}(r) = T_{R_{\text{ref}}}(h_{R_{\text{ref}}}(r)), \quad (2.31)$$

where $N_{R_{\text{ref}}}(\cdot)$ and $T_{R_{\text{ref}}}(\cdot)$ are the target LCR and AFD of the fading model at hand, given by (2.4) and (2.5) for the α - μ channel ($\delta = \alpha$), (2.10) and (2.11) for the η - μ channel ($\delta = \eta$), (2.15) and (2.16) for the κ - μ channel ($\delta = \kappa$), and (2.20) and (2.11) for the

α - η - κ - μ channel, with parameters conditioned to $\text{ref} = \text{L}$ or $\text{ref} = \text{U}$. Furthermore, $h_{R_{\text{ref}}}$ is given by the definition in (2.29).

In the proposed simulator, as already discussed, the rank-matching stage is preceded by a random-mixture stage. Then, in fact, the global statistics are provided as a weighted sum of individual statistics when $\text{ref} = \text{L}$ and $\text{ref} = \text{U}$, the weights being given by the mixture probabilities p_{mix} and $1 - p_{\text{mix}}$, respectively. Combining this with (2.30) and (2.31), we finally obtain the output LCR and AFD of the proposed simulators as

$$N_{\tilde{R}}(r) = p_{\text{mix}}N_{R_{\text{L}}}(h_{R_{\text{L}}}(r)) + (1 - p_{\text{mix}})N_{R_{\text{U}}}(h_{R_{\text{U}}}(r)) \quad (2.32)$$

$$T_{\tilde{R}}(r) = p_{\text{mix}}T_{R_{\text{L}}}(h_{R_{\text{L}}}(r)) + (1 - p_{\text{mix}})T_{R_{\text{U}}}(h_{R_{\text{U}}}(r)). \quad (2.33)$$

2.4 Leveraging the Mixture Probabilities

In this section, we design p_{mix} to render the proposed simulation framework an optimum fit to the theoretical second-order statistics of the α - μ , η - μ , κ - μ , and α - η - κ - μ fading models.

2.4.1 Design Principle for Mixture Probabilities

From (2.32) and (2.33), it can be noticed that the mixture probability p_{mix} directly affects the second-order statistics of the proposed simulator. As a term of comparison, the mixture probability in (2.27) has been originally designed in the context of random mixture alone [69], aiming to render a good fit to the Nakagami- m PDF. But in our scheme, due to the rank-matching stage, the α - μ , η - μ , κ - μ , and α - η - κ - μ PDFs are exactly attained by construction, regardless of the mixture probabilities used in the random-mixture stage. Therefore, we can now tune these probabilities to optimize the match for the second-order statistics, namely, LCR and AFD, as follows.

An appropriate value of p_{mix} can be selected to match the exact LCR or AFD at any given target envelope level (say, r_{th}). This is achieved by solving (2.32) or (2.33) for p_{mix} , yielding

$$p_{\text{mix}} = \frac{N_R(r_{\text{th}}) - N_{R_{\text{U}}}(h_{R_{\text{U}}}(r_{\text{th}}))}{N_{R_{\text{L}}}(h_{R_{\text{L}}}(r_{\text{th}})) - N_{R_{\text{U}}}(h_{R_{\text{U}}}(r_{\text{th}}))} \quad \text{or} \quad (2.34)$$

$$p_{\text{mix}} = \frac{T_R(r_{\text{th}}) - T_{R_{\text{U}}}(h_{R_{\text{U}}}(r_{\text{th}}))}{T_{R_{\text{L}}}(h_{R_{\text{L}}}(r_{\text{th}})) - T_{R_{\text{U}}}(h_{R_{\text{U}}}(r_{\text{th}}))}, \quad (2.35)$$

where $N_R(\cdot)$ and $T_R(\cdot)$ are the LCRs and AFDs of the investigated fading models with the desired fading parameters, given by (2.4) and (2.5) for the α - μ channel, (2.10) and (2.11) for the η - μ channel, (2.15) and (2.16) for the κ - μ channel, and (2.20) and (2.11) for the α - η - κ - μ channel. Moreover, $N_{R_{\text{ref}}}(\cdot)$ and $T_{R_{\text{ref}}}(\cdot)$ are LCR and AFD of the models in terms

of the fading parameters from the random-mixture stage, conditioned to $\text{ref} = \text{L}$ and $\text{ref} = \text{U}$.

In principle, one can plug into (2.34) or (2.35) any target envelope level r_{th} for which the exact LCR or AFD should be satisfied. To gain insight into a suitable choice of r_{th} , we tried initially the mixture probability as in (2.27). Even for that value of p_{mix} , not tailored to our purpose, we observed that the overall match for the LCR and AFD is very good. We also observed that this match is slightly worse at low envelope levels. More importantly, it is often at very low signal levels that system outages occur in practice. Therefore, a good choice for r_{th} is a low envelope level that best fits the outage requirements of the application at hand and the sensitivity of the receiver in operation.

There is a hidden drawback in (2.34) and (2.35). These expressions require the numerical evaluation of $h_{R_{\text{ref}}}(\cdot)$, defined in (2.29) in terms of the CDF and inverse CDF for each fading model, and the numerical evaluation of LCR and AFD for each fading model, using the theoretical statistics presented in Section 2.1. Alternatively, in what follows, we derive simple approximate design expressions for p_{mix} by building on the assumption that $r_{\text{th}} \ll 1$, as suitable in practice. The idea is to replace in (2.34) and (2.35) the exact expressions of $h_{R_{\text{ref}}}(\cdot)$, $N_R(\cdot)$ and $T_R(\cdot)$ by their asymptotic representations as $r_{\text{th}} \rightarrow 0$. Eventually, in Section 2.4.4, we obtain highly accurate, closed-form design expressions for p_{mix} . But first, in Sections 2.4.2 and 2.4.3, we derive the required asymptotic representations. In fact, we derive complete Maclaurin series representations for key first- and second-order statistics of the α - μ , η - μ , and κ - μ fading models [75]. Then, by dropping the terms beyond the first, we obtain the desired asymptotic expressions. For the α - η - κ - μ fading model, we obtain the asymptotic expressions from the series representations given in (2.19) and (2.20).

It is noteworthy that the Maclaurin series representations alone, derived here as byproducts, turn out to be valuable original contributions of this work. These representations can be readily used elsewhere for the analysis and design of various digital communication systems operating over fading channels.

2.4.2 Maclaurin Series for Target Statistics

In this section we obtain the Maclaurin series representations for the CDF, LCR, and AFD of the α - μ , η - μ , and κ - μ fading models. As explained, these representations shall be used in Section 2.4.4 to obtain a simple asymptotic design of the mixture probability p_{mix} . To our best knowledge, the Maclaurin series representations presented here are new [75]. Throughout the text, “ \sim ” means “asymptotically equal to around zero,” i.e., $f(x) \sim g(x) \iff \lim_{x \rightarrow 0} f(x)/g(x) = 1$.

Assume that the CDF of R has a Maclaurin series representation, written as

$$F_R(r) = \sum_{n=0}^{\infty} a_n r^{b_n} \sim a_0 r^{b_0}, \quad (2.36)$$

where b_n is a monotonically increasing function with respect to n and the coefficients a_n and b_n depend on the fading model considered.

Proposition 1. *The Maclaurin series coefficients a_n and b_n for the CDF of the α - μ , η - μ , and κ - μ fading models are respectively given by*

$$a_n = \frac{(-1)^n \mu^{\mu+n}}{(n+\mu)n!\Gamma(\mu)\hat{r}^{\alpha(\mu+n)}} \quad (2.37a)$$

$$b_n = \alpha(\mu+n) \quad (2.37b)$$

$$a_n = \frac{2^{n+2\mu}(-h)^n h^\mu}{(n+2\mu)\Gamma(1+n)\Gamma(2\mu)} \left(\frac{\mu}{\hat{r}^2}\right)^{n+2\mu} {}_2F_1\left(\frac{1-n}{2}, \frac{-n}{2}; \mu + \frac{1}{2}; \frac{H^2}{h^2}\right) \quad (2.38a)$$

$$b_n = 2(2\mu+n) \quad (2.38b)$$

$$a_n = \frac{\mu(\kappa+1)^{\frac{\mu+1}{2}}}{\kappa^{\frac{\mu-1}{2}} \exp(\mu\kappa)\hat{r}^{\mu+1}(n+\mu)} \left(\frac{\mu}{\hat{r}} \sqrt{\kappa(\kappa+1)}\right)^{2n+\mu-1} \frac{U(-n, \mu, \kappa\mu)(\kappa\mu)^{-n}}{\Gamma(1+n)\Gamma(n+\mu)} \quad (2.39a)$$

$$b_n = 2(\mu+n), \quad (2.39b)$$

where ${}_2F_1(\cdot)$ is the hypergeometric function and $U(\cdot)$ is the confluent hypergeometric function [71].

Proof. The Maclaurin series for the PDF of the α - μ , η - μ , and κ - μ fading models were provided in [76]. The Maclaurin series for the corresponding CDF can be readily obtained by integrating the PDF series term by term. ■

Now, assume that the LCR of R also has a Maclaurin series representation, written as

$$N_R(r) = \sum_{n=0}^{\infty} c_n r^{d_n} \sim c_0 r^{d_0}, \quad (2.40)$$

where d_n is a monotonically increasing function with respect to n and the coefficients c_n and d_n depend on the fading model considered.

Proposition 2. *The Maclaurin series coefficients c_n and d_n for the LCR of the α - μ , η - μ , and κ - μ fading models are respectively given by*

$$c_n = \frac{(-1)^n \sqrt{2\pi} f_D \mu^{\mu+n-0.5}}{n!\Gamma(\mu)\hat{r}^{\alpha(\mu+n-0.5)}} \quad (2.41a)$$

$$d_n = \alpha(\mu+n-0.5) \quad (2.41b)$$

$$c_n = \frac{f_D \pi^{3/2} ((1+\eta)\mu)^{2\mu-1/2} (-1)^n \mu^n}{\Gamma(\mu) \eta^{n+\mu} \hat{r}^{2(n+2\mu)-1}} \left[\sum_{m=0}^n \frac{(1+\eta)^{2(n-m)-1/2} (1-\eta^2)^m}{(n-m)! 2^{n+m+2+2\mu}} \right. \\ \left. \left(\frac{4(1+(-1)^m)(1+\eta)}{\Gamma(1+\frac{m}{2})} {}_3F_2 \left(\left\{ \frac{-1}{4}, \frac{1}{4}, \frac{1+m}{2} \right\}, \left\{ \frac{1}{2}, \frac{1+m}{2} + \mu \right\}; \frac{(-1+\eta)^2}{(1+\eta)^2} \right) - \right. \right. \\ \left. \left. \frac{(-1+(-1)^m)(-1+\eta)}{\Gamma(\frac{1+m}{2})} {}_3F_2 \left(\left\{ \frac{1}{4}, \frac{3}{4}, \frac{2+m}{2} \right\}, \left\{ \frac{3}{2}, \frac{m}{2} + \mu + 1 \right\}; \frac{(-1+\eta)^2}{(1+\eta)^2} \right) \right) \right] \quad (2.42a)$$

$$d_n = 2(n+2\mu) - 1 \quad (2.42b)$$

$$c_n = \frac{\sqrt{2\pi\mu} f_D (\kappa+1)^{\frac{\mu}{2}}}{\kappa^{\frac{\mu-1}{2}} \exp(\mu\kappa) \hat{r}^{\mu+1}} \left(\frac{\mu}{\hat{r}} \sqrt{\kappa(\kappa+1)} \right)^{2n+\mu-1} \frac{U(-n, \mu, \kappa\mu) (\kappa\mu)^{-n}}{\Gamma(1+n) \Gamma(n+\mu)} \quad (2.43a)$$

$$d_n = 2(\mu+n) - 1, \quad (2.43b)$$

where ${}_3F_2(\cdot)$ is the regularized generalized PQ hypergeometric function [71].

Proof. By considering the Maclaurin series of the exponential function [77] into the α - μ LCR in (2.4), we eventually obtain

$$N_R(r) = \sum_{n=0}^{\infty} \frac{(-1)^n \sqrt{2\pi} f_D \mu^{\mu+n-0.5}}{n! \Gamma(\mu) \hat{r}^{\alpha(\mu+n-0.5)}} r^{\alpha(\mu+n-0.5)}. \quad (2.44)$$

From (2.44), the coefficients of the Maclaurin series for the α - μ LCR are directly given as in (2.41).

For the η - μ fading model, we start with a transformation of variables in the integrand of (2.10), obtaining

$$N_R(r) = \frac{f_D \sqrt{\pi} ((1+\eta)\mu)^{2\mu-\frac{1}{2}}}{2^{2\mu-2} \eta^\mu \Gamma^2(\mu)} \left(\frac{r}{\hat{r}} \right)^{4\mu-1} \times \\ \int_{-1}^1 \frac{1}{2} (1-x^2)^{\mu-1} \sqrt{1+\eta-(1-\eta)x} \exp \left(\frac{-\mu(1+\eta)^2 r^2}{2\eta \hat{r}^2} \right) \exp \left(\frac{-\mu(1-\eta^2) r^2 x}{2\eta \hat{r}^2} \right) dx. \quad (2.45)$$

By replacing the rightmost exponential function in the integrand of (2.45) with its Maclaurin series and solving the integral, we obtain

$$N_R(r) = \frac{f_D \pi^{3/2} ((1+\eta)\mu)^{2\mu-\frac{1}{2}}}{\sqrt{1+\eta} \Gamma(\mu)} \left(\frac{r}{\hat{r}} \right)^{4\mu-1} \exp \left(\frac{-\mu(1+\eta)^2 r^2}{2\eta \hat{r}^2} \right) \sum_{m=0}^{\infty} \frac{(-1)^m (1-\eta^2)^m \mu^m r^{2m}}{2^{2(1+m+\mu)} \eta^{m+\mu} \hat{r}^{2m}} \times \\ \left(\frac{4(1+(-1)^m)(1+\eta)}{\Gamma(1+\frac{m}{2})} {}_3F_2 \left(\left\{ \frac{-1}{4}, \frac{1}{4}, \frac{1+m}{2} \right\}, \left\{ \frac{1}{2}, \frac{1+m}{2} + \mu \right\}; \frac{(-1+\eta)^2}{(1+\eta)^2} \right) - \right. \\ \left. \frac{(-1+(-1)^m)(-1+\eta)}{\Gamma(\frac{1+m}{2})} {}_3F_2 \left(\left\{ \frac{1}{4}, \frac{3}{4}, \frac{2+m}{2} \right\}, \left\{ \frac{3}{2}, \frac{m}{2} + \mu + 1 \right\}; \frac{(-1+\eta)^2}{(1+\eta)^2} \right) \right). \quad (2.46)$$

Following a similar procedure, we substitute the remaining exponential function in (2.46) by its Maclaurin series, which leads to

$$N_R(r) = \frac{f_D \pi^{3/2} ((1+\eta)\mu)^{2\mu-\frac{1}{2}}}{\sqrt{1+\eta}\Gamma(\mu)} \left(\frac{r}{\hat{r}}\right)^{4\mu-1} \sum_{k=0}^{\infty} \frac{1}{k!} \left(\frac{-\mu(1+\eta)^2 r^2}{2\eta \hat{r}^2}\right)^k \sum_{m=0}^{\infty} \frac{(-1)^m (1-\eta^2)^m \mu^m r^{2m}}{2^{2(1+m+\mu)} \eta^{m+\mu} \hat{r}^{2m}} \times \\ \left(\frac{4(1+(-1)^m)(1+\eta)}{\Gamma(1+\frac{m}{2})} {}_3F_2 \left(\left\{ \frac{-1}{4}, \frac{1}{4}, \frac{1+m}{2} \right\}, \left\{ \frac{1}{2}, \frac{1+m}{2} + \mu \right\}; \frac{(-1+\eta)^2}{(1+\eta)^2} \right) - \right. \\ \left. \frac{(-1+(-1)^m)(-1+\eta)}{\Gamma(\frac{1+m}{2})} {}_3F_2 \left(\left\{ \frac{1}{4}, \frac{3}{4}, \frac{2+m}{2} \right\}, \left\{ \frac{3}{2}, \frac{m}{2} + \mu + 1 \right\}; \frac{(-1+\eta)^2}{(1+\eta)^2} \right) \right). \quad (2.47)$$

Finally, by grouping terms with identical exponents (r being the basis), after algebraic manipulations we obtain

$$N_R(r) = \sum_{n=0}^{\infty} \frac{f_D \pi^{3/2} ((1+\eta)\mu)^{2\mu-1/2} (-1)^n \mu^n}{\Gamma(\mu) \eta^{n+\mu} \hat{r}^{2(n+2\mu)-1}} \left[\sum_{m=0}^n \frac{(1+\eta)^{2(n-m)-1/2} (1-\eta^2)^m}{(n-m)! 2^{n+m+2+2\mu}} \times \right. \\ \left(\frac{4(1+(-1)^m)(1+\eta)}{\Gamma(1+\frac{m}{2})} {}_3F_2 \left(\left\{ \frac{-1}{4}, \frac{1}{4}, \frac{1+m}{2} \right\}, \left\{ \frac{1}{2}, \frac{1+m}{2} + \mu \right\}; \frac{(-1+\eta)^2}{(1+\eta)^2} \right) - \right. \\ \left. \frac{(-1+(-1)^m)(-1+\eta)}{\Gamma(\frac{1+m}{2})} {}_3F_2 \left(\left\{ \frac{1}{4}, \frac{3}{4}, \frac{2+m}{2} \right\}, \left\{ \frac{3}{2}, \frac{m}{2} + \mu + 1 \right\}; \frac{(-1+\eta)^2}{(1+\eta)^2} \right) \right] \times r^{2(n+2\mu)-1}, \quad (2.48)$$

from which the Maclaurin series coefficients for the η - μ LCR are promptly formulated as in (2.42).

For the κ - μ fading model, once again we replace the exponential function and the modified Bessel function of first kind and $(\mu-1)$ -th order in (2.15) by their Maclaurin series representations given in [77], which yields

$$N_R(r) = \frac{\sqrt{2\pi\mu} f_D (1+\kappa)^{\frac{\mu}{2}}}{\kappa^{\frac{\mu-1}{2}} \exp(\mu\kappa) \hat{r}} \left(\frac{r}{\hat{r}}\right)^{\mu} \sum_{k=0}^{\infty} \frac{1}{k!} \left(\frac{-\mu(1+\kappa)r^2}{\hat{r}^2}\right)^k \times \\ \sum_{m=0}^{\infty} \frac{1}{m! \Gamma(m+\mu)} \left(\frac{\mu \sqrt{\kappa(1+\kappa)} r}{\hat{r}}\right)^{2m+\mu-1}. \quad (2.49)$$

By grouping terms with identical exponents, we obtain

$$N_R(r) = \sum_{n=0}^{\infty} \frac{\sqrt{2\pi\mu} f_D (1+\kappa)^{\frac{\mu}{2}}}{\kappa^{\frac{\mu-1}{2}} \exp(\mu\kappa) \hat{r}^{\mu+1}} \left(\frac{\mu \sqrt{\kappa(1+\kappa)} r}{\hat{r}}\right)^{2n+\mu-1} \times \\ \sum_{k=0}^n \frac{1}{k! (n-k)! \Gamma(n-k+\mu)} \left(\frac{-\mu(1+\kappa)}{\hat{r}^2}\right)^k \left(\frac{\mu \sqrt{\kappa(1+\kappa)} r}{\hat{r}}\right)^{-2k} \quad (2.50)$$

Then, after algebraic manipulations, the series reduces to

$$N_R(r) = \sum_{n=0}^{\infty} \frac{\sqrt{2\pi\mu} f_D (\kappa+1)^{\frac{\mu}{2}}}{\kappa^{\frac{\mu-1}{2}} \exp(\mu\kappa) \hat{r}^{\mu+1}} \left(\frac{\mu}{\hat{r}} \sqrt{\kappa(\kappa+1)}\right)^{2n+\mu-1} \frac{U(-n, \mu, \kappa\mu) (\kappa\mu)^{-n}}{\Gamma(1+n) \Gamma(n+\mu)} \times r^{2(\mu+n)-1}, \quad (2.51)$$

where the Maclaurin series coefficients for the κ - μ LCR become apparent as in (2.43). ■

Finally, for the AFD, we can directly use its representation in terms of the CDF and LCR:

$$T_R(r) = \frac{F_R(r)}{N_R(r)} = \frac{\sum_{n=0}^{\infty} a_n r^{b_n}}{\sum_{n=0}^{\infty} c_n r^{d_n}} \sim \frac{a_0}{c_0} r^{b_0-d_0}, \quad (2.52)$$

where a_n , b_n , c_n , and d_n are the CDF and LCR coefficients provided in Propositions 1 and 2.

2.4.3 Asymptotic Expressions for $h_{R_{\text{ref}}}(\cdot)$

Now, we obtain an asymptotic expression, as $r \rightarrow 0$, for the auxiliary function $h_{R_{\text{ref}}}(\cdot)$ also required in (2.34) and (2.35).

As defined in (2.29), $h_{R_{\text{ref}}}(\cdot)$ depends on the envelope CDF and its inverse function. For $r \rightarrow 0$, $h_{R_{\text{ref}}}(\cdot)$ can be asymptotically expressed as

$$h_{R_{\text{ref}}}(r) \sim e_0 r^{f_0}, \quad (2.53)$$

where e_0 and f_0 can be shown to depend exclusively on the asymptotic CDF coefficients, namely, a_0 and b_0 , provided in Proposition 1 with $n = 0$, for the α - μ , η - μ , and κ - μ channels. For the α - η - κ - μ fading model, one finds a_0 and b_0 keeping only the first term, with $n = 0$, in (2.19). After algebraic manipulations, e_0 for the α - μ , η - μ , κ - μ , and α - η - κ - μ fading models are respectively obtained as

$$e_0 = \left(\frac{\hat{r}^{\alpha(\mu_{\text{ref}} - \mu)} \mu^{\mu-1} \Gamma(\mu_{\text{ref}})}{\mu_{\text{ref}}^{\mu_{\text{ref}}-1} \Gamma(\mu)} \right)^{\frac{1}{\alpha\mu_{\text{ref}}}} \quad (2.54)$$

$$e_0 = \left(\frac{4^{\mu-\mu_{\text{ref}}} \mu_{\text{ref}}^{1-2\mu_{\text{ref}}} \Gamma(2\mu_{\text{ref}}) h^{\mu-\mu_{\text{ref}}}}{\mu^{1-2\mu} \hat{r}^{4\mu-4\mu_{\text{ref}}} \Gamma(2\mu)} \right)^{\frac{1}{4\mu_{\text{ref}}}} \quad (2.55)$$

$$e_0 = \left(\frac{\exp(\kappa(\mu_{\text{ref}} - \mu)) \Gamma(\mu_{\text{ref}}) (\kappa + 1)^{\mu-\mu_{\text{ref}}}}{\mu^{1-\mu} \mu_{\text{ref}}^{\mu_{\text{ref}}-1} \Gamma(\mu) \hat{r}^{2(\mu-\mu_{\text{ref}})}} \right)^{\frac{1}{2\mu_{\text{ref}}}} \quad (2.56)$$

$$e_0 = \left(\frac{\exp\left(\frac{(1+p_{\text{ref}}q)\kappa\mu_{\text{ref}}}{\delta_{\text{ref}}}\right) \hat{r}^{\alpha\mu_{\text{ref}}} (\mu\xi)^{\mu} \left(\frac{p}{\eta}\right)^{\frac{p\mu}{1+p}} \Gamma(1+\mu_{\text{ref}})}{\exp\left(\frac{(1+pq)\kappa\mu}{\delta}\right) \hat{r}^{\alpha\mu} (\mu_{\text{ref}}\xi_{\text{ref}})^{\mu_{\text{ref}}} \left(\frac{p_{\text{ref}}}{\eta}\right)^{\frac{p_{\text{ref}}\mu_{\text{ref}}}{1+p_{\text{ref}}}} \Gamma(1+\mu)} \right)^{\frac{1}{\alpha\mu_{\text{ref}}}}, \quad (2.57)$$

and the same f_0 can be found for all fading models mentioned here, such as

$$f_0 = \frac{\mu}{\mu_{\text{ref}}}. \quad (2.58)$$

2.4.4 Asymptotic Design of Mixture Probabilities

Having obtained asymptotic expressions for $h_{R_{\text{ref}}}(\cdot)$, $N_R(\cdot)$ and $T_R(\cdot)$ in Sections 2.4.2 and 2.4.3, we now plug them into (2.34) and (2.35) to yield simple asymptotic

design expressions for p_{mix} , respectively as

$$p_{\text{mix}} \sim \frac{c_0 \times r_{\text{th}}^{d_0} - c_{0\text{U}} \times (e_{0\text{U}} r_{\text{th}}^{f_{0\text{U}}})^{d_{0\text{U}}}}{c_{0\text{L}} \times (e_{0\text{L}} r_{\text{th}}^{f_{0\text{L}}})^{d_{0\text{L}}} - c_{0\text{U}} \times (e_{0\text{U}} r_{\text{th}}^{f_{0\text{U}}})^{d_{0\text{U}}}} \quad (2.59)$$

$$p_{\text{mix}} \sim \frac{\frac{a_0}{c_0} \times r_{\text{th}}^{b_0-d_0} - \frac{a_{0\text{U}}}{c_{0\text{U}}} \times (e_{0\text{U}} r_{\text{th}}^{f_{0\text{U}}})^{b_{0\text{U}}-d_{0\text{U}}}}{\frac{a_{0\text{L}}}{c_{0\text{L}}} \times (e_{0\text{L}} r_{\text{th}}^{f_{0\text{L}}})^{b_{0\text{L}}-d_{0\text{L}}} - \frac{a_{0\text{U}}}{c_{0\text{U}}} \times (e_{0\text{U}} r_{\text{th}}^{f_{0\text{U}}})^{b_{0\text{U}}-d_{0\text{U}}}}, \quad (2.60)$$

where the coefficients a_0 and b_0 are provided in Proposition 1 with $n = 0$, for the α - μ , η - μ , and κ - μ fading channels, and in (2.19), with $n = 0$, for the α - η - κ - μ fading model; the coefficients c_0 and d_0 are provided in Proposition 2 with $n = 0$, for the α - μ , η - μ , and κ - μ fading channels, and in (2.20), with $n = j = 0$, for the α - η - κ - μ fading model; the coefficient e_0 is given by (2.54), (2.55), (2.56), and (2.57) for the α - μ , η - μ , κ - μ , and α - η - κ - μ fading channels, respectively; and, finally, the coefficient f_0 is given by (2.58) for all mentioned scenarios. In (2.59) and (2.60), we added the subscript L or U to some coefficients. This subscript indicates that the coefficient is calculated with fading parameters conditioned to $\text{ref} = \text{L}$ or $\text{ref} = \text{U}$, as applicable.

Let us review what happened in Section 2.4. We started by adjusting p_{mix} via (2.34) or (2.35) to match the exact LCR or AFD at a target envelope level r_{th} . Also, we advocated choosing in practice $r_{\text{th}} \ll 1$, because real-world system outages normally occur at very low signal levels. But there was room for improvement: (2.34) and (2.35) require the numerical evaluation of intricate statistics. Then, building on the assumption $r_{\text{th}} \ll 1$, we replaced these statistics by their asymptotic expressions as $r_{\text{th}} \rightarrow 0$, derived here, leading to the approximate, yet closed-form design solutions in (2.59) and (2.60). Remarkably, these approximate solutions prove highly accurate, even in cases where the assumption $r_{\text{th}} \ll 1$ does not hold. In passing, we derived new useful Maclaurin series representations for the CDF, LCR, and AFD of the α - μ , η - μ , and κ - μ fading models, presented in (2.37)–(2.52).

2.5 Conclusions

In this chapter, a unified sequence-generation scheme for the α - μ , η - μ , κ - μ , and α - η - κ - μ fading channels was proposed, which (i) accommodates arbitrary real values of all fading parameters, (ii) corresponds exactly to the fading models' first-order statistics, and (iii) closely approximates their second-order statistics. As far as we know, there is no other simulation scheme that meets these requirements for the referred fading models. The new scheme corrects a strong limitation of the classic simulation scheme, restricted to discrete values of the μ -parameter, which is quite a severe, impractical constraint. Moreover, the new scheme can be easily implemented with little consumption of time and

memory. In order to optimize the proposed scheme, we derived asymptotic expressions and series representations of essential fading models' statistics. This contribution alone can be useful in various wireless applications. We hope that our simulation framework can serve as a practical design tool to assist in the analysis, dimensioning, and optimization of next-generation wireless systems.

In Chapter 4, Monte Carlo simulations of second-order channel statistics will attest the efficiency of the proposed solution.

3 Unified Asymptotic Analysis of Generalized Wireless Channels

The dynamic nature of a random process can be characterized by means of second-order statistics. For a broad class of Gaussian fading models, covering various physical aspects of the wireless channel, the exact analysis of these statistics yields intricate expressions, which have been explored on a case-by-case basis for particular scenarios. In this chapter, we provide a general asymptotic analysis of second-order statistics at high SNR regime for the general Gaussian-class fading model introduced in [42]. The proposed framework leads to simple, unified, and closed-form expressions that characterize the impact of each physical aspect of the fading in the channel: clustering, non-linearity, correlation, scattered waves, and dominant components. To our knowledge, the correlation between multipath clusters has never before been analyzed for the second-order statistics of a physical fading model. Our results provide a complete, practical, and intuitive description of the dynamic behavior of the system as impacted by the various aspects of multipath fading. We consider the general case, where each multipath cluster has real and arbitrary values of all fading parameters, including the correlation between the clusters. Furthermore, we particularize the analysis for various in-phase–quadrature scenarios, as well as for some well-known fading models in the literature [19–22, 27].

The remainder of this chapter is organized as follows. In Section 3.1, the Gaussian class fading model explored in [42] is revisited. In Section 3.2, the asymptotic second-order statistics of the model are derived and specialized for some particular cases. Finally, Section 3.3 presents the main conclusions. The asymptotic expressions obtained are thoroughly validated in Chapter 4, both by reducing them to known particular cases and via Monte Carlo simulations.

This chapter contains research findings presented in the following articles:

- V. M. Rennó, F. R. A. Parente, and J. C. S. Santos Filho, “Asymptotic Analysis of Second Order Statistics for Gaussian Class Fading Channels,” *IEEE Trans. Wireless Commun.*, 2023, submitted.
- V. M. Rennó, F. R. A. Parente, and J. C. S. Santos Filho, “Análise Assintótica Unificada de Estatísticas de Segunda Ordem para Canais de Classe Gaussiana,” in *XL Simpósio Brasileiro de Telecomunicações e Processamento de Sinais (SBrT2022)*, Santa Rita do Sapucaí, Brasil, Sep. 2022.
DOI: 10.14209/sbrt.2022.1570812932.

3.1 Preliminaries

Ultra-reliability, low latency, and high rate communication with massively connected devices are some of the desired features for the next generations of wireless systems [5–7]. It is known that mmWave communication is a key technology to enable such characteristics [38]. Unfortunately, new propagation challenges in the mmWave band arise as well. For instance, recent experimental results have shown that there is a high correlation between multipath clusters of a wireless signal in mmWave communications, due to a high beamforming gain and an ultra-large channel bandwidth [8]. Also, other factors such as receiver imperfections and correlated Gaussian noise can further contribute to deteriorate the transmitted signal [31, 61].

3.1.1 Physical Model

In order to provide better performance analysis for emerging wireless scenarios, the authors in [42] explored a general Gaussian class fading model. This model contemplates dominant and scattered components with arbitrary powers propagating in a nonlinear environment. In addition, it allows the multipath clusters to be arbitrarily correlated, which is a more realistic assumption. For convenience, let the power B of the wireless communication channel be expressed by

$$B^{\frac{\alpha}{2}} = \sum_{i=1}^M X_i^2, \quad (3.1)$$

where $\alpha > 0$ represents the nonlinearity of the transmission medium [19], M is the number of multipath clusters, and $\mathbf{X} \triangleq [X_1 \ X_2 \ \cdots \ X_M]^T$ follows a multivariate Gaussian PDF with mean vector $\mathbf{m} \triangleq \mathbb{E}(\mathbf{X})$ and covariance matrix $\mathbf{\Sigma} \triangleq \mathbb{E}((\mathbf{X} - \mathbf{m})(\mathbf{X} - \mathbf{m})^T)$ [42]. In particular, $\mathbb{E}(X_i) = m_i$ and $\mathbb{V}(X_i) = \sigma_i^2$, $i \in \{1, \dots, M\}$. The correlation coefficient between the RVs X_i and X_j is defined as $\rho_{i,j} \triangleq (\mathbb{E}(X_i X_j) - \mathbb{E}(X_i)\mathbb{E}(X_j)) / (\mathbb{V}(X_i)\mathbb{V}(X_j))^{1/2}$. As known, the multivariate Gaussian PDF of \mathbf{X} can be expressed as

$$f_{\mathbf{X}}(\mathbf{x}) = \frac{\exp\left(-\frac{1}{2}(\mathbf{x} - \mathbf{m})^T \mathbf{\Sigma}^{-1}(\mathbf{x} - \mathbf{m})\right)}{((2\pi)^M \det(\mathbf{\Sigma}))^{\frac{1}{2}}}. \quad (3.2)$$

Due to this arbitrary correlation between the fading components, the exact analysis of the statistics of the channel B in (3.1) can result in intricate mathematical expressions, with little insight into how different fading aspects affect performance metrics. For instance, the exact analysis of the PDF of B depends on a multidimensional integral over the multivariate Gaussian PDF in (3.2). This integral can be obtained through Brennan's approach [78], and the PDF of the general Gaussian class fading model described

in (3.1) can be calculated as

$$f_B(\beta) = \frac{\alpha \beta^{\frac{\alpha}{2}-1}}{((2^{\frac{2}{M}+3}\pi)^M \det(\mathbf{\Sigma}))^{\frac{1}{2}}} \int_0^{\beta^{\frac{\alpha}{2}}} \int_0^{\beta^{\frac{\alpha}{2}}-x_M^2} \cdots \int_0^{\beta^{\frac{\alpha}{2}}-\sum_{i=3}^M x_i^2} \frac{1}{\prod_{i=1}^M |x_i|} \sum_{i=1}^{2^M} \exp\left(-\frac{1}{2}(\mathbf{x}_i - \mathbf{m})^T \mathbf{\Sigma}^{-1}(\mathbf{x}_i - \mathbf{m})\right) \times dx_2^2 \cdots dx_{M-1}^2 dx_M^2, \quad (3.3)$$

where $\beta \geq 0$, $x_1^2 = \beta^{\frac{\alpha}{2}} - \sum_{i=2}^M x_i^2$, with the vector \mathbf{x}_i being defined for each $i \in \{1, \dots, 2^M\}$ as $\mathbf{x}_1 \triangleq [x_1 \ x_2 \ \cdots \ x_M]^T$, $\mathbf{x}_2 \triangleq [-x_1 \ x_2 \ \cdots \ x_M]^T$, $\mathbf{x}_3 \triangleq [x_1 \ -x_2 \ \cdots \ x_M]^T$, and so on for all possible combinations of the set of components $\{x_i\}_{i=1}^M$.

To avoid the intricacy of the exact approach and provide comprehensive insights into system performance, in [42] an asymptotic analysis at high SNR of the general fading model presented in (3.1) was performed, providing simple, general, closed-form expressions for the model first-order statistics. To accomplish this, a key concept discussed in [62] was used, which demonstrated that the asymptote of the channel PDF around zero determines the system performance at high SNR. Before proceeding to the analysis for the second-order statistics, it is convenient to revisit the first-order statistics derived in [42].

3.1.2 First-Order Statistics

The aim is to obtain the asymptotic PDF of B in (3.3) as $\beta \rightarrow 0$. To this end, the authors in [42] derived initially the asymptotic PDF of \mathbf{X} , then of $\mathbf{X}^2 \triangleq [X_1^2 \ X_2^2 \ \cdots \ X_M^2]^T$, and finally the asymptotic PDF of B , which depends on the sum of X_i^2 for all $i \in \{1, \dots, M\}$. The main steps are reproduced next.

The asymptotic PDF of \mathbf{X} can be obtained from the Maclaurin series expansion in (3.2). Taking only the first term, the asymptotic PDF of \mathbf{X} results in

$$f_{\mathbf{X}}(x) \sim \frac{\exp\left(-\frac{1}{2}\mathbf{m}^T \mathbf{\Sigma}^{-1}\mathbf{m}\right)}{((2\pi)^M \det(\mathbf{\Sigma}))^{\frac{1}{2}}}. \quad (3.4)$$

For convenience, let the covariance matrix $\mathbf{\Sigma}$ be factored as $\mathbf{\Sigma} = \mathbf{D}\mathbf{R}\mathbf{D}$ such that

$$\mathbf{\Sigma} = \text{diag} \begin{bmatrix} \sigma_1 \\ \sigma_2 \\ \vdots \\ \sigma_M \end{bmatrix} \cdot \begin{bmatrix} 1 & \rho_{1,2} & \cdots & \rho_{1,M} \\ \rho_{1,2} & 1 & \cdots & \rho_{2,M} \\ \vdots & \vdots & \ddots & \vdots \\ \rho_{1,M} & \rho_{2,M} & \cdots & 1 \end{bmatrix} \cdot \text{diag} \begin{bmatrix} \sigma_1 \\ \sigma_2 \\ \vdots \\ \sigma_M \end{bmatrix}, \quad (3.5)$$

where \mathbf{D} is a diagonal matrix $M \times M$ and \mathbf{R} is a normalized covariance matrix [42]. Also, using the decomposition in (3.5), let $k_i \triangleq m_i^2/\sigma_i^2$, $\forall i \in \{1, \dots, M\}$, and $\mathbf{K} \triangleq$

$[m_1/\sigma_1 \ m_2/\sigma_2 \ \cdots \ m_M/\sigma_M]^T$, such that $\mathbf{K} = \mathbf{D}^{-1}\mathbf{m}$. Thus, the PDF of \mathbf{X} in (3.4) can be expressed as

$$f_{\mathbf{X}}(x) \sim \frac{\exp\left(-\frac{1}{2}\mathbf{K}^T\mathbf{R}^{-1}\mathbf{K}\right)}{((2\pi)^M \det(\mathbf{R}))^{\frac{1}{2}}} \prod_{i=1}^M \frac{1}{\sigma_i}, \quad (3.6)$$

where $\det(\mathbf{R}) > 0$. Furthermore, through a simple transformation of variables into (3.6), the asymptotic PDF of \mathbf{X}^2 is given by

$$f_{\mathbf{X}^2}(x^2) \sim \frac{\exp\left(-\frac{1}{2}\mathbf{K}^T\mathbf{R}^{-1}\mathbf{K}\right)}{((2\pi)^M \det(\mathbf{R}))^{\frac{1}{2}}} \prod_{i=1}^M \frac{1}{\sigma_i |x_i|}. \quad (3.7)$$

To determine the asymptotic PDF of B in (3.1), a key observation was made in [79]: under certain conditions, a set of positive correlated RVs behaves asymptotically around zero as an equivalent set of positive independent RVs. In particular, (3.7) meets these conditions [79, eq. (5)]. Thus, let $\{\check{X}_i^2\}_{i=1}^M$ be the set of independent RVs asymptotically equivalent to $\{X_i^2\}_{i=1}^M$. Comparing (3.7) with [79, eq. (5)], the asymptotic PDF of \check{X}_i^2 reduces to

$$f_{\check{X}_i^2}(\check{x}_i^2) \sim a_{i,0}(\check{x}_i^2)^{b_{i,0}}, \quad (3.8)$$

in which

$$a_{i,0} = \frac{\exp\left(-\frac{1}{2M}\mathbf{K}^T\mathbf{R}^{-1}\mathbf{K}\right)}{((2\pi)^M \det(\mathbf{R}))^{\frac{1}{2M}}} \prod_{j=1}^M \sigma_j^{-\frac{1}{M}} \quad (3.9a)$$

$$b_{i,0} = -\frac{1}{2}. \quad (3.9b)$$

Replacing (3.8) into [79, eq. (4)], and after some algebraic manipulations, the asymptotic PDF of B is obtained as the convolution of the asymptotic PDFs of $\{\check{X}_i^2\}_{i=1}^M$ [42] as

$$f_B(\beta) \sim a_{B,0}\beta^{b_{B,0}}, \quad (3.10)$$

where

$$a_{B,0} = \alpha \frac{\exp\left(-\frac{1}{2}\mathbf{K}^T\mathbf{R}^{-1}\mathbf{K}\right)}{(2^{M+2} \det(\mathbf{R}))^{\frac{1}{2}} \Gamma(\frac{M}{2})} \prod_{i=1}^M \frac{1}{\sigma_i} \quad (3.11a)$$

$$b_{B,0} = \frac{\alpha M}{4} - 1. \quad (3.11b)$$

The relationship between the power B and the envelope R of the channel is given by $R = \sqrt{B}$. Thus, the asymptotic PDF of the envelope R results in

$$f_R(r) \sim 2r f_B(r^2) \sim 2a_{B,0}r^{2b_{B,0}+1}, \quad (3.12)$$

where $a_{B,0}$ and $b_{B,0}$ are given as in (3.11).

Note that (3.12) provides a simple but comprehensive closed-form characterization of the asymptotic envelope PDF of the channel in terms of all the fading parameters

of the general fading model in (3.1). The framework can give insights into how each physical fading parameter affects the performance of the wireless system at high SNR, which is the region where communications systems often operate. This is indeed a useful tool to analyze and optimize system design while circumventing the complexity of the exact approach. This result will also serve as a basis for the asymptotic analysis of second-order statistics provided next.

3.2 Asymptotic Second-Order Statistics

To provide the complete modeling of a communication medium, one must also estimate the time-varying behavior of the wireless channel through the analysis of the channel's higher-order statistics. These statistics affect dynamic metrics such as the average outage rate and duration, expressed by the LCR and AFD, respectively.

The second-order statistics discussed here concern those related to the temporal derivative of the signal envelope. From the physical model in (3.1), we start by computing the joint distribution of $\{\check{X}_i^2\}_{i=1}^M$ and the time derivative of R , denoted by \dot{R} . Then, we proceed by doing a transformation of variables to obtain the joint distribution of R , \dot{R} , and $\{\check{X}_i^2\}_{i=2}^M$. The ultimate goal is to find the joint distribution of R and \dot{R} and, from that, to derive the LCR and AFD. Next we obtain new, simple, closed-form asymptotic expressions for fundamental second-order statistics of the fading model in (3.1). These expressions characterize the time-varying nature of the wireless channel, for arbitrary values of fading parameters and, more importantly, when multipath clusters are arbitrarily correlated.

3.2.1 LCR and AFD at High SNR

We start by taking the time derivative of both sides of (3.1) in terms of the envelope R (recall that $R = \sqrt{B}$). Isolating the time derivative \dot{R} , we obtain

$$\dot{R} = \frac{\sum_{i=1}^M 2X_i \dot{X}_i}{\alpha R^{\alpha-1}}, \quad (3.13)$$

where \dot{X}_i is the time derivative of X_i .

In [80], the relationship between the multipath components and their respective time derivatives was investigated in detail. Here, following a common practice, we consider isotropic scattering and omnidirectional reception, for which the zero-mean Gaussian RV \dot{X}_i is independent of X_i and has variance given by $\dot{\sigma}_i^2 = 2\pi^2 f_D^2 \sigma_i^2$, where f_D is the maximum Doppler shift in Hertz, and σ_i^2 is the variance of X_i , $i \in \{1, \dots, M\}$ [80]. Furthermore, although the RVs in the set $\{X_i\}_{i=1}^M$ may be correlated, those in the set

$\{\dot{X}_i\}_{i=1}^M$ are mutually independent. In addition, we assume that X_i and \dot{X}_j are also independent, $\forall(i, j)$. Thus, given the knowledge of $\{X_i\}_{i=1}^M$, \dot{R} is a sum of M independent Gaussian RVs with conditional PDF given as

$$f_{\dot{R}|X_1^2, \dots, X_M^2}(\dot{r}|x_1^2, \dots, x_M^2) = \frac{1}{\sqrt{2\pi\sigma_{\dot{r}}^2}} \exp\left(\frac{-\dot{r}^2}{2\sigma_{\dot{r}}^2}\right), \quad (3.14)$$

where $\sigma_{\dot{r}}^2 = \left(4 \sum_{i=1}^M x_i^2 \dot{\sigma}_i^2\right) / \alpha^2 r^{2\alpha-2}$.

In the asymptotic scenario, as detailed in Section 3.1, the set $\{X_i^2\}_{i=1}^M$ of correlated RVs behaves asymptotically around zero as an equivalent set of independent RVs $\{\check{X}_i^2\}_{i=1}^M$. In this way, the joint PDF of the variables $\{\dot{R}, \check{X}_1^2, \dots, \check{X}_M^2\}$ is given as

$$f_{\dot{R}, \check{X}_1^2, \dots, \check{X}_M^2}(\dot{r}, \check{x}_1^2, \dots, \check{x}_M^2) = f_{\dot{R}|\check{X}_1^2, \dots, \check{X}_M^2}(\dot{r}|\check{x}_1^2, \dots, \check{x}_M^2) f_{\check{X}_1^2}(\check{x}_1^2) \dots f_{\check{X}_M^2}(\check{x}_M^2), \quad (3.15)$$

where $f_{\check{X}_i^2}(\cdot)$, $i \in \{1, \dots, M\}$, is asymptotically expressed as in (3.8). The joint PDF of $\{\dot{R}, R, \check{X}_1^2, \dots, \check{X}_M^2\}$ is then obtained from (3.15) through a transformation of RVs. To this end, using $\check{X}_1^2 = R^\alpha - \sum_{i=2}^M \check{X}_i^2$, obtained from the manipulation of (3.1) in terms of the envelope R , the joint PDF $f_{\dot{R}, R, \check{X}_2^2, \dots, \check{X}_M^2}(\cdot, \cdot, \cdot, \dots, \cdot)$ results in

$$f_{\dot{R}, R, \check{X}_2^2, \dots, \check{X}_M^2}(\dot{r}, r, \check{x}_2^2, \dots, \check{x}_M^2) = \alpha r^{\alpha-1} f_{\dot{R}, \check{X}_1^2, \check{X}_2^2, \dots, \check{X}_M^2}\left(\dot{r}, r^\alpha - \sum_{i=2}^M \check{x}_i^2, \check{x}_2^2, \dots, \check{x}_M^2\right). \quad (3.16)$$

In turn, the joint PDF of \dot{R} and R can be obtained by integrating (3.16) using Brennan's approach [78], leading to

$$f_{\dot{R}, R}(\dot{r}, r) = \int_0^{r^\alpha} \int_0^{r^\alpha - \check{x}_M^2} \dots \int_0^{r^\alpha - \sum_{i=3}^M \check{x}_i^2} f_{\dot{R}, R, \check{X}_2^2, \dots, \check{X}_{M-1}^2, \check{X}_M^2}(\dot{r}, r, \check{x}_2^2, \dots, \check{x}_{M-1}^2, \check{x}_M^2) d\check{x}_2^2 \dots d\check{x}_{M-1}^2 d\check{x}_M^2. \quad (3.17)$$

Finally, (3.17) can be used to derive the asymptotic expressions of LCR and AFD, as follows.

The LCR is a second-order statistic that provides the average number of ascending (or descending) crosses per second for a given envelope level. By definition, the LCR of a continuous process can be calculated as [23]

$$N_R(r) = \int_0^\infty \dot{r} f_{\dot{R}, R}(\dot{r}, r) d\dot{r}. \quad (3.18)$$

Thus, substituting the joint PDF $f_{\dot{R}, R}(\cdot, \cdot)$ given in (3.17) into (3.18), with use of (3.14)–(3.16) and the asymptotic PDF of $\{\check{X}_i^2\}_{i=2}^M$ given in (3.8), after some algebraic manipulations, we obtain the asymptotic LCR for the general Gaussian-class fading model as

$$N_R(r) \sim \sqrt{\frac{2}{\pi}} a_{i,0}^M \dot{\sigma}_1 \Gamma(1 + b_{i,0})^M \left(\prod_{i=1}^{M-1} \Gamma(i(1 + b_{i,0})) \right) \left(\prod_{j=1}^M {}_2F_1\left(\frac{-1}{2}; 1 + b_{i,0}; j(1 + b_{i,0}); 1 - \frac{\dot{\sigma}_M^2}{\dot{\sigma}_1^2}\right) \right) \times r^{\alpha(Mb_{i,0} + \frac{2M-1}{2})}. \quad (3.19)$$

This is a general closed-form solution whose elements $a_{i,0}$ and $b_{i,0}$ are the asymptotic coefficients given in (3.9).

The AFD of the fading signal envelope is the average time that the signal spends below a certain envelope threshold. It is given by the ratio between the envelope CDF and LCR, as in (2.11). Using the asymptotic CDF derived by the integration of (3.12) and the asymptotic LCR given in (3.19), we obtain the asymptotic AFD for the general Gaussian-class fading model as

$$T_R(r) \sim \frac{\sqrt{\frac{\pi}{2}} a_{B,0} a_{i,0}^{-M} \dot{\sigma}_1^{-1} \Gamma(1 + b_{i,0})^{-M} \times r^{2(b_{B,0}+1) - \alpha(Mb_{i,0} + \frac{2M-1}{2})}}{(b_{B,0} + 1) \left(\prod_{i=1}^{M-1} \Gamma(i(1 + b_{i,0})) \right) \left(\prod_{j=1}^M {}_2F_1 \left(\frac{-1}{2}; 1 + b_{i,0}; j(1 + b_{i,0}); 1 - \frac{\dot{\sigma}_M^2}{\dot{\sigma}_1^2} \right) \right)}, \quad (3.20)$$

where $a_{B,0}$ and $b_{B,0}$ are the asymptotic coefficients given in (3.11).

The asymptotic expressions of LCR and AFD presented in (3.19) and (3.20), respectively, provide a complete characterization for the dynamic performance of the wireless transmission channel operating at high SNR. This characterization accounts for arbitrary values of many fading parameters, such as the nonlinearity of the transmission medium (α), the number of multipath clusters (M), the average power of the scattered (σ_i^2) and dominant (m_i) waves, and, more generally than previous physical fading models considered elsewhere, the correlation between multipath clusters ($\rho_{i,j}$). All in all, the analysis embraces, as particular cases, a broad class of fading models reported in the literature [19], since it considers all the physical aspects considered therein, in addition to the correlation between the multipath components.

The general scenario discussed above considers that the physical parameters of the multipath components may assume arbitrary values. This is a general condition. Some particular cases can be analyzed in order to further simplify the dynamic asymptotic statistics, given in (3.19) and (3.20), of the fading channel modeled by (3.1). Next, we analyze important particular-case scenarios and fading distributions.

3.2.2 Particular Scenarios

Recent works show that UWB channels in mmWave communications can present a high correlation between the in-phase and quadrature components, due to the high beamforming gain [8, 13–15, 43, 44]. Motivated by this, we now analyze the case in which the RVs $\{X_i\}_{i=1}^M$ in (3.1) are arranged in pairs of correlated in-phase and quadrature components. Let M_x and M_y represent the number of in-phase and quadrature Gaussian components, respectively, such that $M_x + M_y = M$. For convenience, the in-phase components $\{X_i\}_{i=1}^{M_x}$ and the quadrature components $\{X_i\}_{i=M_x+1}^M$ can be organized into a vector form as $\mathbf{X} \triangleq [X_1 \ X_2 \ \cdots \ X_{M_x} \ X_{M_x+1} \ \cdots \ X_M]^T$. In particular, we let the M_x

in-phase components have a fixed value for each fading parameter, i.e., the fading parameters reduce to $m_i = m_x$ and $\sigma_i = \sigma_x$, $\forall i \in \{1, \dots, M_x\}$. Similarly, we assume that the fading parameters of the M_y quadrature components are such that $m_i = m_y$ and $\sigma_i = \sigma_y$, $\forall i \in \{M_x + 1, \dots, M\}$. As for the correlation coefficients between the RVs in \mathbf{X} , we investigate three different scenarios.

3.2.2.1 Correlated In-Phase–Quadrature Components

The first scenario considers that (i) any pair of in-phase components has a fixed value for the correlation coefficient (ρ_x), (ii) any pair of quadrature components has a fixed value for the correlation coefficient (ρ_y), and (iii) there is a non-zero fixed cross-correlation between any pair of in-phase and quadrature components (ρ). In this case, the correlation coefficients can be expressed as

$$\rho_{i,j} = \begin{cases} \rho_x, & \text{if } \{i, j\} \in \{1, \dots, M_x\}; \\ \rho_y, & \text{if } \{i, j\} \in \{M_x + 1, \dots, M\}; \\ \rho, & \text{otherwise.} \end{cases} \quad (3.21)$$

For this scenario, the normalized covariance matrix reduces to

$$\mathbf{R} = \begin{bmatrix} \mathbf{I}_{M_x} + \rho_x \mathbf{I}_{M_x}^c & \rho \mathbf{1}_{M_x \times M_y} \\ \rho \mathbf{1}_{M_y \times M_x} & \mathbf{I}_{M_y} + \rho_y \mathbf{I}_{M_y}^c \end{bmatrix}, \quad (3.22)$$

where \mathbf{I} is the identity matrix, $\mathbf{1}$ is the unitary matrix whose all elements are equal to 1, and \mathbf{I}^c is the complement of the identity matrix, i.e., $\mathbf{I}^c \triangleq \mathbf{1} - \mathbf{I}$. Given the covariance matrix \mathbf{R} in (3.22), we find after algebraic manipulations that (see Appendix B.1)

$$\det(\mathbf{R}) = \frac{(1 - \rho_x)^{M_x-1} (1 - \rho_y)^{M_y-1}}{((1 + (M_x - 1)\rho_x)(1 + (M_y - 1)\rho_y) - M_x M_y \rho^2)^{-1}}. \quad (3.23)$$

Since we have the condition $\det(\mathbf{R}) > 0$ in (3.6), it follows that $\rho_x \in \left(\left(\frac{M_x M_y \rho^2}{1 + \rho_y (M_y - 1)} - 1 \right) \frac{1}{M_x - 1}, 1 \right)$, $\rho_y \in \left(\left(\frac{M_x M_y \rho^2}{1 + \rho_x (M_x - 1)} - 1 \right) \frac{1}{M_y - 1}, 1 \right)$, and $\rho < ((1 + \rho_x (M_x - 1))(1 + \rho_y (M_y - 1))(M_x M_y)^{-1})^{1/2}$. Furthermore, in such case, the entry at the i th line and j th column of the inverse matrix \mathbf{R}^{-1} , say $\xi_{i,j}$, is found as (see Appendix B.2)

$$\xi_{i,j} = \begin{cases} \frac{(1 + \rho_x (M_x - 2))(\rho_y (1 - M_y) - 1) + (M_x - 1)M_y \rho^2}{(\rho_x - 1)((1 + (M_x - 1)\rho_x)(1 + (M_y - 1)\rho_y) - M_x M_y \rho^2)}, & \text{if } i = j, \{i, j\} \in \{1, \dots, M_x\} \\ \frac{\rho_x (1 + (M_y - 1)\rho_y) - M_y \rho^2}{(\rho_x - 1)((1 + (M_x - 1)\rho_x)(1 + (M_y - 1)\rho_y) - M_x M_y \rho^2)}, & \text{if } i \neq j, \{i, j\} \in \{1, \dots, M_x\} \\ \frac{(1 + \rho_y (M_y - 2))(\rho_x (1 - M_x) - 1) + (M_y - 1)M_x \rho^2}{(\rho_y - 1)((1 + (M_y - 1)\rho_y)(1 + (M_x - 1)\rho_x) - M_x M_y \rho^2)}, & \text{if } i = j, \{i, j\} \in \{M_x + 1, \dots, M\} \\ \frac{\rho_y (1 + (M_x - 1)\rho_x) - M_x \rho^2}{(\rho_y - 1)((1 + (M_y - 1)\rho_y)(1 + (M_x - 1)\rho_x) - M_x M_y \rho^2)}, & \text{if } i \neq j, \{i, j\} \in \{M_x + 1, \dots, M\} \\ \frac{-\rho}{((1 + (M_x - 1)\rho_x)(1 + (M_y - 1)\rho_y) - M_x M_y \rho^2)}, & \text{otherwise.} \end{cases} \quad (3.24)$$

Substituting these results into (3.19) and (3.20), the asymptotic LCR and AFD for the Gaussian-class fading model with correlated in-phase and quadrature components are respectively obtained as

$$N_R(r) \sim \frac{\sqrt{\pi} f_d \exp\left(-\frac{1}{2} \mathbf{K}^T \mathbf{R}^{-1} \mathbf{K}\right)}{2^{\frac{M}{2}-1} \sigma_x^{M_x-1} \sigma_y^{M_y} \Gamma\left(\frac{M}{2}\right) ((1-\rho_x)^{M_x-1} (1-\rho_y)^{M_y-1})} \times \frac{\prod_{i=M_x+1}^M {}_2F_1\left(\frac{-1}{2}; \frac{1}{2}; \frac{i}{2}; 1 - \frac{\sigma_y^2}{\sigma_x^2}\right) \times r^{\alpha\left(\frac{M-1}{2}\right)}}{((1+(M_x-1)\rho_x)(1+(M_y-1)\rho_y) - M_x M_y \rho^2)^{\frac{1}{2}}} \quad (3.25)$$

$$T_R(r) \sim \frac{r^{\frac{\alpha}{2}}}{M \sqrt{\pi} f_d \sigma_x \prod_{i=M_x+1}^M {}_2F_1\left(\frac{-1}{2}; \frac{1}{2}; \frac{i}{2}; 1 - \frac{\sigma_y^2}{\sigma_x^2}\right)}, \quad (3.26)$$

where, after the necessary simplifications, the $\mathbf{K}^T \mathbf{R}^{-1} \mathbf{K}$ matrix is given by

$$\mathbf{K}^T \mathbf{R}^{-1} \mathbf{K} = \frac{k_x M_x (1 + (M_y - 1)\rho_y) + k_y M_y (1 + (M_x - 1)\rho_x) - 2\sqrt{k_x k_y} M_x M_y \rho}{((1 + (M_x - 1)\rho_x)(1 + (M_y - 1)\rho_y) - M_x M_y \rho^2)}. \quad (3.27)$$

For ease of notation we use $k_x \triangleq m_x^2/\sigma_x^2$ and $k_y \triangleq m_y^2/\sigma_y^2$.

3.2.2.2 Uncorrelated In-Phase–Quadrature Components

The second scenario is similar to the first one, but now we consider that there is no cross-correlation between the in-phase and quadrature components, i.e., the in-phase and quadrature components are mutually independent. In this case, the correlation coefficients are given as

$$\rho_{i,j} = \begin{cases} \rho_x, & \text{if } \{i, j\} \in \{1, \dots, M_x\}; \\ \rho_y, & \text{if } \{i, j\} \in \{M_x + 1, \dots, M\}; \\ 0, & \text{otherwise.} \end{cases} \quad (3.28)$$

For this case, the normalized covariance matrix reduces to

$$\mathbf{R} = \begin{bmatrix} \mathbf{I}_{M_x} + \rho_x \mathbf{I}_{M_x}^c & \mathbf{0}_{M_x \times M_y} \\ \mathbf{0}_{M_y \times M_x} & \mathbf{I}_{M_y} + \rho_y \mathbf{I}_{M_y}^c \end{bmatrix}, \quad (3.29)$$

where $\mathbf{0}$ is the null matrix. After algebraic manipulations, we find that $\det(\mathbf{R}) = (1 - \rho_x)^{M_x-1} (1 - \rho_y)^{M_y-1} (1 + (M_x - 1)\rho_x) (1 + (M_y - 1)\rho_y)$ (See Appendix B.3). The condition $\det(\mathbf{R}) > 0$ in (3.6) then implies that $\rho_x \in \left(\frac{1}{1-M_x}, 1\right)$ and $\rho_y \in \left(\frac{1}{1-M_y}, 1\right)$. In such a case, the entry at the i th line and j th column of the inverse matrix \mathbf{R}^{-1} reduces to (see

Appendix B.4)

$$\xi_{i,j} = \begin{cases} \frac{1+\rho_x(M_x-2)}{(1-\rho_x)(1+\rho_x(M_x-1))}, & \text{if } i = j, \{i, j\} \in \{1, \dots, M_x\} \\ \frac{-\rho_x}{(1-\rho_x)(1+\rho_x(M_x-1))}, & \text{if } i \neq j, \{i, j\} \in \{1, \dots, M_x\} \\ \frac{1+\rho_y(M_y-2)}{(1-\rho_y)(1+\rho_y(M_y-1))}, & \text{if } i = j, \{i, j\} \in \{M_x + 1, \dots, M\} \\ \frac{-\rho_y}{(1-\rho_y)(1+\rho_y(M_y-1))}, & \text{if } i \neq j, \{i, j\} \in \{M_x + 1, \dots, M\} \\ 0, & \text{otherwise.} \end{cases} \quad (3.30)$$

Using these simplifications into (3.19) and (3.20), the corresponding asymptotic LCR and AFD for this scenario are respectively given by

$$N_R(r) \sim \frac{\sqrt{\pi} f_d \exp\left(-\frac{1}{2} \mathbf{K}^T \mathbf{R}^{-1} \mathbf{K}\right) \prod_{i=M_x+1}^M {}_2F_1\left(\frac{-1}{2}; \frac{1}{2}; \frac{i}{2}; 1 - \frac{\sigma_y^2}{\sigma_x^2}\right) \times r^{\alpha\left(\frac{M-1}{2}\right)}}{2^{\frac{M}{2}-1} \sigma_x^{M_x-1} \sigma_y^{M_y} \Gamma\left(\frac{M}{2}\right) ((1-\rho_x)^{M_x-1} (1-\rho_y)^{M_y-1} (1+(M_x-1)\rho_x)(1+(M_y-1)\rho_y))^{\frac{1}{2}}} \quad (3.31)$$

$$T_R(r) \sim \frac{r^{\frac{\alpha}{2}}}{M \sqrt{\pi} f_d \sigma_x \prod_{i=M_x+1}^M {}_2F_1\left(\frac{-1}{2}; \frac{1}{2}; \frac{i}{2}; 1 - \frac{\sigma_y^2}{\sigma_x^2}\right)}, \quad (3.32)$$

where, after the necessary algebraic manipulations, we have

$$\mathbf{K}^T \mathbf{R}^{-1} \mathbf{K} = \frac{M_x k_x}{(1+(M_x-1)\rho_x)} + \frac{M_y k_y}{(1+(M_y-1)\rho_y)}. \quad (3.33)$$

The two scenarios detailed above can be further particularized. For example, assuming that $M_x = M_y = M/2$, one can consider the scenario in which there is correlation only between the i th in-phase and the i th quadrature components. In such case, the physical model is represented by

$$B^{\frac{\alpha}{2}} = \sum_{i=1}^{M/2} (X_{I_i}^2 + X_{Q_i}^2), \quad (3.34)$$

and the covariance matrix \mathbf{R} reduces to

$$\mathbf{R} = \begin{bmatrix} \mathbf{I}_{M/2} & \rho \mathbf{I}_{M/2} \\ \rho \mathbf{I}_{M/2} & \mathbf{I}_{M/2} \end{bmatrix}, \quad (3.35)$$

where the detailed analysis for the asymptotic LCR and AFD expressions has been omitted for brevity. Note that our results simplify the analysis of the general expressions in (3.19) and (3.20) for emerging communication schemes, such as in mmWave applications [8, 13–15, 43, 44].

3.2.2.3 Commutative Scenario

In high-rate, low-range indoor scenarios expected for future generations of wireless communications, the physical parameters of all multipath clusters may assume

the same value [23, 44, 81]. In this scenario, the fading parameters reduce to $m_i = m$, $\sigma_i = \sigma$, and $\rho_{i,j} = \rho$, $\forall i \neq j$. Accordingly, $k = m^2/\sigma^2$. In [42], it was shown that in this scenario $\det(\mathbf{R}) = (1 - \rho)^{M-1}(1 + \rho(M - 1))$. The condition $\det(\mathbf{R}) > 0$ in (3.6) implies that $\rho \in (\frac{1}{1-M}, 1)$. In such a case, the entry at the i th line and j th column of the inverse matrix \mathbf{R}^{-1} can be obtained as (see [42, Appendix])

$$\xi_{i,j} = \begin{cases} \frac{1+\rho(M-2)}{(1-\rho)(1+\rho(M-1))}, & \text{if } i = j; \\ \frac{-\rho}{(1-\rho)(1+\rho(M-1))}, & \text{otherwise.} \end{cases} \quad (3.36)$$

Using these simplifications into (3.19) and (3.20), the asymptotic LCR and AFD for the commutative scenario are given by

$$N_R(r) \sim \frac{f_D \sqrt{\pi} (1 - \rho)^{\frac{1-M}{2}} \exp\left(\frac{-kM}{2(1+\rho(M-1))}\right)}{\Gamma\left(\frac{M}{2}\right) \sigma^{M-1} 2^{\frac{M}{2}-1} (1 + \rho(M-1))^{\frac{1}{2}}} r^{\alpha(\frac{M-1}{2})} \quad (3.37)$$

$$T_R(r) \sim \frac{r^{\frac{\alpha}{2}}}{M \sqrt{\pi} f_D \sigma}. \quad (3.38)$$

The analysis discussed here provides relevant information about the dynamic performance of the system in terms of each physical fading parameter when all components have the same characteristics. This contributes to the modeling of wireless communication channels in promising indoor technologies [8, 44].

3.2.3 Particular Fading Models

A large number of statistical models from the literature is used to describe the randomness of the short-term fading [19]. Many of them assume independence between the multipath clusters or between the corresponding in-phase and quadrature components—a less comprehensive scenario than the one considered here. As already mentioned, the exact mathematical analysis of the channel statistics becomes increasingly complicated as more aspects of fading are incorporated into the model. To overcome such limitation, it is convenient to asymptotically analyze the dynamic statistics of fading channels popularly discussed in the literature, which turn out to be particular cases of the general Gaussian-class fading model discussed herein.

To characterize the asymptotic dynamic behavior of the wireless channel at high SNR for a broad class of distributions, we reduce our analysis presented in (3.19) and (3.20) to some particular cases. In Table 3.1, we provide the closed-form asymptotic expressions of LCR and AFD for some fading models reported in the literature [19–22, 27]. In this table, (i) the first column lists the fading models under consideration, (ii) the second column contains the original parameterization of the model, (iii) the third column

Table 3.1 – Asymptotic LCR and AFD for particular fading models.

Fading model	Original Parameterization	Proposed Gaussian-Class Model Parameterization	$N_R(r)$	$T_R(r)$
Rayleigh	(Ω) [20]	$\alpha = 2; M = 2; m_i = 0;$ $\sigma_1 = \sigma_2 = \left(\frac{\Omega}{2}\right)^{\frac{1}{2}}.$	$\frac{\sqrt{2\pi}f_D r}{\sqrt{\Omega}}$	$\frac{r}{\sqrt{2\pi}f_D \sqrt{\Omega}}$
Nakagami- m	(m, Ω) [27]	$\alpha = 2; M = 2m; m_i = 0;$ $\sigma_i = \left(\frac{\Omega}{2m}\right)^{\frac{1}{2}}, i \in \{1, \dots, M\}.$	$\frac{\sqrt{2\pi}f_D m^{m-\frac{1}{2}} r^{2m-1}}{\Gamma(m)\Omega^{m-\frac{1}{2}}}$	$\frac{r}{\sqrt{2\pi}f_D \sqrt{m\Omega}}$
α - μ	(α, μ, \hat{r}) [21]	$M = 2\mu; m_i = 0;$ $\sigma_i = \left(\frac{\hat{r}^\alpha}{2\mu}\right)^{\frac{1}{2}}, i \in \{1, \dots, M\}.$	$\frac{\sqrt{2\pi}f_D \mu^{\mu-\frac{1}{2}} r^{\alpha(\mu-\frac{1}{2})}}{\Gamma(\mu)\hat{r}^{\alpha(\mu-\frac{1}{2})}}$	$\frac{r^{\frac{\alpha}{2}}}{\sqrt{2\pi}f_D \sqrt{\mu\hat{r}^\alpha}}$
κ - μ	(κ, μ, \hat{r}) [22]	$\alpha = 2; M = 2\mu; \sum_{i=1}^M m_i^2 = \frac{\kappa\hat{r}^2}{\kappa+1};$ $\sigma_i = \left(\frac{\hat{r}^2}{2\mu(\kappa+1)}\right)^{\frac{1}{2}}, i \in \{1, \dots, M\}.$	$\frac{\sqrt{2\pi}f_D (\mu+\kappa\mu)^{\mu-\frac{1}{2}} r^{2\mu-1}}{\exp(\kappa\mu)\Gamma(\mu)\hat{r}^{2(\mu-\frac{1}{2})}}$	$\frac{\sqrt{(1+\kappa)}r}{\sqrt{2\pi}f_D \sqrt{\mu\hat{r}^2}}$
η - μ	(η, μ, \hat{r}) [22]	$\alpha = 2; M = 4\mu; m_i = 0;$ $\sigma_i = \left(\frac{\eta\hat{r}^2}{2\mu(\eta+1)}\right)^{\frac{1}{2}}, i \in \{1, \dots, \frac{M}{2}\};$ $\sigma_i = \left(\frac{\hat{r}^2}{2\mu(\eta+1)}\right)^{\frac{1}{2}}, i \in \{\frac{M}{2} + 1, \dots, M\}.$	$\sqrt{2\pi}f_D \left(\frac{(1+\eta)\mu}{\hat{r}^2}\right)^{2\mu-\frac{1}{2}} \eta^{-\mu} \times$ ${}_2F_1\left(\frac{-1}{2}; \mu; 2\mu; 1-\eta\right) r^{4\mu-1}$	$\frac{(2\hat{r}\mu)^{-1} \sqrt{\mu(1+\eta)}r}{\sqrt{2\pi}f_D {}_2F_1\left(\frac{-1}{2}; \mu; 2\mu; 1-\eta\right)}$
α - η - κ - μ	$(\alpha, \eta, \kappa, \mu, p, q, \hat{r})$ [19]	$M = 2\mu; \sum_{i=1}^{M_x} m_i^2 = \frac{\eta\kappa q \hat{r}^\alpha}{(\kappa+1)(\eta q+1)};$ $\sum_{i=M_x+1}^{M_x+M_y} m_i^2 = \frac{\frac{1}{2}}{(\kappa+1)(\eta q+1)};$ $\sigma_i = \left(\frac{\eta\hat{r}^\alpha(p+1)}{2\mu p(\eta+1)(\kappa+1)}\right)^{\frac{1}{2}}, i \in \{1, \dots, M_x\};$ $\sigma_i = \left(\frac{\hat{r}^\alpha(p+1)}{2\mu(\eta+1)(\kappa+1)}\right)^{\frac{1}{2}}, i \in \{M_x+1, \dots, M\}.$	$\sqrt{2\pi}f_Y \left(\frac{(1+p)\hat{r}^\alpha}{(1+\eta)(1+\kappa)\mu}\right)^{\frac{1}{2}-\mu} \times$ $\left(\frac{p}{\eta}\right)^{\frac{p\mu}{1+p}} \exp\left(-\frac{(1+pq)(1+\eta)\kappa\mu}{(1+p)(1+q\eta)}\right) \times$ ${}_2F_1\left(\frac{-1}{2}; \frac{p\mu}{1+p}; \mu; 1-\frac{f_Y^2 \eta}{f_Y^2 p}\right) r^{\alpha(\mu-\frac{1}{2})}$	$\frac{\sqrt{(1+\eta)(1+\kappa)}}{\sqrt{2\pi}f_Y \sqrt{\mu\hat{r}^\alpha(1+p)}} \times$ $\frac{\exp\left(\frac{(q-1)(p-\eta)\kappa\mu}{(1+p)(1+q\eta)}\right) r^{\frac{\alpha}{2}}}{{}_2F_1\left(\frac{-1}{2}; \frac{p\mu}{1+p}; \mu; 1-\frac{f_Y^2 \eta}{f_Y^2 p}\right)}$

shows how the parameters of the general fading model in (3.1) are chosen to obtain each particular model, (iv) the fourth column gives the asymptotic LCR expressions, and (v) the fifth column gives the asymptotic AFD expressions. Even though these second-order statistics are given in terms of the original parameterization (second column), the third column shows the correspondence in terms of the parameters considered here (α , M , σ_i , and m_i). The omitted parameters have a trivial equivalence (see [19, Sec. VI] for more details on fading models parameterization). For example, the correspondence for α is not shown in the third column when the nonlinearity parameter is the same parameter for some particular fading model, such as α - μ and α - η - κ - μ . Furthermore, as the particular models assume that the multipath components are mutually independent, the corresponding correlation coefficients are null, that is, $\rho_{i,j} = 0$, $\forall i \neq j$, omitted in the table for simplicity. Finally, it is noteworthy that the real μ -parameter of known fading distributions is a physical continuous version of the number of multipath clusters, represented here by the integer M -parameter [19–22, 27].

The results in Table 3.1 show that the unified analysis of second-order statistics proposed herein can be simplified and explored for several fading models addressed in the technical literature. So, one can determine the asymptotic dynamic performance, in terms of LCR and AFD, for different propagation scenarios and fading distributions. These results are indeed novel and can be readily applied to the performance analysis of a broad variety of communication channels.

3.3 Conclusions

The exact formulation of the dynamic statistics that model the wireless communication channel is challenging, as the expressions are usually given as a function of several integrals.

In this chapter, a general, simple, and unified asymptotic analysis of the wireless communication systems' dynamic performance over fading channels was proposed. Asymptotic expressions were derived in closed form for key second-order statistics of general Gaussian class distributions. The analysis considered the most diverse physical fading phenomena described in the literature, including the correlation between multipath components, a realistic assumption for emerging applications. The analytical expressions were analyzed and reduced to special-case propagation conditions, including particular fading models in the literature and various correlation scenarios for the in-phase and quadrature components.

The proposed analysis can provide useful information on how each fading parameter affects the dynamic performance of wireless systems operating at high SNR.

The results can be readily used to evaluate and optimize applications that are subject to different propagation conditions, such as those envisaged for emerging communication systems.

The analytical results are validated through Monte Carlo simulations for several fading scenarios in Chapter 4.

4 Numerical and Simulation Results

This chapter presents several numerical results that illustrate the behavior of the second-order statistics addressed in this work, namely LCR and AFD, for the different fading scenarios investigated in the previous chapters. Theoretical and simulation results of the second-order statistics are provided in Section 4.1 for the simulation schemes proposed in Chapter 2 for the α - μ , η - μ , κ - μ , and α - η - κ - μ fading channels. Additionally, in Section 4.2, theoretical, simulation, and asymptotic results are provided for the general Gaussian-class fading model analyzed in Chapter 3.

4.1 Simulation Results for the Proposed Simulation Framework

In this section, we present analytical and empirical statistics of the proposed simulation scheme for the α - μ , η - μ , κ - μ , and α - η - κ - μ models, with different values of the fading parameters. Our aim is not to discuss the fading models' statistics themselves; a thorough discussion has already been presented in [19, 21, 22]. Instead, our aim is to illustrate, for a wide range of scenarios, how closely the statistics of the proposed simulation scheme, described in Chapter 2, approximate the theoretical fading models' statistics. Since the match for first-order statistics is perfect by design, here we only cover the second-order statistics (LCR and AFD).

The LCR is shown in Fig. 4.1-(a), Fig. 4.2-(a), and Fig. 4.3-(a), and the AFD, in Fig. 4.1-(b), Fig. 4.2-(b), and Fig. 4.3-(b). The fading models' statistics are represented by solid lines, given by (2.4) and (2.5) for α - μ fading, (2.10) and (2.11) for η - μ fading, (2.15) and (2.16) for κ - μ fading, and (2.20) and (2.11) for α - η - κ - μ fading. The proposed simulator's analytical statistics, given by (2.32) and (2.33), are represented by dashed lines, and their empirical counterparts (i.e., obtained via simulation) are represented by markers. In all simulations, we used $N = 10^7$ samples. For the p_{mix} calibration via (2.59) and (2.60), we use somewhat arbitrarily a normalized envelope level of $r_{\text{th}}/\hat{r} = -25$ dB.

In all simulated scenarios, in the random-mixture stage, the autocorrelated Gaussian components of the physical fading models were generated according to the traditional Jakes/Clark model [74]. In the rank-matching stage, the independent samples with the desired fading parameters of each fading channels were generated through the rejection method proposed in [82].

We select the sample scenarios as follows. In Fig. 4.1-(a) and Fig. 4.1-(b), the unified δ - μ simulator, described in Chapter 2.3 and illustrated in Fig. 2.2, was used in a

worse-than-Rayleigh condition, i.e., with Nakagami- m fading parameter $m \triangleq \mathbb{E}^2(R^2)/\mathbb{V}(R^2)$ less than unity ($m < 1$). In Fig. 4.2-(a) and Fig. 4.2-(b), we consider a better-than-Rayleigh condition for the same δ - μ simulator, i.e., $m > 1$. Both conditions are common in practice [28–31, 33–35]. Then, for each scenario, we pick two cases: $\mu < m$ and $\mu > m$. In each case, the same values of m and μ are used for the α - μ , η - μ , and κ - μ fading models. Based on these values, the corresponding values of α are adjusted using [21]

$$m = \frac{\Gamma^2\left(\mu + \frac{2}{\alpha}\right)}{\Gamma(\mu)\Gamma\left(\mu + \frac{4}{\alpha}\right) - \Gamma^2\left(\mu + \frac{2}{\alpha}\right)}, \quad (4.1)$$

and the corresponding values of η are adjusted using [22]

$$m = 2\mu \left(1 + \left(\frac{H}{h}\right)^2\right)^{-1}, \quad (4.2)$$

where H and h are defined in Section 2.1.2, depending on the format in which the η - μ distribution is used. Finally the corresponding values of κ are adjusted using [22]

$$m = \frac{\mu(1 + \kappa)^2}{1 + 2\kappa}. \quad (4.3)$$

On the other hand, in Fig. 4.3-(a) and Fig. 4.3-(b) the proposed α - η - κ - μ simulator, described in Chapter 2.3 and illustrated in Fig 2.3, was used. The results were found with a set of randomly selected parameters, covering several fading scenarios [19, 38].

It is observed from the figures that the analytical and empirical statistics for the proposed simulation schemes perfectly match each other, as expected. In addition, it is observed that, in general, the simulator's statistics maintain an excellent agreement with the fading models' statistics over the whole range of envelope values, becoming practically indistinguishable as the μ -parameter increases.

A remark is in order. In Fig. 4.1, Fig. 4.2, and Fig. 4.3, note that, for $\mu \geq 0.5$, an exact match is achieved between the models' statistics and the proposed simulator's statistics at envelope level r_{th} , as desired. On the other hand, the match is no longer exact for $\mu < 0.5$ (see scenarios with $\mu = 0.46$ in Fig. 4.1, and $\mu = 0.45$ in Fig. 4.3). This is because, if $\mu < 0.5$ (or, in the α - η - κ - μ case, $\mu_x < 1$ and $\mu_y < 1$), then $\mu_L = 0$ and $\mu_U = 0.5$ (or, in the α - η - κ - μ case, $\mu_U = 1$), causing the input reference sequence R_L in the random-mixture stage to be null. In such a case, the best thing we can do is to choose R_U alone as the output of the random-mixture stage or, equivalently, choose $p_{\text{mix}} = 0$. But then, of course, we can no longer adjust p_{mix} to match the exact statistics at any target envelope level. Hence the imperfect fit at r_{th} . It is noteworthy, however, that even in those extreme, unlikely cases where $\mu < 0.5$ (or $\mu_x < 1$ and $\mu_y < 1$), the overall fit is still very good, with the proposed simulator mimicking the general shape of the fading models' statistics.

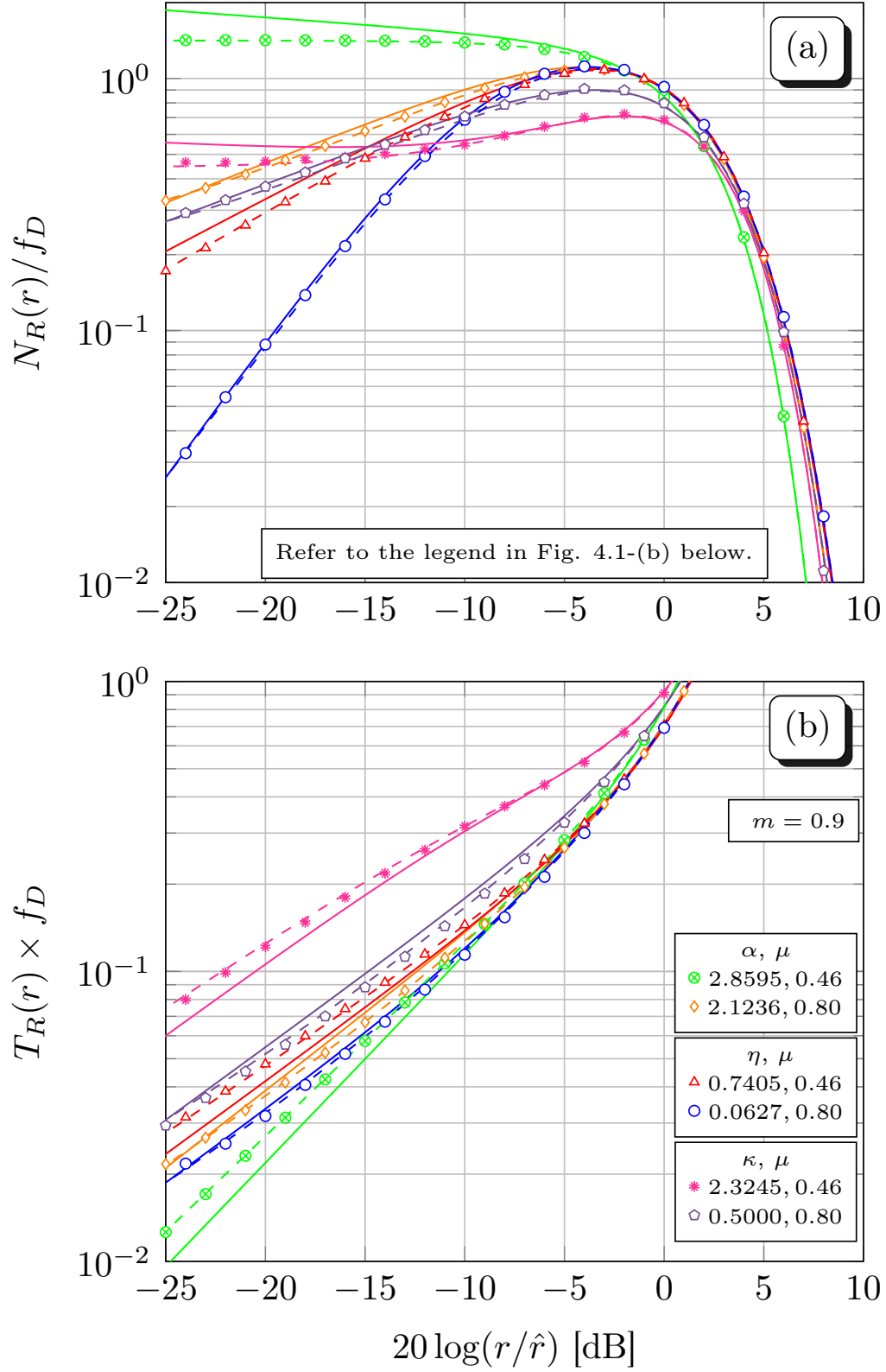


Figure 4.1 – LCR and AFD of the proposed α - μ , η - μ , and κ - μ simulator versus theoretical fading model's statistics in a worse-than-Rayleigh condition.(fading model: solid; proposed simulator, analytical: dashed; proposed simulator, empirical: markers).

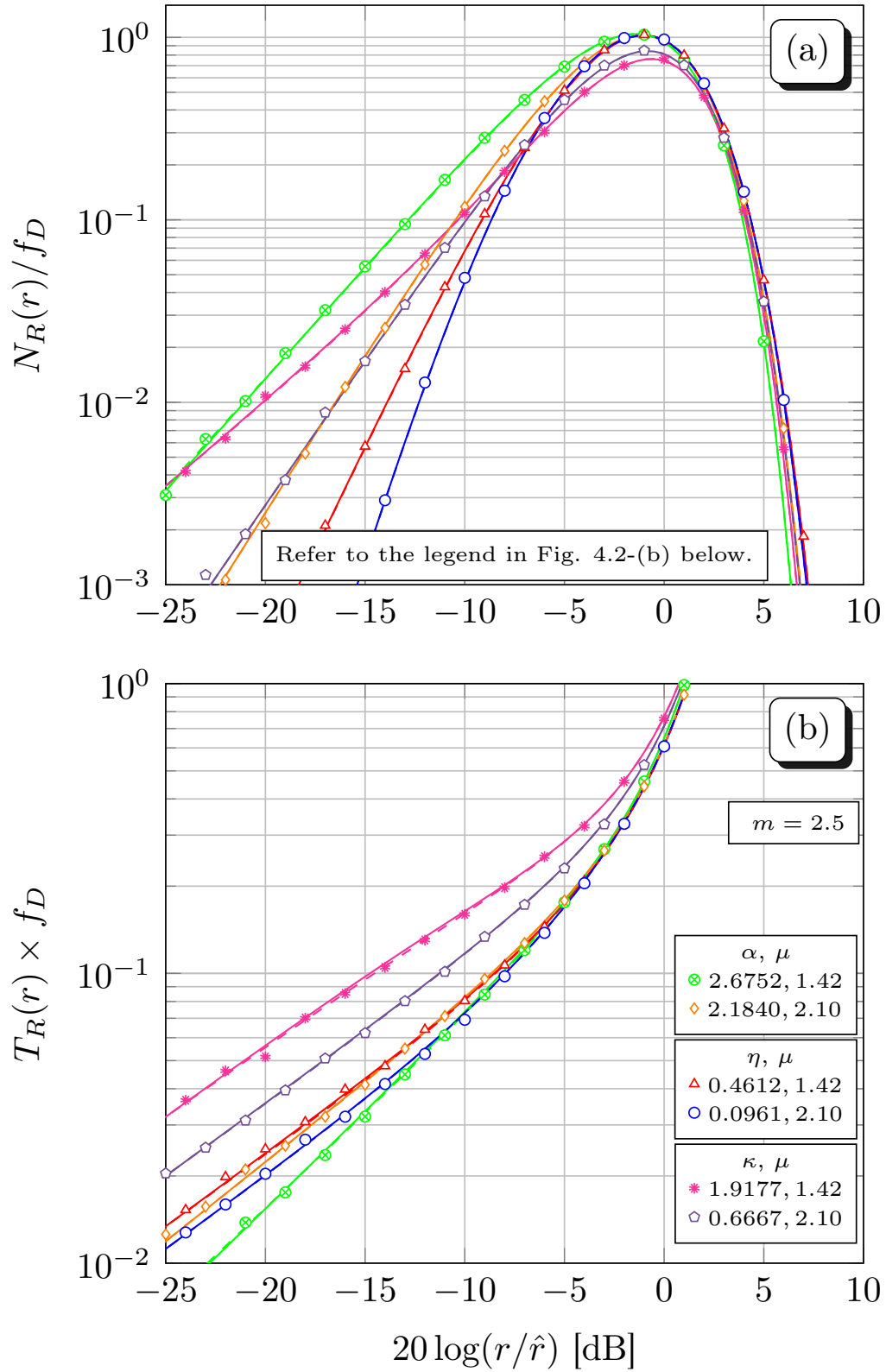


Figure 4.2 – LCR and AFD of the proposed α - μ , η - μ , and κ - μ simulator versus theoretical fading model's statistics in a better-than-Rayleigh condition. (fading model: solid; proposed simulator, analytical: dashed; proposed simulator, empirical: markers).

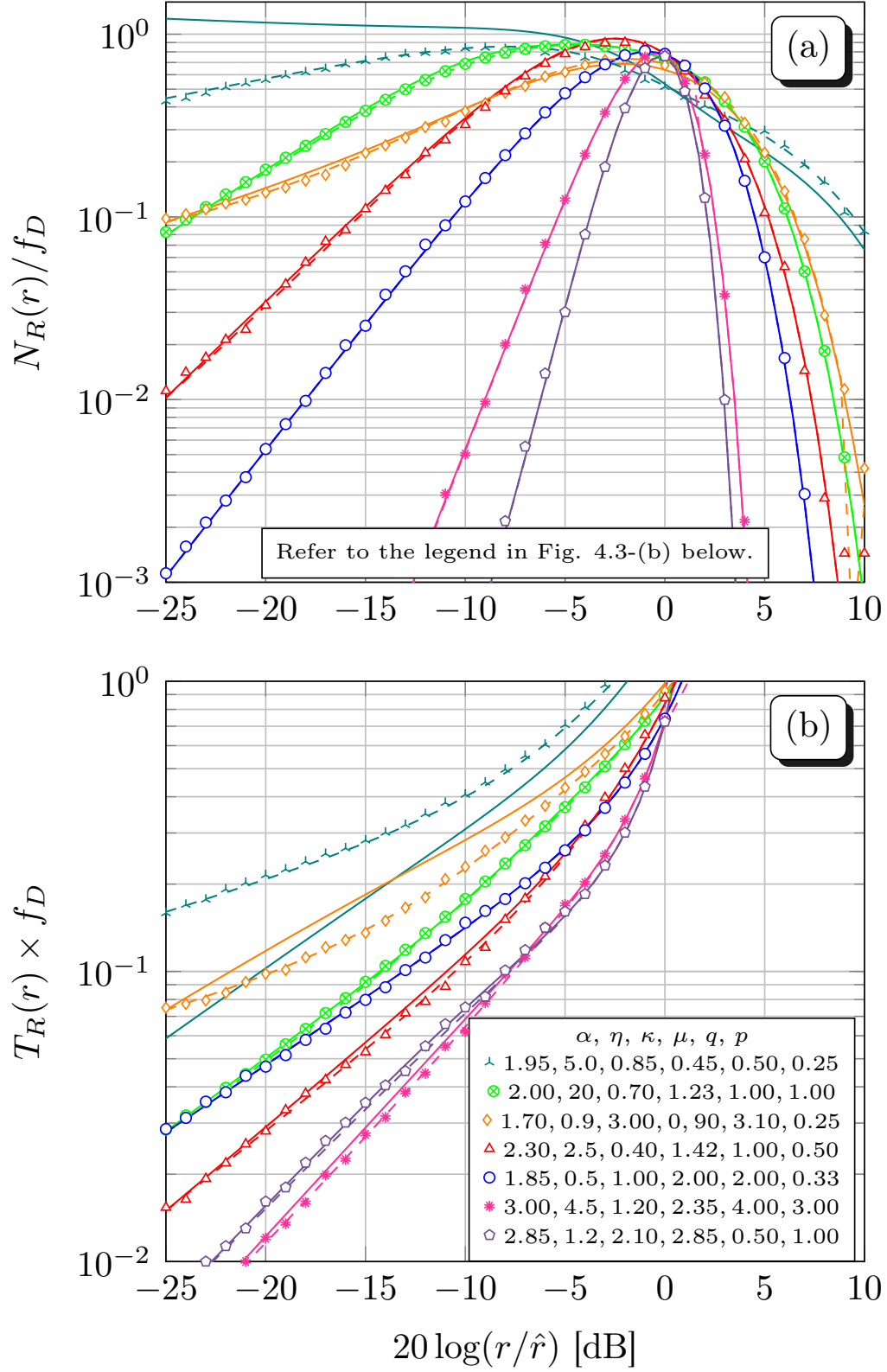


Figure 4.3 – LCR and AFD of the proposed α - η - κ - μ simulator versus theoretical fading model's statistics. (fading model: solid; proposed simulator, analytical: dashed; proposed simulator, empirical: markers).

To our best knowledge, the simulation framework proposed here is the only available solution to date for generating autocorrelated sequences of α - μ , η - μ , κ - μ , and α - η - κ - μ fading processes with real arbitrary values of the μ -parameter, as well as of all other fading parameters.

4.2 Numerical Results for the Proposed Asymptotic Analysis

In this section, considering particular fading models and various correlation scenarios for the in-phase and quadrature components, the asymptotic expressions of LCR and AFD derived in Chapter 3.2 for a general Gaussian-class fading model are validated through Monte Carlo simulations.

Initially, a sequence of $N = 10^7$ realizations was generated for each autocorrelated Gaussian multipath cluster X_i , $i \in \{1, \dots, M\}$, with zero mean, forming an array \mathbf{X}_i of dimension $M \times N$. The autocorrelation of each sequence X_i was adjusted according to the traditional Jakes/Clark model [74]. So, the mean vector \mathbf{m} and the covariance matrix $\mathbf{\Sigma}$ were included via $\mathbf{X} = \mathbf{C}\mathbf{X}_i + \mathbf{m}$, where \mathbf{C} is the Cholesky decomposition of the covariance matrix, that is, $\mathbf{\Sigma} = \mathbf{C}\mathbf{C}^T$ [83, 84]. Finally, the M lines of \mathbf{X} were combined as in (3.1), resulting in a $1 \times N$ sequence for the channel power B and for the envelope R , since $R = \sqrt{B}$. Using the R -sequence, the empirical LCR and AFD were then calculated.

The LCR is shown in Fig. 4.4-(a), Fig. 4.5-(a), and Fig. 4.6-(a), and the AFD, in Fig. 4.4-(b), Fig. 4.5-(b), and Fig. 4.6-(b). In these figures, (i) the asymptotic analytical solutions are represented by solid lines, (ii) the simulation results are represented by markers, and (iii) the theoretical expressions, numerically calculated by Brennan's method [78], are represented by dashed lines.

In Fig. 4.4-(a) and Fig. 4.4-(b), which share the same legend, some well-known fading distributions are illustrated [19, 23]. The asymptotic expressions depicted are those presented in Section 3.2.3. Fig. 4.5-(a) and Fig. 4.5-(b) consider the commutative scenario, described in Section 3.2.2.3, where the asymptotic solutions of the LCR and AFD are given by (3.37) and (3.38). Finally, the correlated and uncorrelated in-phase-quadrature scenarios, described in Section 3.2.2.1 and 3.2.2.2, are illustrated in Fig. 4.6-(a) and Fig. 4.6-(b), in which the asymptotic analytical expressions of the LCR and AFD are given by (3.31), (3.25), (3.32), and (3.26). In all scenarios considered, the fading parameters were chosen at random.

Observe that, in the asymptotic region ($r \rightarrow 0$), the analytical and simulated statistics coincide perfectly with each other for all the fading scenarios, as expected. In addition, the asymptotic expressions have a good overall fit for $r < 0$ dB, the region that

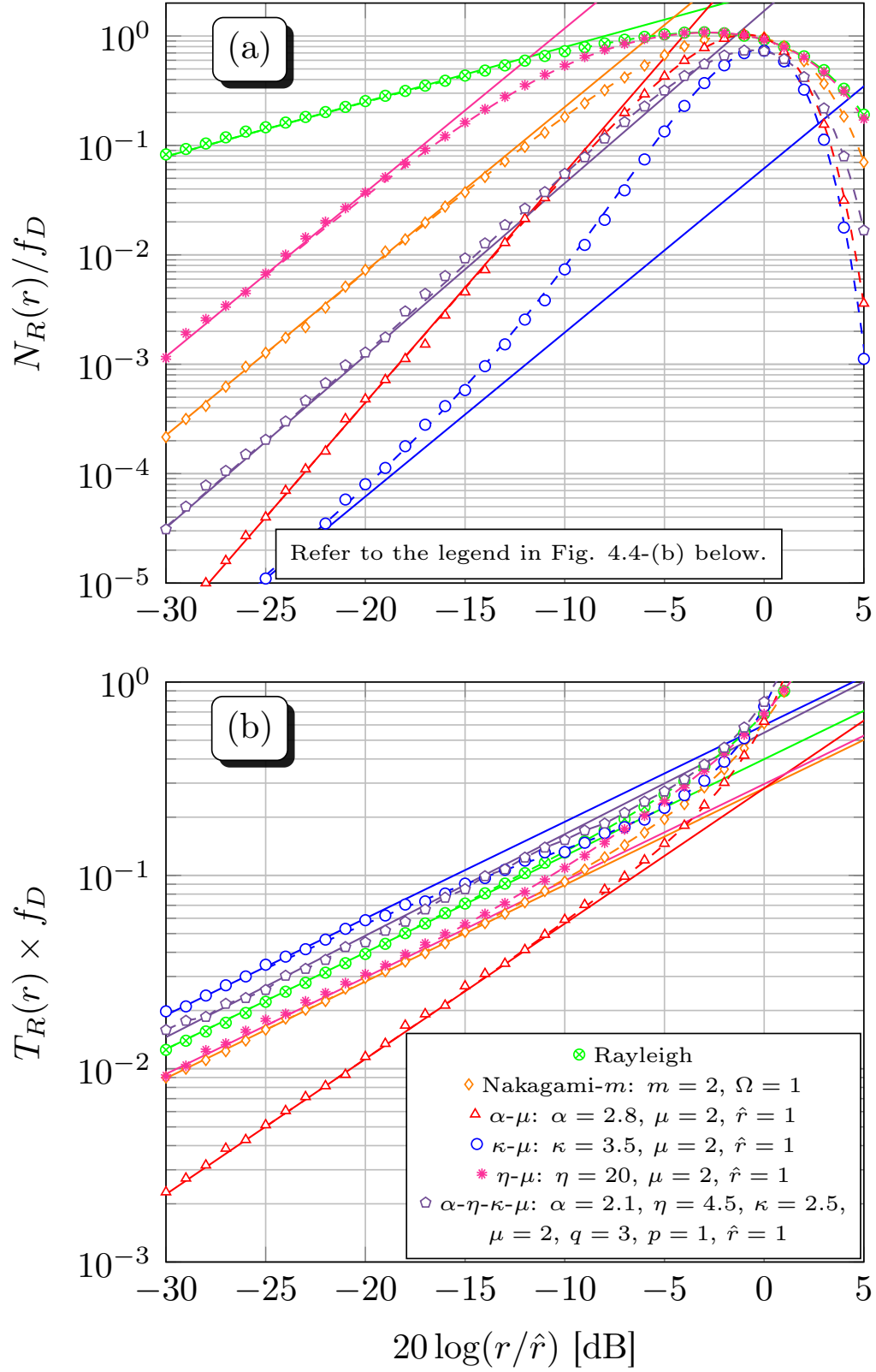


Figure 4.4 – Analytical-asymptotic (solid lines), simulated (markers), and theoretical (dashed lines) LCR and AFD for known particular cases of the Gaussian-class fading model.

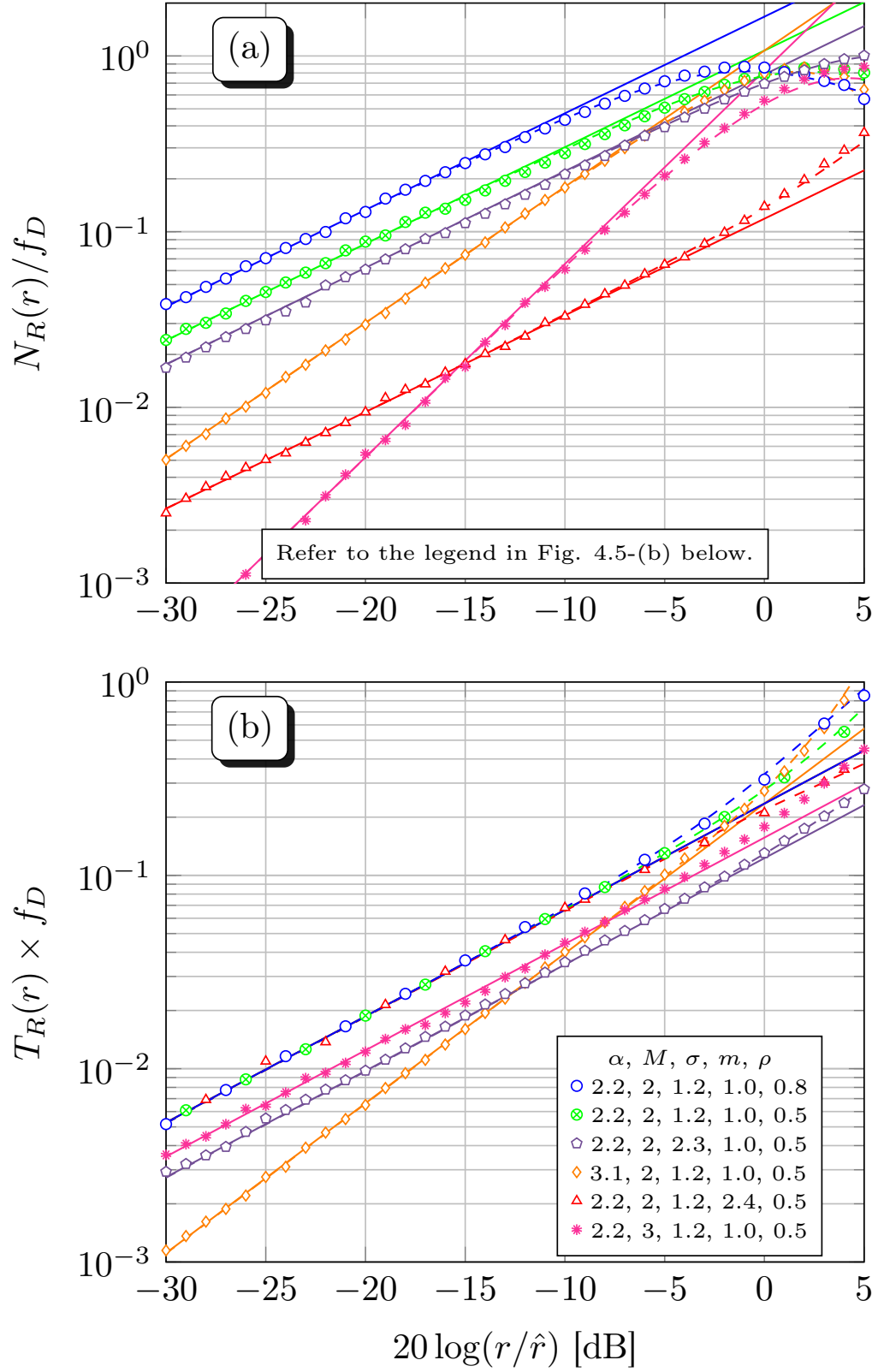


Figure 4.5 – Analytical-asymptotic (solid lines), simulated (markers), and theoretical (dashed lines) LCR and AFD for the commutative scenario of the Gaussian-class fading model.

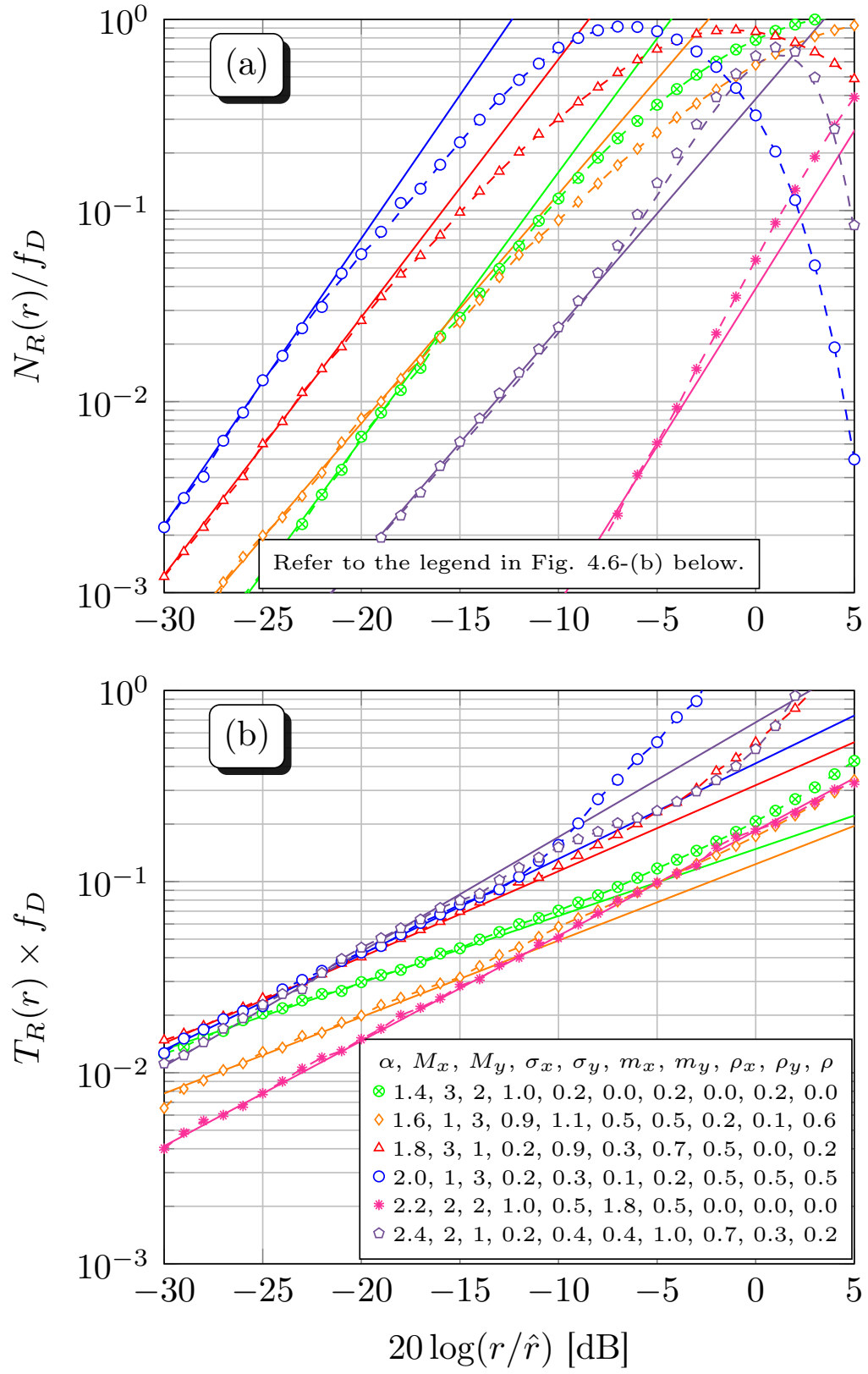


Figure 4.6 – Analytical-asymptotic (solid lines), simulated (markers), and theoretical (dashed lines) LCR and AFD for various in-phase-quadrature scenarios of the Gaussian-class fading model.

governs the high SNR (average) performance [62], most important in practical wireless applications. Moreover, the asymptotic statistics derived here were implemented simply and quickly for all scenarios.

The asymptotic expressions provided here for the dynamic fading metrics were validated for different propagation scenarios, proving to be a practical and useful tool to help model wireless channels in emerging applications.

4.3 Conclusions

In this chapter, the main goal was to show the applicability of the advanced simulation scheme and the unified asymptotic analysis proposed in Chapters 2 and 3, respectively, for several known fading scenarios such as α - μ , η - μ , κ - μ , and α - η - κ - μ , as well as for more general scenarios such as the Gaussian-class fading model in (3.1). Monte Carlo simulations attested the efficiency of the proposed solutions.

The simulation scheme and the unified asymptotic analysis proposed in this work for the different fading environments were both validated through well-known second-order statistics, namely LCR and AFD. To this end, the output sequence of the proposed simulator and the asymptotic statistics were compared with the theoretical statistics of the analyzed fading models. Several fading scenarios were addressed and, in all cases, the simulation results and the asymptotic analysis coincided with the fading model's theoretical statistics.

The simulation framework proposed here produces fading samples that mimic the dynamic behavior of the communication channel for arbitrary real values of the fading parameters, including the μ -parameter. As far as we know, this is the only existing simulation scheme that considers the first- and second-order statistics of the α - μ , η - μ , κ - μ , and α - η - κ - μ fading models while covering arbitrary real values for all fading parameters. Additionally, the asymptotic analysis provided here for the second-order statistics proved to be accurate in the high SNR region of operation. The analysis considers the correlation between multipath clusters, a condition not previously addressed in the literature, yet realistic for current and emerging propagation scenarios.

5 Final Words

This chapter highlights the main contributions of this dissertation and suggests a few research directions for future related works.

5.1 Concluding Remarks

In this thesis, we approached three aspects in the field of wireless fading channels: (i) the development of a simulation framework for autocorrelated fading sequences that contemplates well-known fading distributions in the literature; (ii) the derivation of an asymptotic analysis for key second-order statistics of a general Gaussian-class fading model; and (iii) the validation of these contributions through extensive Monte Carlo simulations.

In the first part of this dissertation (Chapter 2), we focused on the design and analysis of a general and unified simulation method for α - μ , η - μ , κ - μ , and α - η - κ - μ fading channels that (i) embraces arbitrary real values of the μ -parameter. Not less importantly, the proposed method (ii) matches the exact first-order statistics of the fading models and (iii) closely approaches their second-order statistics. The method relies on a cascade of two simulation techniques: random mixture [69] and rank matching [70], a combination that has proven effective for Nakagami- m fading [19, 21, 22, 53]. To our knowledge, this is the only simulator available that meets the requirements (i)–(iii) for the referred fading models. In addition, we develop a new simple approach for optimizing the random-mixture stage and, as a byproduct, we derive new series representations and asymptotic coefficients for essential first- and second-order statistics of the fading models analyzed here. These representations and coefficients constitute a valuable original contribution of this work, which can be used elsewhere in the analysis and design of communication systems over fading channels.

In the second part of this dissertation (Chapter 3), we investigated the time-varying nature of Gaussian-based random processes. The general fading model analyzed is composed of multipath clusters with arbitrary specular components and arbitrary multipath powers propagating in a non-linear environment. Unlike other models in the literature, which assume independence among the clusters or among their in-phase and quadrature components, the investigated model allows them to be arbitrarily correlated, a more realistic assumption to model wireless channels in 5G, 6G and beyond. We proposed an asymptotic analysis for the dynamic metrics of a general class of fading mod-

els [42]. More specifically, we provide new, simple, closed-form expressions for fundamental second-order statistics in high SNR regime, namely LCR and AFD. The analysis is rather comprehensive and was simplified for many particular cases, ranging from Rayleigh distribution to the ultrageneralized α - η - κ - μ distribution, in addition to various correlation scenarios for the in-phase and quadrature components, described and derived here. This analysis seeks to overcome the inherent complexity of the exact approach for higher-order statistics when several physical fading parameters are considered, mainly the correlation between multipath clusters. So, a comprehensive analysis has been introduced at high SNR, a prime regime for most applications, and can be readily applied to evaluate, design, and optimize emerging wireless systems operating in a broad family of propagation scenarios. As an example of promising technology that can benefit from the proposed analysis, mmWave and RIS communications over fading channels are strongly impacted by intracluster correlation [8, 42].

Finally, in the third part of this dissertation (Chapter 4), we provided an extensive validation of the fading simulator proposed in Chapter 2 and the asymptotic analysis proposed in Chapter 3, through Monte Carlo simulations for many different fading scenarios. The second-order statistics, LCR and AFD, were analyzed. It was observed that the analytical and empirical statistics for the proposed simulation schemes (Chapter 2) perfectly match each other and, in general, the simulator's statistics maintain an excellent agreement with the fading models' statistics over the whole range of envelope values. For the proposed asymptotic analysis (Chapter 3), it was observed that, in the asymptotic region, that is, as $r \rightarrow 0$, the analytical and empirical statistics coincide perfectly with each other, as expected, in all the fading scenarios considered. Our solutions proved to be easy, simple, and quick to implement in all those sample examples. This further emphasizes the usefulness of the simulation scheme and asymptotic analysis proposed in this dissertation to model and simulate the dynamic statistics of generalized fading channels.

5.2 Future Research Directions

Some possible directions for future related works are summarized next.

1. An immediate research direction would be the improvement of the fading samples simulator, proposed here for well-known channels, by extending it to cover the general Gaussian-class model discussed in Chapter 3. The objective would be to generate fading samples propagating in a non-linear environment, with arbitrary values of dominant and scattered powers. Furthermore, the samples may bear an arbitrary correlation between an arbitrary real number of multipath clusters. The

validation of the statistics produced by that extended simulator can be attained through the analysis of the theoretical asymptotic statistics discussed here.

2. Another research direction is to obtain the asymptotic second-order statistics of series, parallel, and mixed combinations of multiple independent random processes associated with Gaussian-class fading channels, according to the model discussed in [85]. Then, in addition to considering the correlation between the clusters within each channel, one can consider the correlation between the multiple random processes belonging to the serial, parallel, and mixed combinations of channels. The analysis of such channel combinations is useful in the development of emerging technologies such as RIS communications [14, 15, 86].
3. A third research direction would be to build on the Gaussian Field Theory [87] to design a realistic spatial simulation of fading processes, considering a two- or three-dimensional propagation scenario for the various fading models.

Bibliography

- [1] S. Cherry, “Edholm’s Law of Bandwidth,” *IEEE Spectr.*, vol. 41, no. 7, pp. 58–60, 2004.
- [2] T. Kürner and S. Priebe, “Towards THz Communications-status in Research, Standardization and Regulation,” *Journal of Infrared, Millimeter, and Terahertz Waves*, vol. 35, no. 1, pp. 53–62, 2014.
- [3] G. Davis, “2020: Life with 50 Billion Connected Devices,” in *IEEE International Conference on Consumer Electronics (ICCE)*, 2018.
- [4] L. Ericsson, “More than 50 Billion Connected Devices,” *White Paper*, vol. 14, no. 1, 2011.
- [5] J. G. Andrews, S. Buzzi, W. Choi, S. V. Hanly, A. Lozano, A. C. K. Soong, and J. C. Zhang, “What Will 5G Be?” *IEEE J. Sel. Areas Commun.*, vol. 32, no. 6, pp. 1065–1082, Jun. 2014.
- [6] S. Amakawa, Z. Aslam, J. Buckwater, S. Caputo, A. Chaoub, Y. Chen, Y. Corre, M. Fujishima, Y. Ganghua, and S. Gao, “White Paper on RF Enabling 6G—Opportunities and Challenges from Technology to Spectrum,” *University of Oulu*, 2021.
- [7] M. Banafaa, I. Shayea, J. Din, M. H. Azmi, A. Alashbi, Y. I. Daradkeh, and A. Alhammadi, “6G Mobile Communication Technology: Requirements, Targets, Applications, Challenges, Advantages, and Opportunities,” *Alexandria Engineering Journal*, 2022.
- [8] N. Iqbal, J. Luo, R. Müller, G. Steinböck, C. Schneider, D. A. Dupleich, S. Häfner, and R. S. Thomä, “Multipath Cluster Fading Statistics and Modeling in Millimeter-Wave Radio Channels,” *IEEE Trans. Antennas Propag.*, vol. 67, no. 4, pp. 2622–2632, Jan. 2019.
- [9] T. S. Rappaport, G. R. MacCartney, S. Sun, H. Yan, and S. Deng, “Small-Scale, Local Area, and Transitional Millimeter Wave Propagation for 5G Communications,” *IEEE Trans. Antennas Propag.*, vol. 65, no. 12, pp. 6474–6490, 2017.
- [10] X. Chen, G. Liu, Z. Ma, X. Zhang, W. Xu, and P. Fan, “Optimal Power Allocations for Non-Orthogonal Multiple Access Over 5G Full/Half-Duplex Relaying Mobile Wireless Networks,” *IEEE Trans. Wireless Commun.*, vol. 18, no. 1, pp. 77–92, 2019.

- [11] J. Zheng, Q. Zhang, and J. Qin, "Average Block Error Rate of Downlink NOMA Short-Packet Communication Systems in Nakagami- m Fading Channels," *IEEE Commun. Lett.*, vol. 23, no. 10, pp. 1712–1716, 2019.
- [12] M. Matthaiou, P. J. Smith, H. Q. Ngo, and H. Tataria, "Does Massive MIMO Fail in Ricean Channels?" *IEEE Wireless Commun. Lett.*, vol. 8, no. 1, pp. 61–64, 2019.
- [13] C. L. Miller, P. J. Smith, P. A. Dmochowski, H. Tataria, and M. Matthaiou, "Analytical Framework for Full-Dimensional Massive MIMO With Ray-Based Channels," *IEEE J. Sel. Topics Signal Process.*, vol. 13, no. 5, pp. 1181–1195, 2019.
- [14] Y. Han, W. Tang, S. Jin, C. Wen, and X. Ma, "Large Intelligent Surface-Assisted Wireless Communication Exploiting Statistical CSI," *IEEE Trans. Veh. Technol.*, vol. 68, no. 8, pp. 8238–8242, 2019.
- [15] B. Di, H. Zhang, L. Song, Y. Li, Z. Han, and H. V. Poor, "Hybrid Beamforming for Reconfigurable Intelligent Surface based Multi-User Communications: Achievable Rates With Limited Discrete Phase Shifts," *IEEE J. Sel. Areas Commun.*, vol. 38, no. 8, pp. 1809–1822, 2020.
- [16] M. D. Yacoub, *Foundations of Mobile Radio Engineering*. Routledge, 2019.
- [17] D. Tse and P. Viswanath, *Fundamentals of Wireless Communication*. Cambridge University Press, 2005.
- [18] T. S. Rappaport, *Wireless Communications: Principles and Practice*. Prentice Hall PTR New Jersey, 1996, vol. 2.
- [19] M. D. Yacoub, "The α - η - κ - μ Fading Model," *IEEE Trans. Antennas Propag.*, vol. 64, no. 8, pp. 3597–3610, Aug. 2016.
- [20] L. Rayleigh, "XII. On the Resultant of a Large Number of Vibrations of the same Pitch and of Arbitrary Phase," *The London, Edinburgh, and Dublin Philos. Mag. and J. of Sci.*, vol. 10, no. 60, pp. 73–78, 1880.
- [21] M. D. Yacoub, "The α - μ Distribution: A Physical Fading Model for the Stacy Distribution," *IEEE Trans. Veh. Technol.*, vol. 56, no. 1, pp. 27–34, Jan. 2007.
- [22] M. D. Yacoub, "The κ - μ Distribution and the η - μ Distribution," *IEEE Antennas Propag. Mag.*, vol. 49, no. 1, pp. 68–81, Feb. 2007.
- [23] A. A. Dos Anjos, T. R. R. Marins, C. R. N. Da Silva, V. M. R. Peñarrocha, L. Rubio, J. Reig, R. A. A. De Souza, and M. D. Yacoub, "Higher Order Statistics in a mmWave Propagation Environment," *IEEE Access*, vol. 7, pp. 103 876–103 892, Jul. 2019.

- [24] S. O. Rice, "Statistical Properties of Random Noise Currents," *Selected Papers on Noise and Stochastic Processes*, 1954.
- [25] R. S. Hoyt, "Probability Functions for the Modulus and Angle of the Normal Complex Variate," *The Bell System Technical Journal*, vol. 26, no. 2, pp. 318–359, 1947.
- [26] W. Weibull, "A Statistical Distribution Function of Wide Applicability," *Journal of applied mechanics*, 1951.
- [27] M. Nakagami, "The m -distribution: A General Formula of Intensity Distribution of Rapid Fading," in *Statistical Methods in Radio Wave Propagation*. Elsevier, 1960, pp. 3–36.
- [28] P. K. Chong, S. Yoo, S. H. Kim, and D. Kim, "Wind-Blown Foliage and Human-Induced Fading in Ground-Surface Narrowband Communications at 400 MHz," *IEEE Trans. Veh. Technol.*, vol. 60, no. 4, pp. 1326–1336, May 2011.
- [29] V. M. Rodrigo-Penarrocha, J. Reig, L. Rubio, H. Fernandez, and S. Loredó, "Analysis of Small-scale Fading Distributions in Vehicle-to-Vehicle Communications," *Mobile Information Systems*, 2016.
- [30] S. K. Yoo, P. C. Sofotasios, S. L. Cotton, M. Matthaiou, M. Valkama, and G. K. Karagiannidis, "The η - μ / Inverse Gamma Composite Fading Model," in *IEEE 26th Annual International Symposium on Personal, Indoor, and Mobile Radio Communications (PIMRC)*, Aug. 2015, pp. 166–170.
- [31] N. Bhargav, S. L. Cotton, and D. B. Smith, "An Experimental-Based Analysis of Inter-BAN Co-Channel Interference Using the κ - μ Fading Model," *IEEE Trans. Antennas Propag.*, vol. 65, no. 2, pp. 983–988, Feb. 2017.
- [32] J. F. Paris, "Statistical Characterization of κ - μ Shadowed Fading," *IEEE Trans. Veh. Technol.*, vol. 63, no. 2, pp. 518–526, Feb. 2014.
- [33] F. J. Canete, J. Lopez-Fernandez, C. Garca-Corrales, A. Sanchez, E. Robles, F. J. Rodrigo, and J. F. Paris, "Measurement and Modeling of Narrowband Channels for Ultrasonic Underwater Communications," *Sensors*, vol. 16, no. 2, p. 256, 2016.
- [34] M. G. Doone, S. L. Cotton, and C. Oestges, "An Experimental Investigation into the Impact of Vehicular Traffic on Interpersonal Wearable-to-Wearable Communications Channels," *IEEE Trans. Antennas Propag.*, vol. 65, no. 10, pp. 5418–5430, Oct. 2017.
- [35] P. Karadimas, E. D. Vagenas, and S. A. Kotsopoulos, "On the Scatterers' Mobility and Second Order Statistics of Narrowband Fixed Outdoor Wireless Channels," *IEEE Trans. Wireless Commun.*, vol. 9, no. 7, pp. 2119–2124, Jul. 2010.

- [36] G. Fraidenraich and M. D. Yacoub, "The α - η - μ and α - κ - μ Fading Distributions," in *IEEE 9th International Symposium on Spread Spectrum Techniques and Applications*, 2006, pp. 16–20.
- [37] X. Li, X. Chen, J. Zhang, Y. Liang, and Y. Liu, "Capacity Analysis of α - η - κ - μ Fading Channels," *IEEE Commun. Lett.*, vol. 21, no. 6, pp. 1449–1452, Jun. 2017.
- [38] A. A. dos Anjos, T. R. R. Marins, R. A. A. de Souza, and M. D. Yacoub, "Higher Order Statistics for the α - η - κ - μ Fading Model," *IEEE Trans. Antennas Propag.*, vol. 66, no. 6, pp. 3002–3016, Jun. 2018.
- [39] A. Mathur, Y. Ai, M. R. Bhatnagar, M. Cheffena, and T. Ohtsuki, "On Physical Layer Security of α - η - κ - μ Fading Channels," *IEEE Commun. Lett.*, vol. 22, no. 10, pp. 2168–2171, Oct. 2018.
- [40] A. Goswami and A. Kumar, "Performance Analysis of Multi-Hop Wireless Communication Systems Over α - η - κ - μ Channel," *Physical Commun.*, vol. 33, pp. 9–15, 2019.
- [41] V. M. Rennó, R. A. A. de Souza, and M. D. Yacoub, "On the Generation of White Samples in Severe Fading Conditions," *IEEE Commun. Lett.*, vol. 23, no. 1, pp. 180–183, Jan. 2019.
- [42] F. R. A. Parente, F. d. P. Calmon, and J. C. S. Santos Filho, "High-SNR Performance in Gaussian-Class Fading," in *IEEE International Conference on Communications (ICC)*, 2020, pp. 1–7.
- [43] S. Sun, T. S. Rappaport, M. Shafi, P. Tang, J. Zhang, and P. J. Smith, "Propagation Models and Performance Evaluation for 5G Millimeter-Wave Bands," *IEEE Trans. Veh. Technol.*, vol. 67, no. 9, pp. 8422–8439, 2018.
- [44] S. Schwarz, E. Zöchmann, M. Müller, and K. Guan, "Dependability of Directional Millimeter Wave Vehicle-to-Infrastructure Communications," *IEEE Access*, vol. 8, pp. 53 162–53 171, 2020.
- [45] Y. S. Chow and H. Teicher, *Probability theory: Independence, Interchangeability, Martingales*. Springer Science & Business Media, 2003.
- [46] A. Abdi, K. Wills, H. A. Barger, M. S. Alouini, and M. Kaveh, "Comparison of the Level Crossing Rate and Average Fade Duration of Rayleigh, Rice and Nakagami Fading Models with Mobile Channel Data," in *IEEE 52nd Vehicular Technology Conference*, vol. 4, 2000, pp. 1850–1857 vol.4.

- [47] M. D. Yacoub, J. E. V. Bautista, and L. G. R. Guedes, "On Higher Order Statistics of the Nakagami- m Distribution," *IEEE Trans. Veh. Technol.*, vol. 48, no. 3, pp. 790–794, May 1999.
- [48] D. B. da Costa, J. C. S. Santos Filho, M. D. Yacoub, and G. Fraidenraich, "Second-Order Statistics of η - μ Fading Channels: Theory and Applications," *IEEE Trans. Wireless Commun.*, vol. 7, no. 3, pp. 819–824, Mar. 2008.
- [49] S. L. Cotton and W. G. Scanlon, "Higher-order Statistics for κ - μ Distribution," *Electron. Lett.*, vol. 43, no. 22, Oct. 2007.
- [50] A. A. Dos Anjos, T. R. R. Marins, C. R. N. da Silva, V. M. R. Peñarrocha, L. Rubio, J. Reig, R. A. A. De Souza, and M. D. Yacoub, "Higher Order Statistics in a mmWave Propagation Environment," *IEEE Access*, vol. 7, pp. 103 876–103 892, 2019.
- [51] T. G. Newman and P. L. Odell, *The Generation of Random Variates*. London, U.K.: Charles Griffin, 1971.
- [52] A. Papoulis and S. U. Pillai, *Probability, Random Variables and Stochastic Processes*. New York: McGraw-Hill, 2002.
- [53] J. C. S. Santos Filho, B. V. Teixeira, M. D. Yacoub, and G. T. F. Abreu, "The RM² Nakagami Fading Channel Simulator," *IEEE Trans. Wireless Commun.*, vol. 12, no. 5, pp. 2323–2333, May 2013.
- [54] N. Beaulieu and C. Cheng, "Efficient Nakagami- m Fading Channel Simulation," *IEEE Trans. Veh. Technol.*, vol. 54, no. 2, pp. 413–424, 2005.
- [55] Q. M. Zhu, X. Y. Dang, D. Z. Xu, and X. M. Chen, "Highly Efficient Rejection Method for Generating Nakagami- m Sequences," *Electronics letters*, vol. 47, no. 19, p. 1, 2011.
- [56] R. Cogliatti, R. A. A. de Souza, and M. D. Yacoub, "Practical, Highly Efficient Algorithm for Generating κ - μ and η - μ Variates and a Near-100% Efficient Algorithm for Generating α - μ Variates," *IEEE Commun. Lett.*, vol. 16, no. 11, pp. 1768–1771, 2012.
- [57] R. A. A. de Souza, A. M. O. Ribeiro, and D. Guimarães, "On the Efficient Generation of α - κ - μ and α - η - μ White Samples with Applications," *Int. J. of Antennas and Propag.*, 2015.
- [58] J. C. S. Santos Filho and M. D. Yacoub, "Coloring Non-Gaussian Sequences," *IEEE Trans. Signal Process.*, vol. 56, no. 12, pp. 5817–5822, Dec. 2008.

- [59] B. Liu and D. Munson, "Generation of a Random Sequence having a Jointly Specified Marginal Distribution and Autocovariance," *IEEE Trans. Acoust., Speech, Signal Process.*, vol. 30, no. 6, pp. 973–983, 1982.
- [60] N. C. Beaulieu and K. T. Hemachandra, "Novel Simple Representations for Gaussian Class Multivariate Distributions With Generalized Correlation," *IEEE Trans. Inf. Theory*, vol. 57, no. 12, pp. 8072–8083, 2011.
- [61] M. D. Kulkarni and A. B. Kostinski, "A Simple Formula for Monitoring Quadrature Phase Error with Arbitrary Signals," *IEEE Trans. Geosci. Remote Sens.*, vol. 33, no. 3, pp. 799–802, 1995.
- [62] Z. Wang and G. B. Giannakis, "A Simple and General Parameterization Quantifying Performance in Fading Channels," *IEEE Trans. Commun.*, vol. 51, no. 8, pp. 1389–1398, Aug. 2003.
- [63] A. Chaaban, Z. Rezki, and M. Alouini, "Capacity Bounds and High-SNR Capacity of MIMO Intensity-Modulation Optical Channels," *IEEE Trans. Wireless Commun.*, vol. 17, no. 5, pp. 3003–3017, May 2018.
- [64] H. Kazemi and H. Haas, "Downlink Cooperation with Fractional Frequency Reuse in DCO-OFDMA Optical Attocell Networks," in *IEEE International Conference on Communications (ICC)*, 2016, pp. 1–6.
- [65] J. Si, Z. Li, J. Cheng, and C. Zhong, "Asymptotic Secrecy Outage Performance for TAS/MRC Over Correlated Nakagami- m Fading Channels," *IEEE Trans. Commun.*, vol. 67, no. 11, pp. 7700–7714, 2019.
- [66] L. Kong, G. Kaddoum, and Z. Rezki, "Highly Accurate and Asymptotic Analysis on the SOP Over SIMO α - μ Fading Channels," *IEEE Commun. Lett.*, vol. 22, no. 10, pp. 2088–2091, 2018.
- [67] N. Varshney, A. K. Jagannatham, and L. Hanzo, "Asymptotic SER Analysis and Optimal Power Sharing for Dual-Phase and Multi-Phase Multiple-Relay Cooperative Systems," *IEEE Access*, vol. 6, pp. 50 404–50 423, 2018.
- [68] B. Zhu, J. Cheng, H. T. Cheng, R. Selea, and L. Wu, "An Asymptotic Study of Hierarchical Diversity Reception Over Rician Channels With Arbitrary Correlation," *IEEE Trans. Veh. Technol.*, vol. 65, no. 5, pp. 3299–3311, 2016.
- [69] G. T. F. Abreu, "On the Moment-Determinance and Random Mixture of Nakagami- m Variates," *IEEE Trans. Commun.*, vol. 58, no. 9, pp. 2561–2575, Sep. 2010.

- [70] J. C. S. Santos Filho, M. D. Yacoub, and G. Fraidenraich, "A Simple Accurate Method for Generating Autocorrelated Nakagami- m Envelope Sequences," *IEEE Commun. Lett.*, vol. 11, no. 3, pp. 231–233, Mar. 2007.
- [71] M. Abramowitz and I. A. Stegun, *Handbook of Mathematical Functions with Formulas, Graphs, and Mathematical Tables*. New York: Dover, 1972.
- [72] J. Marcum, "A Statistical Theory of Target Detection by Pulsed Radar," *IRE Trans. Inf. Theory*, vol. 6, no. 2, pp. 59–267, Apr. 1960.
- [73] C. R. N. da Silva, G. R. D. L. Tejerina, and M. D. Yacoub, "The α - η - κ - μ Fading Model: New Fundamental Results," *IEEE Trans. Antennas Propag.*, vol. 68, no. 1, pp. 443–454, 2020.
- [74] W. C. Jakes, *Microwave Mobile Communications*. Wiley, 1974.
- [75] "Taylor series," <https://mathworld.wolfram.com/>, accessed: 2023-06-02.
- [76] V. Perim, J. D. V. Sanchez, and J. C. S. Santos Filho, "Asymptotically Exact Approximations to Generalized Fading Sum Statistics," *IEEE Trans. Wireless Commun.*, vol. 19, no. 1, pp. 205–217, 2020.
- [77] A. Jeffrey and D. Zwillinger, *Table of Integrals, Series, and Products*. Elsevier, 2007.
- [78] D. G. Brennan, "Linear Diversity Combining Techniques," *Proc. IRE*, vol. 47, no. 6, pp. 1075–1102, Jun. 1959.
- [79] F. R. A. Parente and J. C. S. Santos Filho, "Asymptotically Exact Framework to Approximate Sums of Positive Correlated Random Variables and Application to Diversity-Combining Receivers," *IEEE Wireless Commun. Lett.*, vol. 8, no. 4, pp. 1012–1015, Aug. 2019.
- [80] I. B. G. Pôrto and M. D. Yacoub, "On the Phase Statistics of the κ - μ Process," *IEEE Trans. Wireless Commun.*, vol. 15, pp. 4732–4744, Jul. 2016.
- [81] T. R. R. Marins *et al.*, "Fading Evaluation in the mm-Wave Band," *IEEE Trans. Commun.*, vol. 67, no. 12, pp. 8725–8738, Sep. 2019.
- [82] V. M. Rennó, "Geração de Amostras do Modelo de Desvanecimento α - η - κ - μ e Aplicações," Master's thesis, Instituto Nacional de Telecomunicações, 2018.
- [83] R. A. Horn and C. R. Johnson, *Matrix analysis*. Cambridge university press, 2012, vol. 1.

-
- [84] “Cholesky factorization,” <https://www.mathworks.com/help/matlab/ref/chol.html>, accessed: 2023-06-01.
- [85] L. Yang and M.-s. Alouini, “Level Crossing Rate over Multiple Independent Random Processes: an Extension of the Applicability of the Rice Formula,” *IEEE Trans. Wireless Commun.*, vol. 6, no. 12, pp. 4280–4284, 2007.
- [86] G. R. L. Tejerina, C. R. N. Silva, R. A. A. Souza, and M. D. Yacoub, “On the Extended η - μ Model: New Results and Applications to IRS-Aided Systems,” *IEEE Trans. Veh. Technol.*, vol. 72, no. 4, pp. 4133–4142, 2023.
- [87] N. Kang and N. G. Makarov, “Gaussian Free Field and Conformal Field Theory,” *Mathematics Subject Classification*, 2011.

Appendices

APPENDIX A – Supporting Material for Chapter 2

A.1 Illustrative Example for the Proposed Simulator

Consider the proposed simulator for the α - μ , η - μ , and κ - μ (δ - μ , generically) fading channels, shown in Fig. A.1, and the proposed simulator for the α - η - κ - μ fading channel, shown in Fig. A.2. In this section, to aid understanding, we illustrate the simulation process through the generation of an output sequence \check{R} consisting of 9 samples.

First, two reference sequences are generated using the classic simulation method. Assume that, for a given mixture probability value, the reference sequence R_L (shown in orange) with fading parameters δ , μ_L , and \hat{r} (Fig. A.1), or α , η , κ , μ_L , q , p_L , and \hat{r} (Fig. A.2), consists of 4 samples. Accordingly, assume that the reference sequence R_U (shown in blue) with fading parameters δ , μ_U , and \hat{r} (Fig. A.1), or α , η , κ , μ_U , q , p_U , and \hat{r} (Fig. A.2), consists of 5 samples. The output sequence R_{ref} (part in blue, part in orange) of the random-mixture stage is formed by concatenating R_L and R_U in any order, resulting in a 9-sample sequence.

The output of the random-mixture stage provides the input to the rank-matching stage. The global output δ - μ (Fig. A.1) or α - η - κ - μ (Fig. A.2) sequence, \check{R} , is obtained from the reference sequence R_{ref} (from the random-mixture stage) and a set of 9 δ - μ (Fig. A.1) or α - η - κ - μ (Fig. A.2) samples, R_I (shown in red), drawn independently according to the desired fading parameters δ , μ , and \hat{r} , or α , η , κ , μ , q , p , and \hat{r} . The

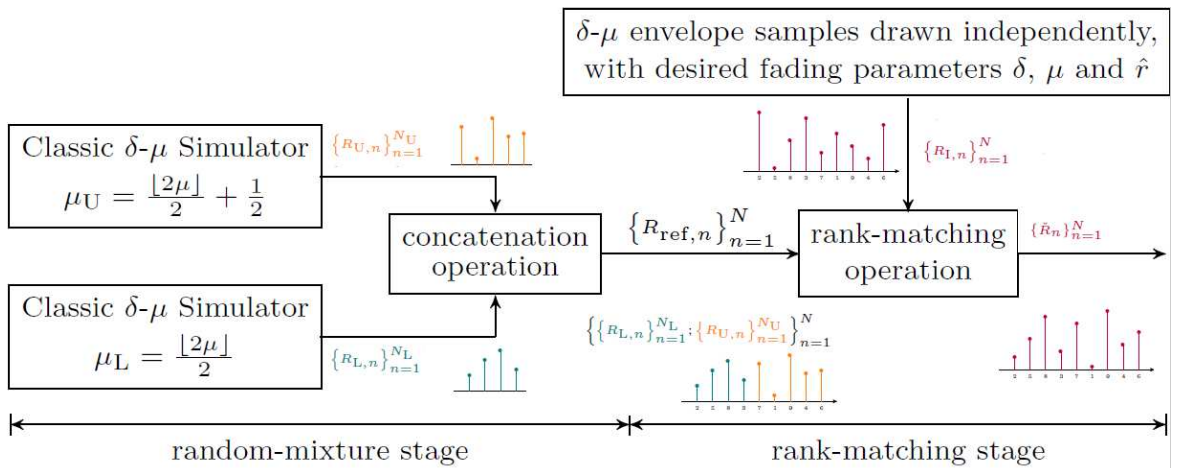


Figure A.1 – Illustrative example of the proposed simulation framework for α - μ , η - μ , and κ - μ fading.

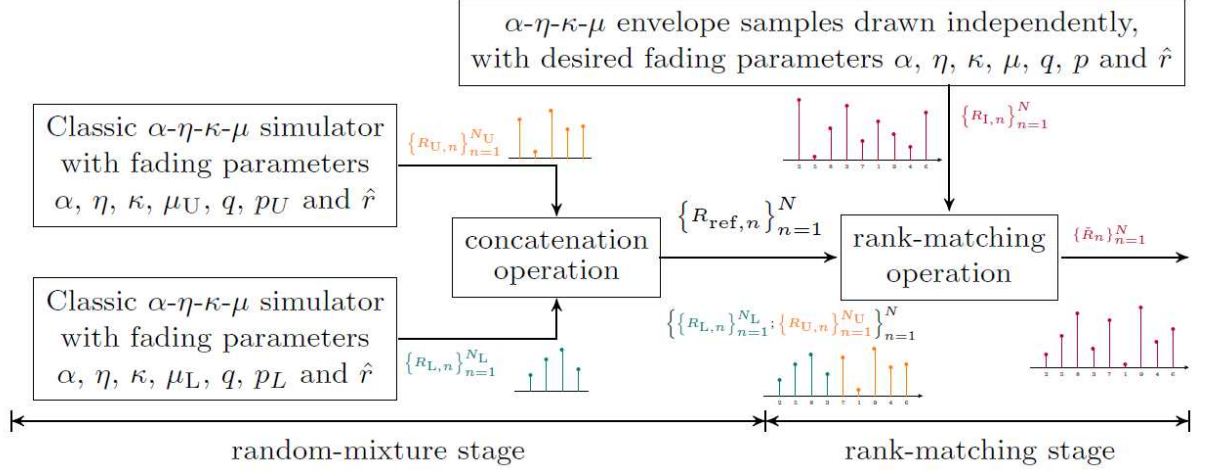


Figure A.2 – Illustrative example of the proposed simulation framework for α - η - κ - μ fading.

global output sequence \check{R} (also shown in red) is a rearrangement of the samples in R_I , such that the ranking of the samples in \check{R} exactly match that of the samples in the reference sequence R_{ref} : their minima occur in the same position, their second minima occur in the same position, and so on. In other words, the samples in \check{R} inherit their values from R_I , but their order is determined by R_{ref} .

APPENDIX B – Supporting Material for Chapter 3

B.1 The Determinant of R for Correlated In-Phase–Quadrature Components

In order to find the determinant of \mathbf{R} in in-phase and quadrature scenarios with non-zero cross correlation, we can perform elementary matrix operations. To improve the understanding of the process, we can rewrite (3.22) as follows

$$\mathbf{R} = \begin{bmatrix} 1 & \rho_x & \dots & \rho_x & \rho & \rho & \dots & \rho \\ \rho_x & 1 & \dots & \rho_x & \rho & \rho & \dots & \rho \\ \vdots & \vdots & \ddots & \vdots & \vdots & \vdots & \ddots & \vdots \\ \rho_x & \rho_x & \dots & 1 & \rho & \rho & \dots & \rho \\ \rho & \rho & \dots & \rho & 1 & \rho_y & \dots & \rho_y \\ \rho & \rho & \dots & \rho & \rho_y & 1 & \dots & \rho_y \\ \vdots & \vdots & \ddots & \vdots & \vdots & \vdots & \ddots & \vdots \\ \rho & \rho & \dots & \rho & \rho_y & \rho_y & \dots & 1 \end{bmatrix}. \quad (\text{B.1})$$

Starting from (B.1), we subtract the M_x th column from the other $M_x - 1$ columns and subtract the M th column from its other $M - 1$ to $M_x + 1$ columns, i.e.,

$$\mathbf{R}' = \begin{bmatrix} 1 - \rho_x & 0 & \dots & \rho_x & 0 & 0 & \dots & \rho \\ 0 & 1 - \rho_x & \dots & \rho_x & 0 & 0 & \dots & \rho \\ \vdots & \vdots & \ddots & \vdots & \vdots & \vdots & \ddots & \vdots \\ \rho_x - 1 & \rho_x - 1 & \dots & 1 & 0 & 0 & \dots & \rho \\ 0 & 0 & \dots & \rho & 1 - \rho_y & 0 & \dots & \rho_y \\ 0 & 0 & \dots & \rho & 0 & 1 - \rho_y & \dots & \rho_y \\ \vdots & \vdots & \ddots & \vdots & \vdots & \vdots & \ddots & \vdots \\ 0 & 0 & \dots & \rho & \rho_y - 1 & \rho_y - 1 & \dots & 1 \end{bmatrix}. \quad (\text{B.2})$$

By adding the first $M_x - 1$ lines of (B.2) to its M_x th line and adding the $M - 1$

to $M_x + 1$ lines of (B.2) to its M th line, we attain

$$\mathbf{R}'' = \begin{bmatrix} 1 - \rho_x & 0 & \dots & \rho_x & 0 & 0 & \dots & \rho \\ 0 & 1 - \rho_x & \dots & \rho_x & 0 & 0 & \dots & \rho \\ \vdots & \vdots & \ddots & \vdots & \vdots & \vdots & \ddots & \vdots \\ 0 & 0 & \dots & 1 + (M_x - 1)\rho_x & 0 & 0 & \dots & M_x\rho \\ 0 & 0 & \dots & \rho & 1 - \rho_y & 0 & \dots & \rho_y \\ 0 & 0 & \dots & \rho & 0 & 1 - \rho_y & \dots & \rho_y \\ \vdots & \vdots & \ddots & \vdots & \vdots & \vdots & \ddots & \vdots \\ 0 & 0 & \dots & M_y\rho & 0 & 0 & \dots & 1 + (M_y - 1)\rho_y \end{bmatrix}. \quad (\text{B.3})$$

Now we add the M th line, multiplied by $-1/M_y$, to each of the lines in the range of $M - 1$ to $M_x + 1$ lines. Finally, we add the M_x th line, multiplied by $(-M_y\rho)/(1 + (M_x)\rho_x)$, to the M th line, resulting in

$$\mathbf{R}''' = \begin{bmatrix} 1 - \rho_x & 0 & \dots & \rho_x & 0 & 0 & \dots & \rho \\ 0 & 1 - \rho_x & \dots & \rho_x & 0 & 0 & \dots & \rho \\ \vdots & \vdots & \ddots & \vdots & \vdots & \vdots & \ddots & \vdots \\ 0 & 0 & \dots & 1 + (M_x - 1)\rho_x & 0 & 0 & \dots & M_x\rho \\ 0 & 0 & \dots & 0 & 1 - \rho_y & 0 & \dots & \rho_y - \frac{1 + (M_y - 1)\rho_y}{M_y} \\ 0 & 0 & \dots & 0 & 0 & 1 - \rho_y & \dots & \rho_y - \frac{1 + (M_y - 1)\rho_y}{M_y} \\ \vdots & \vdots & \ddots & \vdots & \vdots & \vdots & \ddots & \vdots \\ 0 & 0 & \dots & 0 & 0 & 0 & \dots & 1 + (M_y - 1)\rho_y - \frac{M_x M_y \rho^2}{1 + (M_x - 1)\rho_x} \end{bmatrix}. \quad (\text{B.4})$$

It is known that elementary matrix operations do not change the determinant of the original matrix [83], and as (B.4) is upper triangular, we have the determinant of \mathbf{R} as in (3.23).

B.2 The Inverse of \mathbf{R} for Correlated In-Phase–Quadrature Components

The covariance matrix in (3.22) can be rewritten as follows

$$\mathbf{R} = \begin{bmatrix} \mathbf{A}_{M_x \times M_x} & \mathbf{B}_{M_x \times M_y} \\ \mathbf{C}_{M_y \times M_x} & \mathbf{D}_{M_y \times M_y} \end{bmatrix}, \quad (\text{B.5})$$

where $\mathbf{A}_{M_x \times M_x} = \mathbf{I}_{M_x} + \rho_x \mathbf{I}_{M_x}^c$, $\mathbf{B}_{M_x \times M_y} = \rho \mathbf{1}_{M_x \times M_y}$, $\mathbf{C}_{M_y \times M_x} = \rho \mathbf{1}_{M_y \times M_x}$ and $\mathbf{D}_{M_y \times M_y} = \mathbf{I}_{M_y} + \rho_y \mathbf{I}_{M_y}^c$.

As in this case the matrices $\mathbf{A}_{M_x \times M_x}$ and $\mathbf{D}_{M_y \times M_y}$ are invertible, the inverse matrix of (B.5) is given by [83]

$$\mathbf{R}^{-1} = \begin{bmatrix} \mathbf{A}_{M_x \times M_x} & \mathbf{B}_{M_x \times M_y} \\ \mathbf{C}_{M_y \times M_x} & \mathbf{D}_{M_y \times M_y} \end{bmatrix}^{-1} = \begin{bmatrix} (\mathbf{A} - \mathbf{B}\mathbf{D}^{-1}\mathbf{C})^{-1} & -(\mathbf{A} - \mathbf{B}\mathbf{D}^{-1}\mathbf{C})^{-1}\mathbf{B}\mathbf{D}^{-1} \\ -(\mathbf{D} - \mathbf{C}\mathbf{A}^{-1}\mathbf{B})^{-1}\mathbf{C}\mathbf{A}^{-1} & (\mathbf{D} - \mathbf{C}\mathbf{A}^{-1}\mathbf{B})^{-1} \end{bmatrix}, \quad (\text{B.6})$$

where the matrices dimensions have been omitted for brevity.

Following the definition in (B.6), and after extensive algebraic manipulations, the entry at the i th line and j th column of \mathbf{R}^{-1} from (3.22), say $\xi_{i,j}$, is obtained as in (3.24).

B.3 The Determinant of R for Uncorrelated In-Phase–Quadrature Components

In order to find the determinant of \mathbf{R} in in-phase and quadrature scenarios with zero cross correlation, we can perform elementary matrix operations. To improve the understanding of the process, we can rewrite (3.29) as follows

$$\mathbf{R} = \begin{bmatrix} 1 & \rho_x & \dots & \rho_x & 0 & 0 & \dots & 0 \\ \rho_x & 1 & \dots & \rho_x & 0 & 0 & \dots & 0 \\ \vdots & \vdots & \ddots & \vdots & \vdots & \vdots & \ddots & \vdots \\ \rho_x & \rho_x & \dots & 1 & 0 & 0 & \dots & 0 \\ 0 & 0 & \dots & 0 & 1 & \rho_y & \dots & \rho_y \\ 0 & 0 & \dots & 0 & \rho_y & 1 & \dots & \rho_y \\ \vdots & \vdots & \ddots & \vdots & \vdots & \vdots & \ddots & \vdots \\ 0 & 0 & \dots & 0 & \rho_y & \rho_y & \dots & 1 \end{bmatrix}, \quad (\text{B.7})$$

Starting from (B.7), we subtract the M_x th column from the other $M_x - 1$ columns and subtract the M th column from the other $M - 1$ to $M_x + 1$ columns, i.e.,

$$\mathbf{R}' = \begin{bmatrix} 1 - \rho_x & 0 & \dots & \rho_x & 0 & 0 & \dots & 0 \\ 0 & 1 - \rho_x & \dots & \rho_x & 0 & 0 & \dots & 0 \\ \vdots & \vdots & \ddots & \vdots & \vdots & \vdots & \ddots & \vdots \\ \rho_x - 1 & \rho_x - 1 & \dots & 1 & 0 & 0 & \dots & 0 \\ 0 & 0 & \dots & 0 & 1 - \rho_y & 0 & \dots & \rho_y \\ 0 & 0 & \dots & 0 & 0 & 1 - \rho_y & \dots & \rho_y \\ \vdots & \vdots & \ddots & \vdots & \vdots & \vdots & \ddots & \vdots \\ 0 & 0 & \dots & 0 & \rho_y - 1 & \rho_y - 1 & \dots & 1 \end{bmatrix}. \quad (\text{B.8})$$

By adding the first $M_x - 1$ lines of (B.8) to its M_x th line and adding the $M - 1$ to $M_x + 1$ lines of (B.8) to its M th line, we attain

$$\mathbf{R}'' = \begin{bmatrix} 1 - \rho_x & 0 & \dots & \rho_x & 0 & 0 & \dots & 0 \\ 0 & 1 - \rho_x & \dots & \rho_x & 0 & 0 & \dots & 0 \\ \vdots & \vdots & \ddots & \vdots & \vdots & \vdots & \ddots & \vdots \\ 0 & 0 & \dots & 1 + (M_x - 1)\rho_x & 0 & 0 & \dots & 0 \\ 0 & 0 & \dots & 0 & 1 - \rho_y & 0 & \dots & \rho_y \\ 0 & 0 & \dots & 0 & 0 & 1 - \rho_y & \dots & \rho_y \\ \vdots & \vdots & \ddots & \vdots & \vdots & \vdots & \ddots & \vdots \\ 0 & 0 & \dots & 0 & 0 & 0 & \dots & 1 + (M_y - 1)\rho_y \end{bmatrix}. \quad (\text{B.9})$$

Since elementary matrix operations do not change the determinant of the original matrix [83], and as (B.9) is upper triangular, we have

$$\det(\mathbf{R}) = (1 - \rho_x)^{M_x - 1} (1 - \rho_y)^{M_y - 1} (1 + (M_x - 1)\rho_x) (1 + (M_y - 1)\rho_y). \quad (\text{B.10})$$

B.4 The Inverse of R for Uncorrelated In-Phase–Quadrature Components

The covariance matrix in (3.29) can be rewritten as follows


$$\mathbf{R} = \begin{bmatrix} \mathbf{A}_{M_x \times M_x} & \mathbf{0}_{M_x \times M_y} \\ \mathbf{0}_{M_y \times M_x} & \mathbf{B}_{M_y \times M_y} \end{bmatrix}, \quad (\text{B.11})$$






where $\mathbf{A}_{M_x \times M_x} = \mathbf{I}_{M_x} + \rho_x \mathbf{I}_{M_x}^c$ and $\mathbf{B}_{M_y \times M_y} = \mathbf{I}_{M_y} + \rho_y \mathbf{I}_{M_y}^c$. (B.11) is a diagonal block matrix. This matrix is invertible if and only if each of the main blocks is invertible [83]. Thus, the inverse matrix of (B.11) is given by


$$\mathbf{R}^{-1} = \begin{bmatrix} \mathbf{A}_{M_x \times M_x}^{-1} & \mathbf{0}_{M_x \times M_y} \\ \mathbf{0}_{M_y \times M_x} & \mathbf{B}_{M_y \times M_y}^{-1} \end{bmatrix}. \quad (\text{B.12})$$

By the definition of matrices $\mathbf{A}_{M_x \times M_x}$ and $\mathbf{B}_{M_y \times M_y}$, both are invertible and, after algebraic manipulations, the entry at the i th line and j th column of \mathbf{R}^{-1} from (3.29), say $\xi_{i,j}$, is obtained as in (3.30).

APPENDIX C – Permission to Reproduce Copyrighted Material



 Home
  Help
  Live Chat
  Sign in
  Create Account



Requesting permission to reuse content from an IEEE publication

On the Generation of Autocorrelated π , $-\pi$, and $-\pi$ Fading Sequences

Author: Vanessa Mendes Rennó

Publication: IEEE Transactions on Antennas and Propagation

Publisher: IEEE

Date: December 2022

Copyright © 2022, IEEE

Thesis / Dissertation Reuse

The IEEE does not require individuals working on a thesis to obtain a formal reuse license, however, you may print out this statement to be used as a permission grant:

Requirements to be followed when using any portion (e.g., figure, graph, table, or textual material) of an IEEE copyrighted paper in a thesis:

- 1) In the case of textual material (e.g., using short quotes or referring to the work within these papers) users must give full credit to the original source (author, paper, publication) followed by the IEEE copyright line © 2011 IEEE.
- 2) In the case of illustrations or tabular material, we require that the copyright line © [Year of original publication] IEEE appear prominently with each reprinted figure and/or table.
- 3) If a substantial portion of the original paper is to be used, and if you are not the senior author, also obtain the senior author's approval.

Requirements to be followed when using an entire IEEE copyrighted paper in a thesis:

- 1) The following IEEE copyright/ credit notice should be placed prominently in the references: © [year of original publication] IEEE. Reprinted, with permission, from [author names, paper title, IEEE publication title, and month/year of publication]
- 2) Only the accepted version of an IEEE copyrighted paper can be used when posting the paper or your thesis on-line.
- 3) In placing the thesis on the author's university website, please display the following message in a prominent place on the website: In reference to IEEE copyrighted material which is used with permission in this thesis, the IEEE does not endorse any of [university/educational entity's name goes here]'s products or services. Internal or personal use of this material is permitted. If interested in reprinting/republishing IEEE copyrighted material for advertising or promotional purposes or for creating new collective works for resale or redistribution, please go to http://www.ieee.org/publications_standards/publications/rights/rights_link.html to learn how to obtain a License from RightsLink.

If applicable, University Microfilms and/or ProQuest Library, or the Archives of Canada may supply single copies of the dissertation.

BACK
CLOSE WINDOW

Um Simulador Fase-Envoltória para o Processo alpha-mu

Vanessa Mendes Rennó, José Cândido Silveira Santos Filho

DOI: 10.14209/SBRT.2020.1570648767

Keywords: **distribuição alpha-mu** **canais de desvanecimento** **simulação**

Abstract

O esquema clássico para simulação de processos de desvanecimento alpha-mu restringe o parâmetro mu a valores inteiros ou múltiplos de 1/2. Neste trabalho, propõe-se um esquema de simulação mais realista, capaz de acomodar valores reais arbitrários para o parâmetro mu, como observado na prática. Não menos importante, o esquema proposto abrange fase e envoltória, cumpre de forma exata as estatísticas de primeira ordem do modelo alpha-mu, e bem aproxima as de segunda ordem. Todas essas estatísticas são analisadas em detalhe.

 DOWNLOAD
Um Simulador Fase-Envoltória para o Processo α - μ On The Generation of Autocorrelated α - η - κ - μ Fading Sequences

Conference Proceedings: 2021 IEEE Statistical Signal Processing Workshop (SSP)

Author: Vanessa Mendes Rennó

Publisher: IEEE

Date: 11 July 2021

Copyright © 2021, IEEE

Thesis / Dissertation Reuse

The IEEE does not require individuals working on a thesis to obtain a formal reuse license, however, you may print out this statement to be used as a permission grant:

Requirements to be followed when using any portion (e.g., figure, graph, table, or textual material) of an IEEE copyrighted paper in a thesis:

- 1) In the case of textual material (e.g., using short quotes or referring to the work within these papers) users must give full credit to the original source (author, paper, publication) followed by the IEEE copyright line © 2011 IEEE.
- 2) In the case of illustrations or tabular material, we require that the copyright line © [Year of original publication] IEEE appear prominently with each reprinted figure and/or table.
- 3) If a substantial portion of the original paper is to be used, and if you are not the senior author, also obtain the senior author's approval.

Requirements to be followed when using an entire IEEE copyrighted paper in a thesis:

- 1) The following IEEE copyright/ credit notice should be placed prominently in the references: © [year of original publication] IEEE. Reprinted, with permission, from [author names, paper title, IEEE publication title, and month/year of publication]
- 2) Only the accepted version of an IEEE copyrighted paper can be used when posting the paper or your thesis online.
- 3) In placing the thesis on the author's university website, please display the following message in a prominent place on the website: In reference to IEEE copyrighted material which is used with permission in this thesis, the IEEE does not endorse any of [university/educational entity's name goes here]'s products or services. Internal or personal use of this material is permitted. If interested in reprinting/republishing IEEE copyrighted material for advertising or promotional purposes or for creating new collective works for resale or redistribution, please go to http://www.ieee.org/publications_standards/publications/rights/rights_link.html to learn how to obtain a License from RightsLink.

If applicable, University Microfilms and/or ProQuest Library, or the Archives of Canada may supply single copies of the dissertation.

 BACK

 CLOSE WINDOW



Biblioteca da SBrT

Um Simulador Aprimorado para Processos α - η - κ - μ

Vanessa Mendes Rennó, José Cândido Silveira Santos Filho

DOI: [10.14209/sbrt.2021.1570723489](https://doi.org/10.14209/sbrt.2021.1570723489)Keywords: **processo α - η - κ - μ** **simulação** **canais de desvanecimento**

Abstract

O modelo estatístico α - η - κ - μ oferece uma descrição geral e unificada para todos os elementos essenciais do desvanecimento de curto prazo. Em um trabalho recente, propusemos um simulador para o processo α - η - κ - μ que comporta a faixa plena de valores para os parâmetros do modelo e cumpre as suas estatísticas de primeira e segunda ordens de forma satisfatória. Entretanto, nessa proposta, o ajuste de um parâmetro-chave de simulação foi feito por meio de rotinas numéricas complexas, tornando o simulador menos atraente para equipes de projeto de sistemas sem fio do mundo real. Neste trabalho, aprimoramos esse arcabouço de simulação com base em coeficientes assintóticos das estatísticas α - η - κ - μ . A nova abordagem resulta em expressões simples e fechadas para o ajuste do referido parâmetro-chave, reduzindo o custo computacional do simulador.

DOWNLOAD


Biblioteca da SBrT

Análise Assintótica Unificada de Estatísticas de Segunda Ordem para Canais de Classe Gaussiana

Vanessa Mendes Rennó, Francisco Raimundo Albuquerque Parente, José Cândido Silveira Santos Filho

DOI: [10.14209/sbrt.2022.1570812932](https://doi.org/10.14209/sbrt.2022.1570812932)Keywords: **Alta relação sinal-ruído** **análise assintótica** **canal de desvanecimento** **estatísticas de segunda ordem**

Abstract

A natureza dinâmica de um processo aleatório pode ser caracterizada por meio de estatísticas de segunda ordem. Para uma ampla classe gaussiana de modelos de desvanecimento abrangendo vários aspectos físicos do canal sem fio, a análise exata dessas estatísticas produz expressões intrincadas, que têm sido exploradas caso a caso para cenários particulares. Neste trabalho, fornecemos uma análise assintótica geral das estatísticas de segunda ordem em regime de alta relação sinal-ruído para os diversos modelos de desvanecimento da classe gaussiana referida. O arcabouço proposto conduz a expressões simples, unificadas e em forma fechada, capazes de caracterizar o impacto de cada aspecto físico do desvanecimento sobre o canal. Dessa forma, nossos resultados fornecem uma descrição completa, prática e intuitiva do comportamento dinâmico do sistema. As expressões assintóticas obtidas são validadas minuciosamente, tanto reduzindo-as a casos particulares conhecidos quanto por meio de simulações de Monte Carlo.

DOWNLOAD
